Aus dem Fachbereich Medizin
der Johann Wolfgang Goethe-Universität
Frankfurt am Main

betreut am
Zentrum der Inneren Medizin
Medizinische Klinik 2
Direktor: Prof. Dr. Hubert Serve

Roles of MARCH5 and SASH3 in oncogenic signalling in B-cell Non-Hodgkin lymphoma

Dissertation
zur Erlangung des Doktorgrades der theoretischen Medizin
des Fachbereichs Medizin
der Johann Wolfgang Goethe-Universität
Frankfurt am Main

vorgelegt von
Tanja Wotapek

aus Offenbach am Main

Frankfurt am Main, 2021

Aus dem Fachbereich Medizin
der Johann Wolfgang Goethe-Universität
Frankfurt am Main

betreut am
Zentrum der Inneren Medizin
Medizinische Klinik 2
Direktor: Prof. Dr. Hubert Serve

Roles of MARCH5 and SASH3 in oncogenic signalling in B-cell Non-Hodgkin lymphoma

Dissertation
zur Erlangung des Doktorgrades der theoretischen Medizin
des Fachbereichs Medizin
der Johann Wolfgang Goethe-Universität
Frankfurt am Main

vorgelegt von
Tanja Wotapek

aus Offenbach am Main

Frankfurt am Main, 2021

Dekan:	Prof. Dr. Stefan Zeuzem
Referent:	Prof. Dr. Thomas Oellerich
Korreferntin:	Prof. Dr. Evelyn Ullrich
Tag der mündlichen Prüfung:	27.04.2022

Contents

List of Figures

List of Tables

Abbreviations

7AAD	7-Aminoactinomycin D
ABB	Annexin binding buffer
ABC-DLBCL	Activated B-cell like DLBCL
AKT	Protein kinase B = PKB
APAF1	Apoptotic protease activating factor 1
APC	Allophycocyanin
BAD	Bcl2-associated agonist of cell death
BAK	BCL2 Antagonist/Killer 1
BAX	Bcl-2-associated X protein
BCA	Bicinchoninic acid
BCL2	B-cell lymphoma protein 2
BCL2A1	BCL2 Related Protein A1
BCL-B	B-cell lyphoma protein B
BCL-W	B-cell lymphoma protein W
BCL-XL	B-cell lymphoma-extra large
BCR	B-cell receptor
BFP	Blue fluorescent protein
BH	BCL2 homology domain
BID	BH3 Interacting Domain Death Agonist
BIK	BCL2 Interacting Killer
BIM	Bcl-2 Interacting Mediator Of Cell Death
BLK	B Lymphocyte Kinase
BLNK	B-cell linker protein
BMF	Bcl2 Modifying Factor
B-NHL	B-cell NHL
BOK	Bcl-2 related ovarian killer
BSA	Bovine serum albumine
BTK	Bruton's tyrosine kinase
CARD11	Caspase Recruitment Domain Family Member 11
CBM	CARD11-BCL10-MALT1 complex
c-cbl	Casitas B-Lineage Lymphoma Proto-Oncogene
CD19	Cluster of differentiation 19
CD2AP	CD2-associated protein

CD79a/b	Cluster of differentiation 79a/b
cDNA	Copy DNA
CLL	Chronic lymphocytic leukemia
CLP	Common lymphoid progenitor
CMP	Common myeloic progenitor
CRISPR	clustered regularly interspaced short palindromic repeats
CSS	Crispr screen score
CST	Cell Signaling Technologies
D (segment)	Diversity segment
DAG	Diacylglyceride
dFCS	Dialysed FCS
DLBCL	Diffuse large B-cell lymphoma
DMEM	Dulbecco's Modified Eagle's Medium
DMSO	Dimethyl sulfoxide
DNA	Desoxyribo nucleic acid
DPBS	Dulbecco's phosphate buffered saline
Drp-1	Dynamin-1-like protein
DUB	Deubiquitinating enzyme
EDTA	Ethylenediaminetetraacetic acid
EGFP	Enhanced green fluorescent protein
ER	Endoplasmic reticulum
EZH2	Enhancer of zeste homolog 2
FCS	Fetal calv serum
Fis1	Fission, mitochondrial 1
FOXO1	Forkhead box protein O 1
FYN	Tyrosine-protein kinase
GALV	gibbon ape leukaemia virus
GCB-DLBCL	Germinal center B-cell like DLBCL
GO	Gene Ontology
GOBP	GO Biological Process
GOCC	GO Cellular Component
GOMF	GO Molecular Function
GSEA	Gene Set Enrichment Analysis
HDR	Homology-directed repair
HECT	Homologous to E6-associated protein C-terminus
HEK293T	Human embryonic kidney cell line
HL	Hodgkin's lymphoma
HRK	Harakiri
HRP	Horseraddish peroxidase

HSC	Hematopoietic stem cell
ICAM-1	Intercellular Adhesion Molecule 1
IGHV	Immunoglobulin heavy chain
IP	Immunoprecipitation
IP3	Inositol trisphosphate
IRF8	Interferon regulatory factor 8
ITAM	Immunoreceptor tyrosine-based activation motifs
J (segment)	Joining segment
LDL	Low density lipoprotein
LYN	Lck/Yes-Related Novel Protein Tyrosine Kinase
MAPK	Mitogen-activated protein kinase
MARCH5	Membrane Associated Ring-CH-Type Finger 5
MCL	Mantle cell lyphoma
MCL1	MCL1 apoptosis regulator
MCL-1	Myeloid Cell Leukemia Sequence 1
MFF	Mitochondrial fission factor
Mfn2	Mitofusin 2
MHC	Major histocompatibility complex
MOI	Multiplicity of infection
MOMP	Mitochondrial outer membrane permeabilisation
MPP	Multipotent progenitor cells
mRNA	Messenger RNA
MS	Mass spectrometry
MTCH2	Mitochondrial carrier 2
mTOR	Mechanistic target of rapamycin
MTT	3-(4,5-Dimethyl-2-thiazolyl)-2,5-diphenyl-2H-tetrazoliumbromid
MYD88	Myeloid differentiation primary response 88
NFAT	Nuclear factor of activated T cells
NF-κB	Nuclear factor κB
NGS	Next generation sequencing
NHEJ	Non homologous end joining
NHL	Non-Hodgkin's lymphoma
NOXA	Pro-apoptotic BCL2 family protein, latin for damage
PARP	Poly (ADP-ribose) polymerase
PCR	Polymerase chain reaction
PenStrep	Penicillin-Streptomycin
PI3K	Phosphatidylinositol-4,5-Bisphosphate 3-Kinase
PKCβ	Protein kinase C β
PLCγ2	Phospholipase γ 2

PUMA	p53 upregulated modulator of apoptosis
qRT-PCR	Quantitative real-time PCR
RAG 1/2	Recombination activating gene 1/2
RAS	Rat sarcome viral oncogene
RBR	RING-in-between-RING
RING	Really interesting new gene
RNA	Ribonucleic acid
ROS	Reactive oxygen species
RPMI	Roswell Park Memorial Institute cell culture medium
rSAP	Recombinant shrimp alkaline phosphatase
RSS	Recombination signal sequences
SAM	Sterile alfa motif
SASH3	SH3 containing lymphocyte protein 1
SCT	Stem cell transplantation
SDS	Sodium dodecylsulfate
SDS-PAGE	SDS-Polyacrylamide gel electrophoresis
sgRNA	Single guide RNA
SH2	SRC homology 2
SH3	SRC homology 3
SH3KBP1	SH3 domain-containing kinase-binding protein 1
SILAC	Stable Isotope Labelling of Amino Acids by Cell Culture
SOX11	SRY-Box Transcription Factor 11
SYK	Spleen tyrosine kinase
tBID	Truncated BID
TBST	Tris-buffered saline with Tween20
TCR	T-cell receptor
TLR9	Toll-like receptor 9
TMT	Tandem mass tags
TNFα	Tumor necrosis factor α
TUBE	Tandem ubiquitin binding entitiy
UBE2K	Ubiquitin conjugating enzyme E2 K
UPS	Ubiquitin proteasome system
V (segment)	Variable segment
VSV-G	Vesicular stomatitis virus protein G
Y	Tyrosine

1 Abstract

1.1 Abstract

Despite major improvements of the therapy, many B-cell Non-Hodgkin's lymphoma (B-NHL) entities still have a poor prognosis. New therapeutic options are urgently needed. Therefore this study sets out to investigate oncogenic signalling pathways in the two B-NHL entities mantle cell lymphoma (MCL) and diffuse large B-cell lymphoma (DLBCL) in order to define new potential therapeutic targets.
MCL cells overexpress the anti-apoptotic protein BCL-2, thereby they evade apoptosis. With venetoclax, the first-in-class BCL-2 specific inhibitor was approved and achieved good response rates in MCL. However, some cases display intrinsic or acquired resistance to venetoclax. In order to improve the therapy, this study aimed to identify genes which confer sensitivity or resistance towards venetoclax upon their respective knockout. To this end, a genome-wide CRISPR/Cas9-based loss-of-function screen was conducted in the MCL cell line Maver-1. The E3 ubiquitin ligase MARCH5 was identified as one of the top hits conferring sensitivity towards venetoclax upon its knockout. This finding was validated in a competitive growth assay including two more MCL cell lines, Jeko-1 and Mino. MARCH5 knockout also sensitised Jeko-1 cells towards venetoclax even though this cell line was insensitive towards venetoclax in its wild-type form. Using BH3 profiling, an increased dependency on BCL-2 of MARCH5-depleted cells confirmed this finding. The sensitisation was found to be based on induction of apoptosis upon MARCH5 knockout and to an even higher extent upon additional treatment of MARCH5-depleted cells with venetoclax. As already described for epithelial cancer entities, the BCL-2 family members MCL-1 and NOXA were upregulated in MCL cell lines upon MARCH5 knockout. This led to the hypothesis that MARCH5 is a potential regulator of intrinsic apoptosis with NOXA as a key component. A competitive growth assay with MARCH5 and NOXA co-depleted cells revealed a partial reversion of the BCL-2 sensitisation compared to MARCH5 knockout alone. Furthermore, mass spectrometry-based methods were used to gain more insight into other cellular pathways and networks which might be regulated in a MARCH5-dependent manner. In an interactome analysis, proteins which regulate mitochondrial morphology, such as Drp-1 were identified as MARCH5 interactors. Besides this expected finding, interaction between MARCH5 and several members of the BCL-2 family as well

as a potential connection between MARCH5 and vesicular trafficking was discovered. As expected, an ubiquitinome analysis of MARCH5-depleted cells revealed decreased levels of MCL-1 and NOXA ubiquitination. Additionally, a potential role of MARCH5 in the ubiquitination of several members of the cell cycle regulatory pathway was discovered. Based on the broad spectrum of cellular pathways which seem to be regulated in a MARCH5-dependent manner, it was hypothesised that MARCH5 primarily regulates BCL-2 family members which in turn regulate intrinsic apoptosis on the one hand and additionally are involved in the regulation of various other pathways on the other hand.
In summary, this study provides insight into a MARCH5-dependent MCL1-1/NOXA axis in MCL cells and potential implications into related cellular processes.

In addition to the anti-apoptotic pathways described above, B-cell receptor (BCR) signalling is known to provide a pro-survival signal to both normal and malignant B-cells. Targeting the BCR signalling pathway therefore is a promising therapeutic target for B-cell malignancies. In order to gain more insight into the differential modes of BCR signalling of ABC- and GCB-DLBCL cells, genes/proteins which displayed differential essentiality in ABC- and GCB-DLBCL cells were aimed to be defined. Consequently, data sets from a CRISPR/Cas9-based loss-of-function screen were re-analysed. SASH3 was identified as a gene which was essential for GCB- but not for ABC-DLBCL cells. Since this protein is known to be involved in T-cell receptor (TCR)-signalling, SASH3 was assumed to play a potential role in BCR signalling as well and was therefore investigated in more detail. A competitive growth assay confirmed that SASH3 knockout was toxic exclusively for GCB-DLBCL cell lines. An interactome analysis in ABC- and GCB-DLBCL cells revealed interaction between SASH3 and many components of the proximal BCR signalling pathway as well as several downstream signalling pathways such as the PI3K or the NF-κB pathway. An integration of the interactome with data from the CRISPR/Cas9-based loss-of-function screen revealed differential essentiality of the SASH3-interacting proteins in ABC- and GCB-DLBCL cells. It was hypothesised that SASH3 might regulate PI3K signalling on which GCB- but not ABC-DLBCL cells are known to dependent. Discontinuation of the regulation of PI3K signalling could therefore be exclusively toxic to GCB-DLBCL cells.
Taken together, this study describes a subtype-specific dependency of GCB-DLBCL cells on SASH3. Furthermore, the SASH3 interactome has been investigated in B-cells for the first time, thereby highlighting a potential role in proximal BCR signalling and involvement in specific BCR-related downstream signalling pathways.

1.2 Zusammenfassung

Trotz bedeutender Verbesserungen der Therapie haben viele B-Zell Non-Hodgkin-Lymphome (B-NHL) noch immer eine schlechte Prognose. Neue Optionen für die Therapie werden dringend benötigt. Daher wurden in dieser Studie onkogene Signalwege in den beiden B-NHL-Entitäten Mantelzellylmphom (MCL) und Diffus Großzelliges B-Zell-Lymphom (DLBCL) untersucht, um neue potentielle therapeutische Zielstrukturen zu ermitteln.
MCL Zellen überexprimieren das anti-apoptotische Protein BCL-2 und entgehen somit der Apoptose. Mit Venetoclax wurde der erste BCL-2-spezifische Inhibitor klinisch zugelassen und erzielte gute Ansprechraten im MCL. Allerdings zeigen einige Fälle intrinsische oder erworbene Resistenzen gegenüber Venetoclax. Um die Therapie zu optimieren, beabsichtigte diese Studie Gene zu identifizieren, die bei ihrem jeweiligen Knockout Sensitivität oder Resistenz gegenüber Venetoclax vermitteln. Zu diesem Zweck wurde ein genomweiter CRISPR/Cas9-basierter *loss-of-function* Screen in der MCL-Zelllinie Maver-1 durchgeführt. Die E3 Ubiquitinligase MARCH5 wurde als einer der Top-Hits identifiziert, welche Sensitivität gegenüber Venetoclax bei ihrem jeweiligen Knockout vermitteln. Dieses Ergebnis wurde in einem kompetitiven Zellproliferationsassay zusammen mit zwei weiteren MCL-Zelllinien, Jeko-1 und Mino, validiert. Knockout von MARCH5 sensitivierte auch Jeko-1 Zellen gegenüber Venetoclax, obwohl diese Zelllinie in ihrer Wildtyp-Form unempfindlich gegenüber Venetoclax war. Dieses Ergebnis wurde durch eine erhöhte BCL-2-Abhängigkeit MARCH5-depletierter Zellen bestätigt, welche mittels BH3 Profiling identifiziert wurde. Die Sensitivierung basierte auf einer Induktion der Apoptose nach MARCH5-Knockout und in noch höherem Maße bei Behandlung von MARCH5-depletierten Zellen mit Venetoclax. Wie bereits für epitheliale Krebsentitäten beschrieben, waren die BCL-2-Proteine MCL-1 und NOXA in MARCH5-depletierten MCL Zellen heraufreguliert. Dies führte zu der Hypothese, dass MARCH5 ein potentieller Regulator des intrinsischen Apoptose-Signalweges mit NOXA als einer Hauptkomponente sein könnte. Ein kompetitiver Zellproliferationsassay mit MARCH5 und NOXA co-depletierten Zellen zeigte eine partielle Umkehr der BCL-2-Sensitivierung im Vergleich zu alleinigem MARCH5-Knockout. Zusätzlich wurden Massenspektrometrie-basierte Methoden verwendet, um weitere Einblicke in andere zelluläre Signalwege und Netzwerke zu erhalten, welche möglicherweise durch MARCH5 reguliert werden. In einer Interaktom-Analyse wurden Proteine wie Drp-1, welche die mitochondriale Morphologie regulieren, als MARCH5-Interaktionspartner identifiziert. Neben diesem erwarteten Ergebnis wurde eine Interaktion zwischen MARCH5 und verschiedenen BCL-2-Proteinen sowie eine potentielle Verbindung zwischen MARCH5 und dem Vesikeltransport entdeckt. Wie

erwartet, zeigte eine Analyse des Ubiquitinoms MARCH5-depletierter Zellen verminderte Niveaus von MCL-1- und NOXA-Ubiquitinierung. Zusätzlich wurde eine mögliche Rolle von MARCH5 in der Ubiquitinierung von verschiedenen Bestandteilen der Zellzyklus-Regulation entdeckt. Basierend auf dem breiten Spektrum zellulärer Signalwege, die MARCH5-abhängig reguliert zu sein scheinen, wurde die Hypothese entwickelt dass MARCH5 primär BCL-2-Proteine reguliert, welche wiederum einerseits den intrinsischen Apoptose-Signalweg und andererseits verschiedene weitere Signalwege regulieren.
Zusammmengefasst bietet diese Studie weitere Einblicke in eine MARCH5-abhängige MCL-1/NOXA-Achse in MCL Zellen und potentielle Auswirkungen auf verwandte zelluläre Signalwege.

Zusätzlich zu den oben beschriebenen anti-apoptotischen Signalwegen ist bekannt, dass der B-Zell-Rezeptor (BCR) ein Überlebenssignal für normale und maligne Zellen bereitstellt. Der BCR Signalweg ist daher ein vielversprechendes therapeutisches Target in B-Zell Malignomen. Um weitere Einblicke in die unterschiedlichen Modalitäten des BCR-Signalwegs in ABC- und GCB-DLBCL-Zellen zu erhalten, sollten Gene/Proteine definiert werden, welche eine unterschiedliche Essentialität in ABC- und GCB-DLBCL-Zellen zeigen. Zu diesem Zweck wurden Daten eines CRISPR/Cas9-basierten *loss-of-function* Screens erneut analysiert. SASH3 wurde als essentielles Gen für GCB- jedoch nicht für ABC-DLBCL-Zellen identifiziert. Da dieses Protein bekanntermaßen im T-Zell-Rezeptor (TCR)-Signalweg beteiligt ist, wurde angenommen, dass es ebenfalls im BCR-Signalweg eine Rolle spielt und daher detailliert untersucht. Ein kompetitiver Zellproliferationsassay bestätigte dass SASH3 ausschließlich für GCB-DLBCL-Zelllinien toxisch war. Eine Interaktom-Analyse in ABC- und GCB-DLBCL-Zellen zeigte eine Interaktion zwischen SASH3 und vielen Komponenten des proximalen BCR-Signalweges sowie verschiedenen nachgeschalteten Signalwegen wie dem PI3K- oder NF-κB-Signalweg. Durch Integration von Daten der Interaktom-Analyse und Daten des CRISPR/Cas9-basierten *loss-of-function*-Screens wurde eine differentielle Essentialität der SASH3-interagierenden Proteine in ABC- und GCB-DLBCL-Zellen gezeigt. Es wurde angenommen, dass SASH3 den PI3K-Signalweg reguliert, welcher bekanntermaßen essentiell für GCB- aber nicht für ABC-DLBCL-Zellen ist. Eine Unterbrechung der Regulation des PI3K-Signalwegs könnte daher ausschließlich für GCB-DLBCL-Zellen toxisch sein.
Zusammengefasst beschreibt diese Studie eine subtypspezifische SASH3-Abhängigkeit von GCB-DLBCL-Zellen. Weiterhin wurde das SASH3-Interaktom erstmals in B-Zellen untersucht und hob eine potentielle Rolle im proximalen BCR-Signalweg sowie Beteiligung in nachgeschalteten BCR-spezifischen Signalwegen hervor.

2 Introduction

2.1 B-cell Non-Hodgkin lymphoma

Various malignant diseases, such as leukaemia and lymphoma, can emerge from B- and T-cells. Lymphoma can be divided into two major classes: Hodgkin (HL) and non-Hodgkin lymphoma (NHL). The latter account for approx. 90% of all lymphoma cases and encompass a very heterogeneous group of diseases. 85-90% of NHL cases are derived from B-cells (B-NHL), the remainder originates from T- and NK-cells. Usually, the disease develops in lymph nodes, but may also occur in virtually all other tissues. The aggressiveness of the disease and thus the prognosis for the patient depends on the specific B-NHL subtype.[1]

During B-cell development, oncogenic events may occur at any developmental stage, which is illustrated in Figure 2.1. A culmination of several oncogenic events can then lead to the emergence of B-cell neoplasia. The developmental setting of the affected (often termed the "normal B-cell counterpart")[2] cell plus the acquired oncogenic transformation then define the resulting tumour cell. This study will focus on two B-NHL subgroups, namely mantle cell lymphoma and diffuse large B-cell lymphoma.

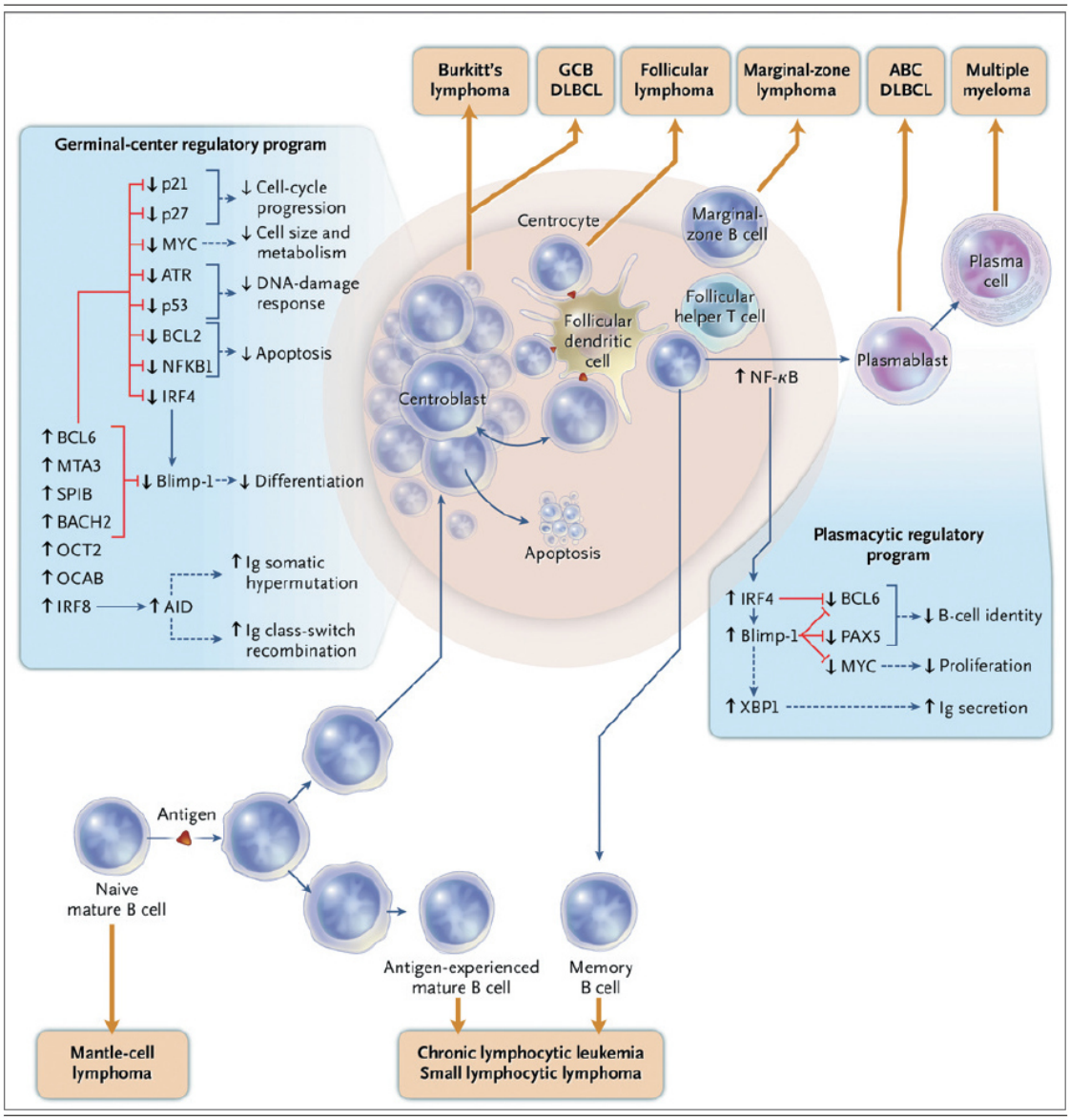

Figure 2.1: **B-NHL may arise from any developmental stage of a B-cell. Reproduced with permission from[3].**

As illustrated in Figure 2.2, overall survival is highly differential in each B-NHL subtype. MCL and DLBCL have the lowest survival probability of the four B-NHL subtypes compared.

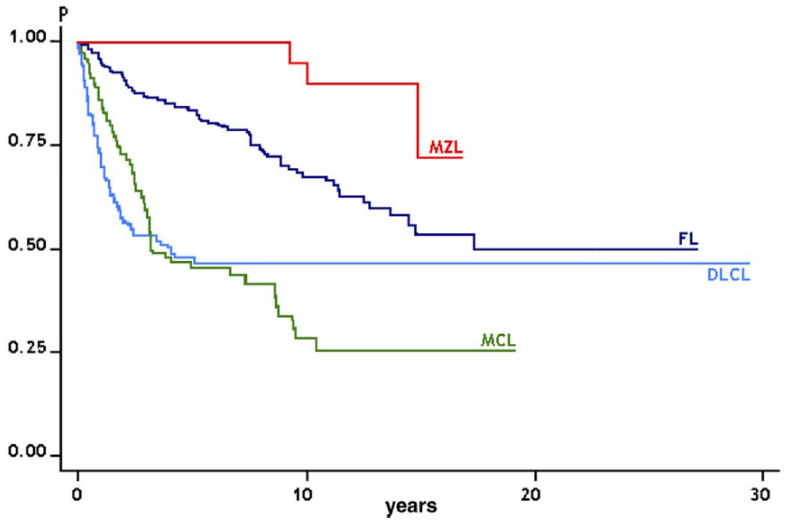

Figure 2.2: **B-NHL subtypes have differential survival probabilities. MZL = Marginal zone lymphoma; FL = Follicular lymphoma; DLCL = Diffuse large B-cell lymphoma; MCL = Mantle cell lymphoma. Figure from[4]. Copyright obtained from The American Society of Hematology.**

2.1.1 Mantle cell lymphoma

Mantle cell lymphoma (MCL) accounts for 3-10% of all newly diagnosed B-NHL cases in Western countries[5] and is generally considered incurable due to its frequent relapses and occurrence of chemotherapy resistance mechanisms.[6] MCL most frequently occurs in elderly males, with a median age of 65-70 years.[7] Currently, there is no standard therapy scheme for the treatment of MCL patients. For patients with indolent disease courses which do not exhibit symptoms at diagnosis, it is safe to defer treatment initiation until symptoms occur. For patients who require immediate onset of therapy, there are several options, depending on the fitness of the patient, disease status and comorbidities. Chemotherapy intensity is adapted to the patient's fitness and stem cell transplantation (SCT) is conducted when feasible. Rituximab, an anti-CD20 antibody, is usually administered. Additional targeted small molecule therapeutics, such as ibrutinib (BTK inhibitor), venetoclax (BCL2 inhibitor), lenalidomide (immunomodulatory drug) and others are applied when possible. Many clinical trials are ongoing to evaluate the best combination of chemotherapy and targeted therapeutics.[5]

Generally, MCL cells comprise a mature B-cell receptor (BCR). The hallmark of MCL cells is the translocation t(11;14)(q13;q32), which puts the *CCND1* gene (encoding the cell cycle regulatory protein cyclin D1) under the control of the *IGHV* (immunoglobulin heavy chain) enhancer. This leads to constitutive expression of cyclin D1. The cells thus are uncoupled from the cell cycle control. Secondary ge-

netic aberrations then transform the cell into a MCL cell. Such secondary events may be deregulation of the apoptosis machinery, the DNA damage response, further impairment of the cell cycle or activation of potentially oncogenic pathways, such as NF-κB signalling, mTOR signalling etc.[7]

The 2016 update of the WHO classification of lymphoid malignancies distinguishes between five MCL variants which arise from two pathways. B-cells with non- or minimally mutated IGHV plus expression of the transcription factor SOX11 can give rise to classical MCL (MCL cells predominantly reside in the mantle zone of lymph follicles in the lymph node), which may progress to blastoid or pleomorphic MCL. A second pathogenic pathway involves cells which have a hypermutated IGHV but do not overexpress SOX11. These cells typically reside in germinal centres and can be transported to peripheral blood, bone marrow and spleen. Despite the fact that these cells are considered genetically more stable than classical MCL cells, secondary transformations may occur which eventually lead to progression of the disease to more aggressive variants.[6]

Expression of the neural transcription factor SOX11 is unique to MCL cells. It was seen to be involved in MCL pathogenesis. Since it is not expressed in normal B-cells, it is established as an MCL biomarker.[8]

2.1.2 Diffuse large B-cell lymphoma

Diffuse large B-cell lymphoma (DLBCL) is the most common form of B-NHL and accounts for approx. 30-40% of cases.[3] Approximately 50-60% of all patients can be cured by application of immunochemotherapy. If patients develop resistances against the commonly used therapeutic agents or relapse, the outcome is poor.[9] DLBCL is a very heterogeneous disease. In 2000, Alizadeh *et al.* achieved a first breakthrough in characterizing DLBCL subgroups. The working group conducted gene expression profiling in 96 samples (normal and malignant) and found two distinct clusters. One group expressed genes which resembled activated B-cells (thus termed activated B-cell like (ABC)-DLBCL), the second group expressed genes which correspond to germinal centre B-cells (therefore termed germinal centre B-cell like (GCB)-DLBCL). Some cases could not be allocated to either subgroup and therefore remain unclassified. ABC- and GCB-DLBCL cases not only differ in their gene expression profile, patients in these two subgroups also have strikingly different prognoses, with the GCB subtype as the more favourable one.[10] In 2018, Chapuy *et al.* as well as Schmitz *et al.* took another approach to define subclasses of DLBCL cases with respect to new, more specific therapeutic options for each subgroup. In contrast to Alizadeh *et al.*, Chapuy *et al.* and Schmitz *et al.* focussed on recurrent genetic alterations. The resulting new DLBCL subgroups were defined by co-occurring genetic

aberrations. Schmitz *et al.* found four new groups: the MCD group was defined by co-occuring MYD88 and CD79B mutations; the BN2 subgroup was characterised by BCL6 fusions and NOTCH2 mutations; the N1 group was based on NOTCH1 mutations, EZH2 mutations and BCL2 translocations were found in the EZB group. With respect to progression-free survival and overall survival, it was seen that EZB and BN2 cases were more favourable than N1 and MCD cases.[11] Chapuy *et al.* defined 5 clusters (C1-C5) which were each characterized by a specific set of genetic driver mutations. This led to the identification of a new low-risk ABC-DLBCL subset and two distinct GCB-DLBCL subsets, among others.[12]

2.2 B-cells

In order to understand malignant transformations in B-NHL entities, it is important to have comprehensive knowledge about the physiological functions of B-cells, their development and signalling pathways.

2.2.1 Development

Lymphocytes, like all other peripheral blood cells, are derived from hematopoietic stem cells (HSCs). These pluripotent cells reside in the bone marrow and can give rise to any type of peripheral blood cell. HSCs develop into multipotent progenitor cells (MPPs) which then commit towards myeloid or lymphoid cells by differentiating in either common myeloid or common lymphoid progenitors (CMPs or CLPs, respectively). CLPs then can give rise to B-, T- and NK-cells which leave the bone marrow and migrate to the peripheral blood.[13]

B-cells need to undergo further maturation steps before they are fully capable of their immune functions. They carry an immature pre-B-cell receptor (BCR). In the process called V(D)J recombination, the pre-BCR matures to a fully functional BCR. The mammalian BCR is encoded by three loci: the IgH, κ and λ locus. Each locus is composed of variable (V) and joining (J) segments, the IgH locus additionally contains diversity (D) segments. Each locus contains tens to hundreds of each segment. Recombination of the V, (D) and J segments leads to diversification of the resulting BCR specificity. The recombined immunoglobulin genes can undergo additional somatic hypermutations in order to refine the BCR specificity. As a first step of V(D)J recombination, the nucleases recombination activating gene 1 and 2 (RAG1 and 2, respectively) induce double-strand breaks at recombination signal sequences (RSS) which precede each V, D or J segment. Subsequently, the DNA break is repaired which leads to recombination of the respective segments.[14]

Finally, B-cells which contain a recombined, mature BCR need to undergo quality

control to make sure that the respective B-cell does not induce an immune response upon recognizing self-antigens. Apoptosis is induced in highly self-reactive B-cells. If this step is skipped, autoimmune diseases may occur.[15]

2.2.2 Physiology

Mature B-cells mainly reside in gut-associated lymphoid tissues and in lymph follicles in lymph nodes and the spleen. Lymphocytes represent the adaptive immune system. In contrast to the innate immune system, the adaptive immune system is shaped by antigen contacts. As described above, B- and T-cell receptors are highly diverse. Upon detection of a foreign antigen, they induce an immune response. B-cells whose BCR specifically recognized the respective antigen clonally proliferate and eventually differentiate to plasma cells. Soluble antibodies specific to the respective antigen are produced and released by the plasma cells. Besides this central purpose, B-cells fulfil a plethora of other functions. They serve as antigen presenting and co-stimulatory cells to induce and regulate T-cell functions. Furthermore, B-cells produce cytokines which are involved in the regulation of other immune cell types.[16]

2.2.3 B-cell receptor signalling

Physiological B-cell receptor signalling

The BCR is a transmembrane complex which is assembled of a pair of light- and heavy-chain immunoglobulins. This complex is coupled to a heterodimer (Igα and Igβ; CD79A and CD79B, respectively) which contains immunoreceptor tyrosine-based activation motifs (ITAMs). CD79A and CD79B each contain one ITAM motif which in turn contains two tyrosine residues. Normal BCR signalling can be divided into three steps: signal initiation, propagation and integration. The initiation phase comprises all early signalling events which involve the BCR itself. During the propagation step, the signal is amplified by production of second messengers and activation of downstream signalling pathways. In the final integration phase, the upstream signalling events culminate in the alteration of gene expression by regulation of transcription factors.[17]

Binding of a ligand to the BCR initiates the BCR signalling cascade. One ligand binds to several BCR molecules and thereby cross-links them. This in turn leads to phosphorylation of the ITAMs by SRC family kinases such as Lck/Yes-Related Novel Protein Tyrosine Kinase (LYN), FYN and B lymphocyte kinase (BLK). Phosphorylation of both ITAM-tyrosine residues is necessary to create a SRC homology 2 (SH2) domain-specific binding site. Cytoplasmic tyrosine kinases which contain SH2

domains such as spleen tyrosine kinase (SYK) are recruited to this binding site and are subsequently activated.[17] With this, the signal initiation phase is completed. Next, the signal is propagated through various downstream signalling pathways.
Activated SYK recruits B-cell linker (BLNK) and SH3 domain-containing kinase-binding protein 1 (SH3KBP1) which drive the phosphorylation of Bruton's tyrosine kinase (BTK) and phospholipase C γ 2 (PLCγ2). Phosphorylated PLCγ2 hydrolyses phosphatidylinositol-4,5-bisphosphate (PI(4,5)2), resulting in diacylglycerol (DAG) and inositol triphosphate (IP3). The latter induces Ca^{2+} mobilization from intracellular Ca^{2+} stores. Elevated Ca^{2+} levels in combination with DAG activate protein kinase Cβ (PKCβ). Activated PKCβ in turn activates many signalling cascades, such as the nuclear factor κB (NF-κB) pathway via the adaptor protein caspase recruitment domain family member 11 (CARD11).[18]
Additionally, BCR signalling is enhanced by signalling of the BCR co-receptor CD19, which is activated simultaneously with the BCR. Phosphorylation of CD19 tyrosine motifs by LYN creates binding sites for Phosphatidylinositol-4,5-bisphosphate 3-kinase (PI3K).[17] PI3K activity recruits further signalling molecules such as BTK and protein kinase B (AKT), which initiates the respective downstream signalling pathways. Taken together, during the BCR signalling propagation phase the following downstream signalling pathways are activated: NF-κB, PI3K, mitogen-activated protein kinase (MAPK), nuclear factor of activated T cells (NFAT) and rat sarcoma viral oncogene (RAS) signalling.[18]
The activation of the above mentioned downstream signalling pathways eventually result in modulation of gene expression via transcription factor regulation (signal integration). Proliferation, clonal expansion, differentiation and antibody production are the final outcomes of B-cell activation and BCR signalling.[17] Figure 2.3 summarises the complexity of BCR signalling.

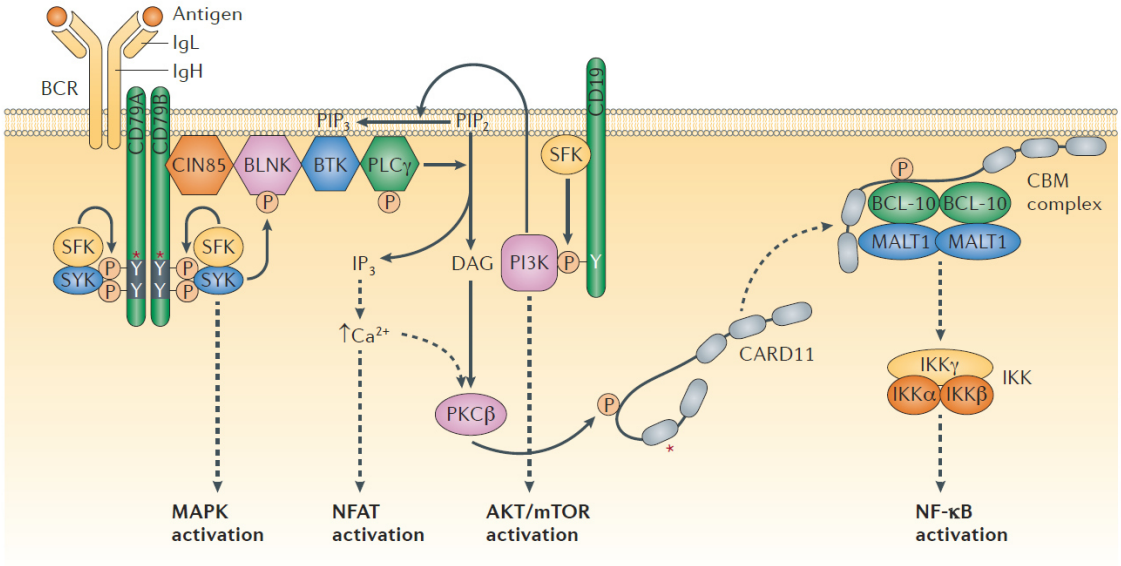

Figure 2.3: **Overview about physiological BCR signalling. Figure from[18]. Copyright obtained from Springer Nature.**

BCR signalling in DLBCL cells

BCR signalling in ABC-DLBCL cells

Activated B-cell like diffuse large B-cell lymphoma (ABC-DLBCL) cells are characterized by their dependency on NF-κB signalling. CARD11, which as part of the CARD11-BCL10-MALT1 (CBM) complex regulates NF-κB signalling activity, is mutated in approx. 10% of ABC-DLBCL cases. This mutation constitutively activates NF-κB signalling and uncouples the cells from dependency on CD79A/B. In 2010, Davis *et al.* characterized a new signalling mode in ABC-DLBCL cells which was termed "chronic active BCR signalling". This study found that CARD11 wild-type cells depend on central BCR signalling components such as BTK, which was contrary to CARD11 mutated cells. This finding linked NF-κB activation to BCR signalling. Like physiologic BCR signalling, chronic active BCR signalling activates many downstream signalling pathways (see Figure 2.4a). Importantly, in ABC-DLBCL but not in GCB-DLBCL cells, BCRs on the membrane are often found in clusters, which is reminiscent of physiological BCR signalling. This suggests the involvement of auto-antigens in the pathomechanism of chronic active BCR signalling. However, until now the involvement of auto-antigens has not been confirmed, yet.[19] Generally, there is a number of recurrent mutations in specific sites of the BCR signalling cascade which render the signalling pathway active. Two examples for this are mutations in the ITAMs of CD79A/B (mutated in 29% of ABC-DLBCL cases, but only 3% of GCB-DLBCL cases) and mutations in the BCR itself (CD79A/B), which minimises the activity of negative feedback loops.[20]

In 2018, a distinct BCR signalling mechanism in ABC-DLBCL cells was discov-

ered. It was observed that a certain subgroup of ibrutinib-sensitive ABC-DLBCL cells strongly depends on Toll-like receptor 9 (TLR9), Myeloid differentiation primary response 88 (MyD88) and the BCR itself. In physiologic B-cells, TLR9 resides in endosomes and signals via the adaptor MyD88. Upon antigen-engagement, the BCR is internalized. In certain ABC-DLBCL cells, the endosome containing the TLR9/MyD88 complex and the endosome containing the BCR fuse and form a new signalling unit. The so-called My-T-BCR complex activates PI3K and NF-κB signalling via co-localisation with mTOR complexes.[21]

BCR signalling in GCB-DLBCL cells

BCR signalling in germinal centre-like (GCB)-DLBCL cells is critically different from BCR signalling in ABC-DLBCL cells. It is described as "tonic" or "toncogenic" BCR signalling. This mode of BCR signalling was first described in Burkitt's lymphoma cells. Knockout or inhibition of SYK is toxic to GCB-DLBCL cells. Furthermore, the cells strongly depend on PI3K signalling, but in contrast to ABC-DLBCL cells, they are independent of NF-KB signalling. Deletion of antigen-binding sites in the BCR did not lead to reduced viability of the cells. It is therefore assumed that autoantigens are not involved in the pathogenesis of GCB-DLBCL cells. Overall, BCR signalling in GCB-DLBCL cells can be described as a constitutive PI3K signalling which is dependent on SYK and LYN, whereas all other downstream pathways which are characteristic for normal as well as chronic active BCR signalling are extinguished (see Figure 2.4b).[20;22]

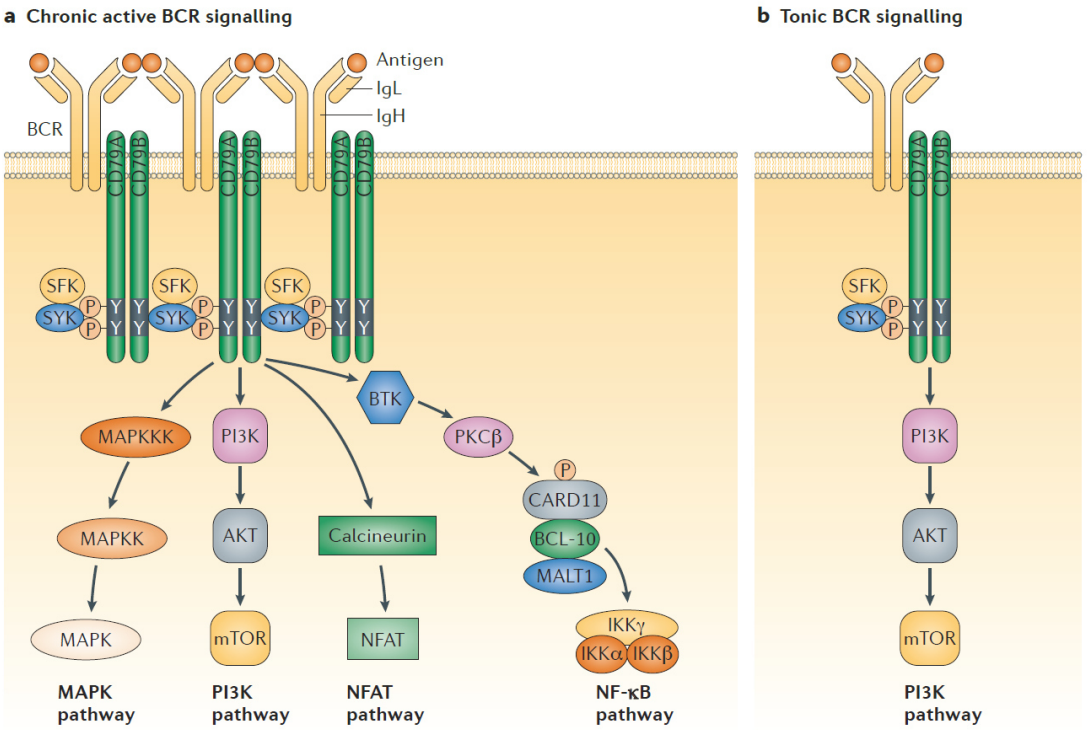

Figure 2.4: **Schematic of chronic active vs. tonic BCR signalling. Figure from[18]. Copyright obtained from Springer Nature.**

BCR signalling inhibitors

As described in section 2.2.3, B-cell Non-Hodgkin lymphoma (B-NHL) entities are dependent on BCR signalling. Thus, inhibition of BCR signalling is a promising therapeutic target.

In 2013, the first-in-class BTK inhibitor ibrutinib achieved a response rate of 68% in a phase 2 clinical trial and was subsequently approved for relapsed/refractory mantle cell lymphoma.[23] Approval for several other B-NHL entities soon followed. Ibrutinib irreversibly binds to cysteine 481 in the ATP binding pocket of BTK.[24] One of the most common mechanisms of acquired ibrutinib resistances is therefore a mutation at the C481 site which prevents ibrutinib binding and therefore keeps BTK signalling active. Other resistance mechanisms involve increased and permanent activation of pathways downstream of BTK, such as the PI3K signalling pathway.[25] A number of second-generation BTK inhibitors have been developed since the approval of ibrutinib. The major advantage of these new compounds is the lower rate of off-target effects. Currently, acalabrutinib and zanubrutinib are clinically approved for application in several B-NHL entities. Moreover, several clinical trials are ongoing in order to evaluate combination therapies including a BTK inhibitor.[24]

Besides BTK inhibition, there are other possible targets in the BCR signalling pathway. An overview about therapeutic targets in the BCR signalling pathway is de-

picted in Figure 2.5. Inhibition of SYK and PI3K has been studied in various B-NHL entities. Idelalisib was the first-in-class PI3K inhibitor, fostamatinib was the first SYK inhibitor to be clinically approved. Studies concerning possible combinations with standard chemotherapy regimens are currently ongoing. Also for SYK and PI3K inhibition, resistance mechanisms are emerging which emphasises the need for more research to restore the capacities of the respective inhibitors.[26]

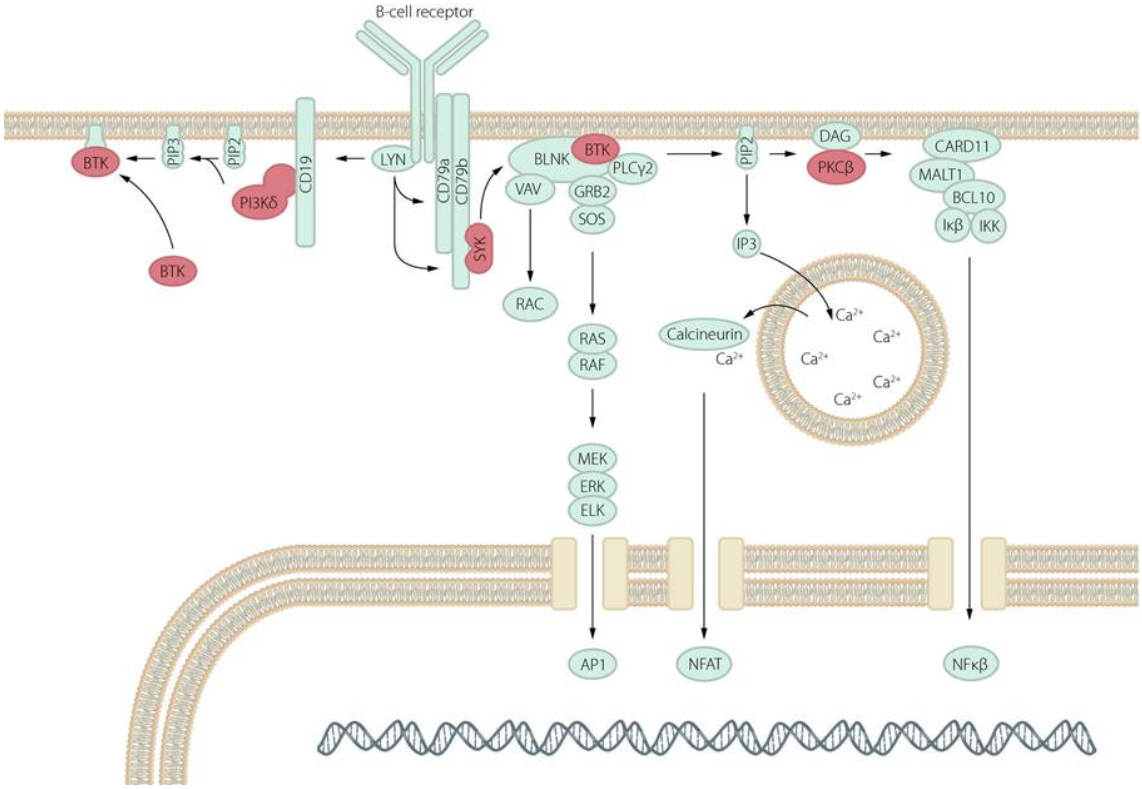

Figure 2.5: **Therapeutic targets in the BCR signalling pathway. All proteins which are depicted in red are targets for small molecule inhibitors. Figure from[27]. Copyright obtained from John Wiley and Sons.**

SASH3

This study investigates SAM and SH3 domain-containing protein 3 (SASH3; also called SH3 containing lymphocyte protein 1, SLY1) in context with BCR signalling. SASH3 is a 42 kDa protein which was first described by Beer *et al.* as a novel protein cloned from a murine T cell lymphoma library. It was seen that this protein is mainly expressed in lymphoid cells.[28] As indicated by the nomenclature, SASH3 contains a SRC homology 3 (SH3) domain and a sterile alpha motif (SAM). SH3 domains are very common motifs which can be found in a broad variety of proteins. This indicates that SH3 domains are capable of conferring many different functions.[29] Also SAM domains can be found in many different proteins, e.g. scaffolding proteins,

transcriptional and translational regulators as well as kinases.[30]
Besides the structure and the expression pattern, very little is known about SASH3. In B- and T-cells, it was seen in various studies that SASH3 plays a role in proliferation and development.[31;32;33] In contrary, in NK cells, SASH3 seems to act as a ribosomal protein. SASH3-deficient NK cells are impaired in their tumour clearance abilities[34]. Besides the SAM and SH3 domain, SASH3 contains a nuclear localization signal. This enables the protein to shuttle between cytoplasm and nucleus, most probably to enable BCR/TCR signal transduction[31;33]. By contrast, in NK cells, SASH3 is constitutively localized in the cytoplasm.[34]
SASH3 shows sequence similarity to various known signalling proteins, such as CD2-associated protein (CD2AP), tyrosine kinase MET, Casitas B-Lineage Lymphoma Proto-Oncogene (c-Cbl) and guanidine-exchange factor Vav.[28] It is therefore reasonable to consider SASH3 as a novel signalling adaptor protein.

2.3 Ubiquitin-proteasome system

2.3.1 Importance for cellular homeostasis

Regulation of protein turnover is a crucial step in cellular homeostasis. The ubiquitin-proteasome system (UPS) is responsible for targeted degradation of proteins. For proteins such as cyclins and transcription factors it is important to limit their half-lives. This ensures that pathways and cellular processes which are regulated by such proteins are only active for a limited time. Therefore, the UPS regulates a broad variety of cellular processes, such as cell cycle, development, apoptosis and signalling pathways.[35] On the other hand, the UPS is part of a cellular quality control system. Misfolded proteins are quickly tagged for proteasomal degradation in order to avoid accumulation.[36]
Deregulation of UPS components can lead to accumulation or aberrant degradation of certain proteins which promotes the development of diseases such as cancer. In haematological malignancies, a number of E3 ligases have been shown to be mutated or altered in their expression. Yang and Staudt describe a number of proteins such as A20 involved in the UPS which are specifically altered in lymphoid malignancies. These are promising new targets for targeted cancer therapy.[37]

2.3.2 The ubiquitin code

Ubiquitin is a globular 76 amino acid protein which is highly conserved from yeast to man.[35] It contains seven lysine residues which can be ubiquitinated themselves. This is the most important feature for the formation of polyubiquitin chains.[38] Ubiquitination of target proteins can occur in different patterns, which is also called the

ubiquitin code. The simplest kind of ubiquitination is the attachment of a single ubiquitin molecule to a target protein (monoubiquination). Often multiple lysine residues of a target protein are monoubiquitinated, this pattern is termed multi-monoubiquitination. Furthermore, target proteins can be tagged by polyubiquitin chains. Here, ubiquitin moieties are connected via their lysine residues (Lys6, Lys11, Lys27, Lys29, Lys33, Lys48, Lys63). Alternatively, a methionine residue (Met1) can be utilized for the formation of polyubiquitin chains. The lysine or methionine residue which is used for formation of the polyubiquitin chain determinates the topology of the resulting chain. Therefore, each of the eight linkage types has a different function (see Figure 2.6) The most prominent type is Lys48 (K48) linkage, which generates a signal for proteasomal degradation of the tagged protein. Approximately half of the polyubiquitin chains are formed via Lys48 linkage. Lys63 is the second prominent linkage type. Proteins which are Lys63 polyubiquitinated are tagged for lysosomal degradation via the autophagic pathway. Additionally, mixed linkage or branched polyubiquitin chains may occur which then modulate certain cellular pathways in a context-specific manner.[39]

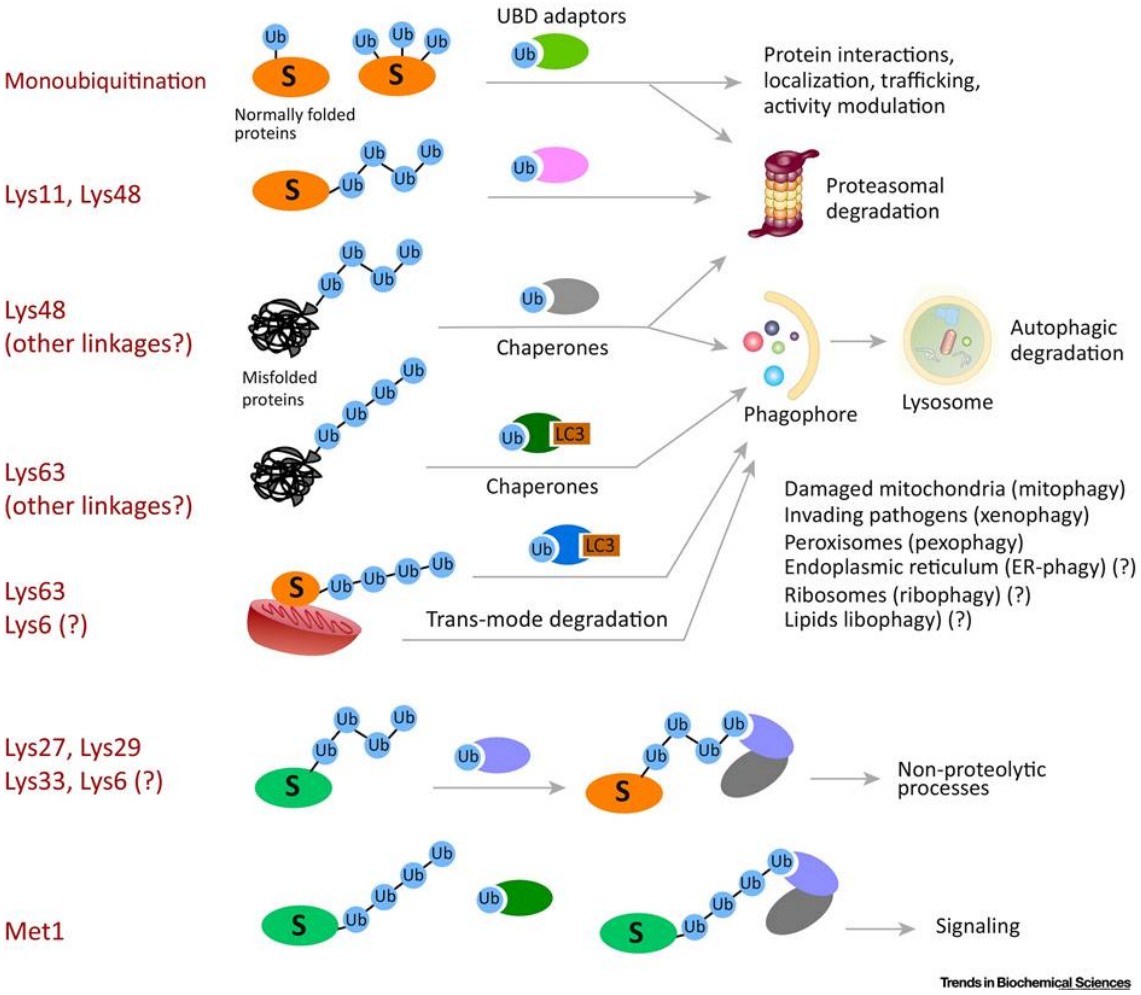

Figure 2.6: **Overview about properties and outcomes of the ubiquitin code. Figure taken from[39]. Copyright obtained from Elsevier publishing group.**

2.3.3 Ubiquitin ligases and mechanism of ubiquitination

Attachment of ubiquitin molecules to target proteins is a three-step process which is catalysed by three ubiquitin ligases (E1-3). E1 ligases activate ubiquitin in an ATP-dependent manner. The activated ubiquitin is transferred to an E2 ligase. Eventually, E3 ligases catalyse the transfer of the activated ubiquitin molecule from the E2 ligase to the target protein.[39] Only two E1 enzymes are known in mammals (UBA1 and UBA6). Approximately 40 E2 ligases and more than 600 E3 ligases have been discovered so far.[40] Substrate specificity is mediated by E2 and E3 ligases.[41] E3 ligases can be divided in three subgroups: homologous to E6-associated protein C-terminus (HECT), really interesting new gene (RING) and RING-in-between-RING (RBR) E3 ligases. RING-type E3 ligases constitute the largest subgroup with more than 600 members. Some RING E3 ligases consist of multiple subunits or are constituted of homo- or heterodimers.[40] MARCH5 is an E3 ligase which seems

to be involved in the regulation of mitochondrial morphology and intrinsic apoptosis. It is described in more detail in chapter 3.4. HECT-type E3 ligases consist of an N-terminal and a C-terminal lobe which interact with each other during the process of transferring the ubiquitin molecule to the target protein. The smallest E3 ligase family is the RBR-type family. 14 members have been discovered in the human genome so far. These proteins consist of two RING domains. Ubiquitin-loaded E2 ligases are recruited to RING1 whereas the attachment of ubiquitin to the target protein is mediated by RING2.[40]

A growing body of evidence documents a pathogenic role for E3 ligases in human cancers. The abundancy of tumour suppressors and promoters can be regulated by their targeted degradation via E3 ligases. For example, protein levels of the tumour suppressor p53 are regulated by various E3 ligases which in turn influences pathogenesis in cervical, lung, prostate, hepatocellular, breast and ovarian cancers, leukaemia, melanoma and many other tumour entities.[40]

Ubiquitination can be reversed by deubiquitinating enzymes (DUBs). Approximately 100 genes encoding DUBs are known in the human genome. DUBs can be subclassified in cysteine proteases and metalloproteinases. Dysregulation leads to aberrant protein stability and just like ubiquitin ligases DUBs thus can be involved in the pathogenesis of various diseases.[42]

2.3.4 MARCH5

MARCH5 (Membrane-Associated Ring-CH-Type Finger 5; also termed mitochondrial ubiquitin ligase, MITOL) was first described by Yonashiro *et al.* in 2006. It is a 31 kDa E3 ubiquitin ligase belonging to the RING-type family. MARCH5 is located in the mitochondrial outer membrane and comprises four transmembrane domains.[43]

Not much is known about the precise functional context of MARCH5. During the last years, MARCH5 was mainly regarded to be involved in two distinct relations: regulation of mitochondrial morphology and regulation of the intrinsic apoptotic pathway.

Mitochondria are not rigid organelles but their structure is constantly reshaped by fission and fusion cycles. It was observed that mitochondria display abnormal shapes if MARCH5 was knocked out. MARCH5 was seen to interact with dynamin-1-like protein (Drp1), the mitochondrial fission factor Fis1 and mitofusin 2 (Mfn2) which are known regulators of mitochondrial morphology.[43;44;45]

MCL1 is an anti-apoptotic BCL-2 family protein, but is also involved in the regulation of mitochondrial morphology. Recently, a potential involvement of MARCH5 in the regulation of the intrinsic apoptotic pathway was described. It was seen that be-

sides MCL-1, also NOXA was upregulated in MARCH5 depleted cells.[46;47;48] NOXA is a p53-regulated pro-apoptotic BH3 only protein. Subramanian et al. observed that MARCH5 depleted cells are sensitized towards BCL2/BCL-XL inhibition with ABT-737 and suggested a new mode of p53-independent NOXA regulation[48].
Haschka *et al.* proposed a network in which MCL-1 is ubiquitinated by MARCH5 in a NOXA-dependent manner. NOXA degradation might be dependent on additional ubiquitin ligases. However, they found both NOXA and MCL-1 to be ubiquitinated by MARCH5 in a TUBE IP.[47]
In summary, MARCH5 is involved in the following pathways:

- Protein quality control and maintenance of mitochondrial integrity: misfolded proteins (e.g. mSOD1) are recognized and ubiquitinated by MARCH5 which leads to their rapid degradation. Accumulation of misfolded proteins would otherwise lead to mitochondrial malfunction and eventually to cell death.
- Regulation of mitochondrial fission and fusion via Drp1, Mff and other factors.
- Involvement in the formation of mitochondria-ER contact sites which serve for the exchange of calcium and lipids.[49]

2.4 Apoptosis

2.4.1 Overview and common executive pathway

For tissue homeostasis and during development, it is inevitable for cells to be capable of undergoing programmed cell death. Among other mechanisms, apoptosis is one type of cell death. Once this cascade has been initiated, the cellular contents are demolished. An impressive manifestation is nuclear condensation.
To date, three major apoptosis pathways have been studied in detail: the extrinsic, the intrinsic and the granzyme B pathway (see Figure 2.7).[50] Each pathway is initiated in a unique way. Eventually, all pathways join a common executive pathway, the caspase cascade. Caspases are endoproteases which initially are present as inactive procaspases. All apoptosis pathways culminate in recruitment of initiator caspases (caspase-8, -9) which are activated by dimerisation. Executioner caspases (caspase-3, -6, -7) are then cleaved and thus activated by the initiator caspases. The executioner caspases then cleave their respective target proteins which ultimately leads to cell destruction.[51]
The extrinsic pathway is initiated by binding of a ligand such as FasL or TNFα to a membrane-bound death receptor. This leads to signal propagation into the cytoplasm where caspase-8 is recruited and self-activated (Taylor et al. 2008). The intrinsic pathway is governed by proteins of the BCL-2 family, details about this

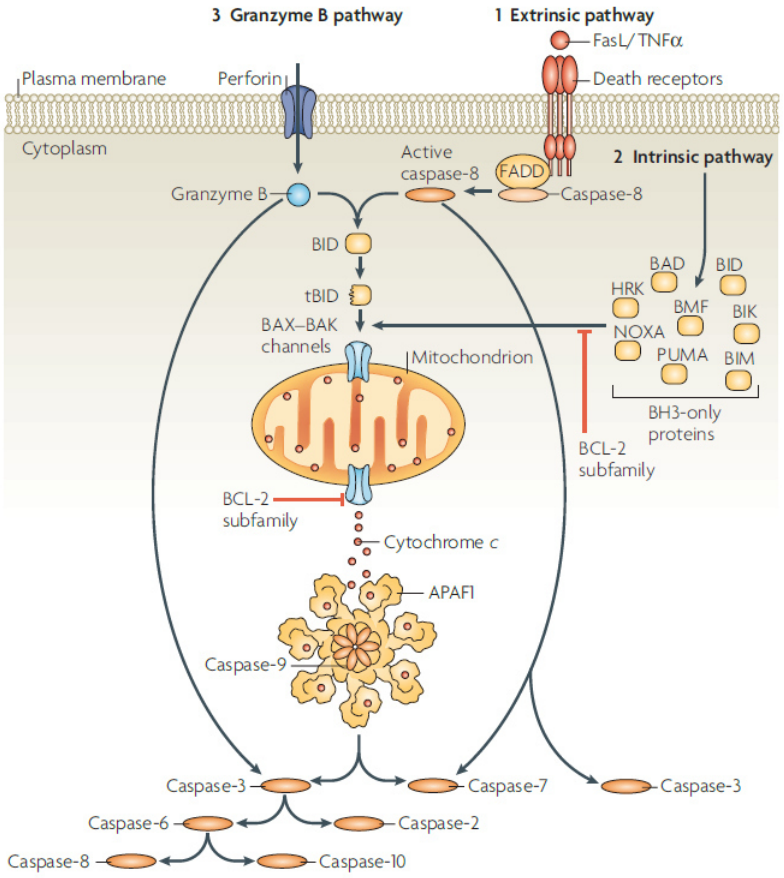

Figure 2.7: **Overview about apoptosis pathways. Figure from[50]. Copyright obtained from Springer Nature.**

pathway are described in chapter 4.2. Finally, the caspase cascade can also be activated via the granzyme B pathway. Granzyme B and perforin-containing granules are released from cytotoxic T-cells as well as NK-cells. Perforin inserts a pore into the target cell membrane, enabling the protease granzyme B to enter the cell, where it cleaves and activates caspase-3.[50]

2.4.2 Intrinsic apoptotic pathway

BCL-2 family: structure and regulation

BCL2 family members can be divided into three subclasses according to their function: pro-apoptotic, anti-apoptotic and effector proteins. All proteins are characterized by a specific pattern of BCL-2 homology (BH) domains, of which 4 are known (BH1-4). The anti-apoptotic proteins BCL-2, BCL-XL, BCL-W, MCL-1, BCL2A1 and BCL-B each contain a BH1, 2, 3 and 4 domain. The pro-apoptotic effector proteins BAX, BAK and BOK are characterized by the presence of a BH1, -2 and -3 domain but lack a BH4 domain. Finally, a third group of BCL-2 family proteins

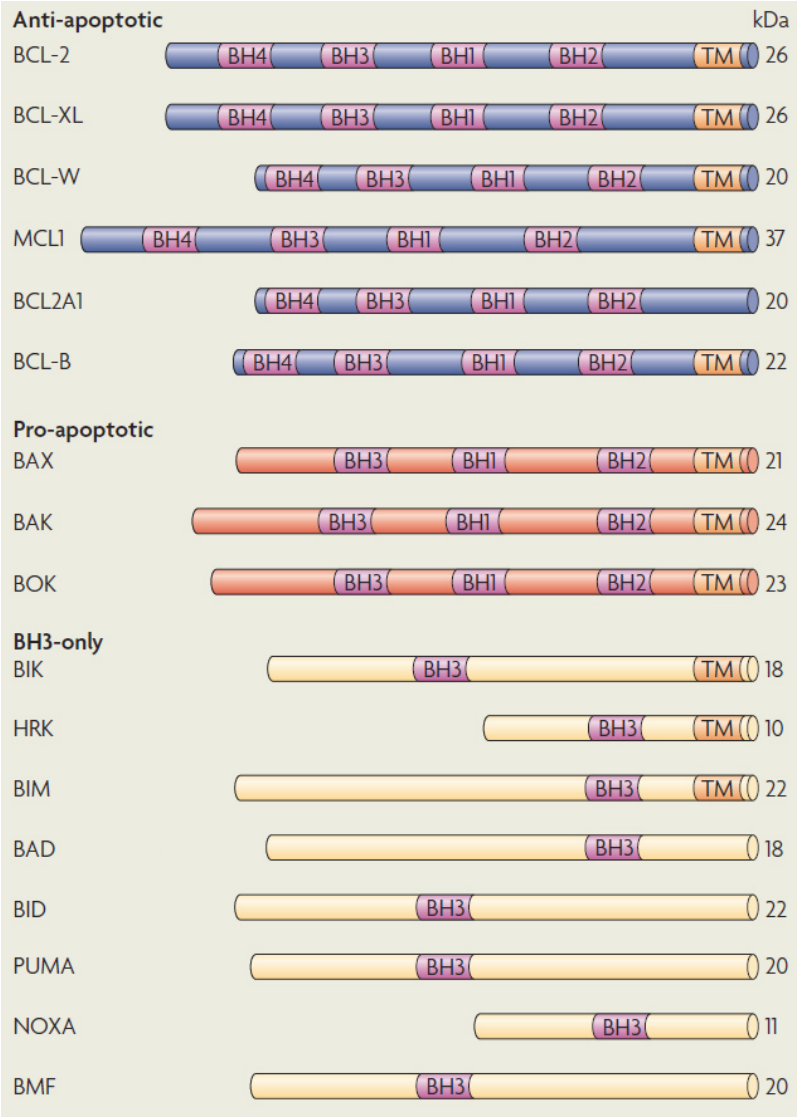

Figure 2.8: **Structure and function of BCL-2 family proteins. Figure from[50]. Copyright obtained from Springer Nature.**

is characterized by containing only a BH3 domain, thus called BH3 only proteins. These proteins (namely BIK, HRK, BIM, BAD, BID, PUMA, NOXA and BMF) possess pro-apoptotic functions but are regulated in different ways.[50] An overview about structure and function of each BCL-2 family protein is depicted in Figure 2.8.

In order to regulate the intrinsic apoptosis pathway, the BCL-2 family proteins are capable of several interactions with each other. The effector proteins BAX and BAK can be directly activated by the pro-apoptotic BCL-2 family members BIM, truncated BID (tBID) and PUMA. This can in turn be prevented via sequestration of BIM, tBID and PUMA by anti-apoptotic BCL-2 family members such as BCL-2 and MCL1. Anti-apoptotic BCL-2 family members can furthermore prevent apoptosis by direct binding and sequestration of the effector proteins BAX and BAK.[52]

Several feedback loops and redundancies make sure that a cell which is definitively designated for apoptosis cannot reverse the balance of pro-and anti-apoptotic BCL-2 family proteins and apoptosis cannot be activated inadvertently on the other hand. Cellular levels of each BCL-2 family protein contribute to a cell's susceptibility towards apoptosis. Protein levels can either be regulated on the transcriptional level or by post-transcriptional modifications such as ubiquitination. This indicates an important role for the ubiquitin-proteasome system (see chapter 2.3.[52]
As described, pro- and anti-apoptotic BCL2 family proteins need to be balanced under physiological conditions. In a healthy cell, the balance is slightly shifted towards anti-apoptotic proteins. But if the pro-apoptotic proteins barely outweigh the anti-apoptotic proteins, the cell is more susceptible to apoptosis. The cell is then primed for apoptosis. A method to determine a cell's apoptotic priming is BH3 profiling.[52]

Pathway mechanism

Pro- and anti-apoptotic BCL-2 family proteins are balanced under physiological conditions. The pro-apoptotic BH3 only proteins function as sensors for various types of cellular stress. For example, DNA damage induces p53 which in turn induces NOXA and PUMA transcription. Once the balance of pro-and anti-apoptotic BCL-2 family members has definitively shifted towards apoptosis, the signalling mechanism is activated. BAX and BAK oligomerise and insert pores into the mitochondrial outer membrane. The exact mechanism of the pore formation and the exact mode of BAK/BAK oligomerisation are still not fully elucidated. Once the mitochondrial outer membrane has been permeabilised, cytochrome c, which normally resides in the mitochondrial intermembrane space, is released into the cytoplasm. It binds to apoptotic protease activating factor 1 (APAF1). Multimeres of cytochrome c and APAF1 form the so called apoptosome, a structure which activates caspase-9 and therefore activates the common executive pathway, which is described above.[53]

Deregulation of the intrinsic apoptosis pathway in B-NHL

Resistance to apoptosis has been described as a hallmark of cancer by Hanahan and Weinberg in 2000.[54] BCL-2 was identified as a driver of resistance towards apoptosis in haematological malignancies. Follicular lymphoma (FL) is characterized by the translocation t(14;18)(q32;q21) which places *BCL2* under the control of the immunoglobulin heavy chain (*IGH*) transcriptional enhancer, which leads to constitutive overexpression of the anti-apoptotic protein BCL-2. A pathomechanistic role for BCL-2 was subsequently also found in other B-NHL subtypes, such as CLL and

DLBCL.[55]
The mode of BCL-2 overexpression differs in B-NHL subtypes. In GCB-DLBCL, it may be caused by the translocation t(14;18) whereas in ABC-DLBCL BCL-2 is upregulated by transcriptional mechanisms or copy number alterations.[56] In MCL, BCL-2 overexpression is caused by *BCL2* amplifications in most cases.[57]
Considering these aspects, BCL-2 inhibition represents a promising therapeutic strategy for B-NHL.

2.4.3 Venetoclax

Besides BCL-2 itself, other BCL-2 family members are commonly overexpressed in haematological malignancies and thus are interesting structures for novel therapeutic agents. A group of small molecules which were designed for this purpose are so called BH3 mimetics. As the name suggests, these agents function by mimicking BH3 only proteins. They directly bind to anti-apoptotic BCL-2 proteins with high affinity, thereby antagonizing them.[55]
With venetoclax, the first BCL-2-specific BH3 mimetic was available. By binding of venetoclax to BCL 2, it displaces other BH3 only proteins already bound to BCL-2 (e.g. BIM) which are then free to activate BAX and BAK or inhibit other anti-apoptotic BH3 only proteins.[58] It was approved for treatment of various haematological malignancies in 2016.[59]
Upon treatment with venetoclax, malignant cells tend to upregulate other anti-apoptotic BLC-2 proteins (mainly MCL-1 and BCL-XL) in order to circumvent induction of apoptosis. In DLBCL, additional upregulation of AKT was observed. Treatment of these cells with NVP-BEZ235, a dual PI3K/mTOR inhibitor achieved MCL-1 downregulation and re-sensitisation of venetoclax-resistant cells. In MCL, co-treatment with ibrutinib (a BTK inhibitor) is especially effective. Besides blocking BCR signalling, ibrutinib treatment leads to mobilisation of malignant cells from nodal tissues. Venetoclax has been observed to be more effective in blood than in lymph tissue. The ibrutinib-venetoclax combination therefore has a dual effect.[60] This combination was investigated in a phase II clinical trial in relapsed/refractory mantle cell lymphoma patients and showed 71% overall response rate.[61]

2.5 Aim of the study

During the last years, small molecule inhibitors in combination with standard chemotherapeutic regimens have become a valuable tool in therapy of haematological malignancies. There is a broad spectrum of potential targets and many of the compounds have achieved good responses. However, there are still cases in each entity

which do not respond to the inhibitors or develop resistances over time. This study therefore aimed to investigate cellular survival pathways such as BCR signalling and resistance towards apoptosis in order to define new potential therapeutic targets or to maximise the impact of approved inhibitors such as venetoclax.

2.5.1 MARCH5

As one of the central characteristics of cancer, resistance to apoptosis is a promising target for cancer therapy. Venetoclax, a BCL-2-specific inhibitor, has achieved good response rates and is approved for a number of haematological diseases, including mantle cell lymphoma. This study aimed to identify proteins which upon their knockout sensitise MCL cells towards venetoclax by use of a CRISPR/Cas9-based loss-of-function screen. MARCH5 was identified as such a sensitising protein. In subsequent experiments, the role of MARCH5 in the regulation of intrinsic apoptosis was supposed to be examined in more detail, e.g. by use of mass spectrometry-based experiments.

2.5.2 SASH3

In order to shed more light on differences between BCR signalling in ABC- and GCB-DLBCL cells, genes with differential essentiality for these two entities were supposed to be defined. For this, data from a a CRISPR/Cas9-based loss-of-function screen which was conducted in a collaborating laboratory, were analysed. SASH3 depletion was found to be of differential toxicity for ABC- and GCB-DLBCL cell lines. Since SASH3 is described as a potential signalling adapter protein, a possible connection to BCR signalling was examined in subsequent analyses.

3 Material and methods

3.1 Cell culture

3.1.1 General cell culture methods

For this study, three human MCL cell lines and five human DLBCL cell lines were used, which are detailed in table 3.1.

Table 3.1: **Cell lines used for this study**

Disease	Cell line	Reference
MCL	Jeko-1	[62]
	Maver-1	[63]
	Mino	[64]
ABC-DLCBL	TMD8	[65]
	Riva	[66]
GCB-DLBCL	DOHH2	[67]
	SU-DHL-5	[68]
	WSU-DLCL2	[69]

All cell lines were engineered to stably express Cas9 by the Staudt laboratory (NIH, Bethesda, USA). Single cell cloning and validation of Cas9 activity was conducted in this collaborating laboratory, as well. Cell line identity was authenticated by STR profiling upon first cultivation in the Oellerich laboratory. The cells were regularly tested for mycoplasma contamination using a PCR protocol published by Uphoff and Drexler.[70]

DLBCL and mantle cell lymphoma cell lines were cultured in Advanced RPMI (Cat. No. 12633020, Thermo Fisher Scientific, Waltham, MA, USA) supplemented with 5% heat-inactivated fetal calf serum (FCS; Cat. No. 7524, Sigma Aldrich, St. Louis, MO, USA) and 2 mM L-glutamine (Cat. No. 25030123, Thermo Fisher Scientific, Waltham, MA, USA). Cells were splitted three times per week to maintain a cell density of approx. $0.3x10^6$ cells/ml.

HEK293T cells were cultured in Dulbecco's Modified Eagle Medium (DMEM; Cat. No. 41965062, Thermo Fisher Scientific, Waltham, MA, USA) supplemented with 10% heat-inactivated FCS and 2 mM L-glutamine. The cells were splitted three times per week to maintain <80% confluency.

All cells were kept at 37°C in a humidified milieu containing 5% CO2 (HeraCell 240i incubator, Thermo Fisher Scientific, Waltham, MA, USA).

3.1.2 Cell viability assay (MTT assay)

In order to monitor sensitivity of a cell line towards an inhibitor, a 96-well approach was used. Here, cells were incubated with various concentrations of a certain inhibitor for four days. Subsequently, a tetrazolium salt was added and metabolised to a purple metabolite by viable cells. Intensity of the purple colour was proportional to the percentage of viable cells.

In detail, the optimal number of cells per well was individually determined for each cell line in a separate approach in advance. The respective number of cells in 50 µl complete medium was added to each well of a 96-well microtiter plate. The specific inhibitor, venetoclax (Cat. No. HY15532-5mg, MedChemExpress, Monmouth Junction NJ, USA) was diluted separately. For this, the range of desired concentrations to be tested was determined first. Venetoclax was tested in a range of 0.61 nM – 10 μM. First, the inhibitor was diluted in complete medium to a concentration of 20 μM. Subsequently, serial 1:4 dilutions were performed, resulting in complete media samples containing 20 μM – 1.2 nM venetoclax, respectively. Additionally, complete medium containing DMSO was prepared. 50 μl of each dilution were added to the cells, resulting in a 1:2 in-well dilution which finally resulted in the desired dilution range of 10 μM – 0.61 nM. Each dilution was tested in triplicates. Additionally, a blank sample was prepared. For this, 100 μl complete medium were added to three wells which did not contain cells. The plate was incubated for four days at 37°C in the cell culture incubator. On day four, 25 μl 3-(4,5-Dimethyl-2-thiazolyl)-2,5-diphenyl-2H-tetrazoliumbromid (MTT) solution (2 g/l MTT (Cat. No. 20395.03, Serva, Heidelberg, Germany)) in DPBS (Cat. No. 14190-094, Thermo Fisher Scientific, Waltham, MA, USA) were added to each well and incubated for 4 h at 37°C. During this time, viable cells metabolized the yellowish water-soluble tetrazolium salt MTT to water-insoluble purple formazan. The intensity of the purple metabolite was proportional to the percentage of viable cells. Cells were lysed by addition of 100 μl stopping solution (25% (w/v) SDS (Cat. No. 2326.3), 50% N,N-Dimethylformamide (Cat. No. T921.1, both Roth, Karlsruhe, Germany), pH 4.5) per well. The plate was further incubated at 37°C. The following day, the samples were analysed using a plate reader device (Infinite M200 Pro, Tecan, Männedorf, Switzerland). Here, dual wavelength measurement with λ=560 nm as measurement wavelength (A_{560}) and λ=620 nm (A_{620}) as reference wavelength was performed. Viability was calculated as follows: first, the difference between A_{560} and A_{620} was

calculated which served for background correction. Secondly, the mean of the corrected absorbance values for each triplicate was calculated. Blank correction was conducted by subtracting the mean blank absorbance value from each mean sample value. Finally, the percentage of viable cells was calculated by normalisation of blank corrected sample values on the mean blank corrected absorbance value of DMSO-treated cells. Mean inhibitory concentrations (IC_{50}) were calculated using the online tool Quest Graph^{TM} IC_{50} Calculator (AAT Bioquest, Inc., Sunnyvale, CA, USA).

3.2 Bacterial culture and manipulation

3.2.1 Transformation

E. coli Stbl3 are engineered to easily incorporate DNA using the heat shock method. For this, 60 μl bacterial suspension were thawed on ice and subsequently incubated with 100 ng of the respective plasmid DNA or the ligation mix for 30 min. A heat shock (42°C, 30 sec) caused the formation of temporary pores in the bacterial cell wall which allowed influx of plasmid DNA into the bacterial cell. The samples were incubated on ice for 2 min. Subsequently, 300 μl S.O.C. medium (complex bacterial growth medium which allows maximum transformation efficiency; Cat. No. 15544-034, Thermo Fisher Scientific, Waltham, MA, USA) were added and the bacterial cell suspension was incubated at 37°C in an Eppendorf thermomixer while shaking at 700 rpm. For re-transformations, 50 μl bacterial suspension were subsequently plated on LB agar plates containing 100 μg/ml ampicillin (LB Amp plates). For transformations in the course of plasmid cloning, the bacterial suspension was centrifuged after incubation. Most of the supernatant was removed, the cells were resuspended in the remaining medium and subsequently plated on LB Amp plates. The plates were incubated at 37°C overnight. Only bacterial cells which incorporated the respective plasmid coding for an ampicillin resistance would grow on the LB agar containing ampicillin.

3.2.2 Mini preparation

4 ml LB medium containing 100 μg/ml ampicillin (LB Amp medium) were inoculated with a single colony and incubated at 37°C while shaking at 200 rpm in a bacterial shaker for approx. 16 h. On the next day, plasmid DNA was isolated from the bacteria using the GeneJET Plasmid Miniprep kit (Cat. No. K0503, Thermo Fisher Scientific, Waltham, MA, USA) according to the manufacturer's instructions. Here, bacterial cells were harvested, lysed and the lysate was applied to a silica membrane-based spin column which bound plasmid DNA. After washing of

the DNA, it was eluted from the membrane with ddH_2O. Plasmid DNA concentration was determined using a spectral photometer (NanoDrop 2000C, Thermo Fisher Scientific, Waltham, MA, USA).

3.2.3 Midi preparation

In order to purify plasmid DNA in a larger scale, 4 ml LB Amp medium were inoculated with a single bacterial colony and incubated at 37°C while shaking at 200 rpm in a bacterial shaker for approx. 6-8 h (starter culture). 200 ml LB Amp medium were then inoculated with the starter culture and incubated at 37°C while shaking at 200 rpm overnight. On the next day, plasmid DNA was purified from the bacteria using the NucleoBond Xtra Midi Plus EF kit (Cat. No. 740422.5, Macherey-Nagel, Düren, Germany) according to the manufacturer's instructions. Shortly, the bacteria were harvested and lysed. The lysate was applied to a silica-membrane based column which bound plasmid DNA. After washing, the plasmid DNA was eluted from the membrane. For desalting and concentration, the plasmid DNA contained in the eluate was bound to a syringe filter supplied with the kit. After washing, plasmid DNA was eluted from the filter with ddH_2O. Plasmid DNA concentration was determined using the NanoDrop 2000C.

3.3 Protein biochemical methods

3.3.1 Western blotting

Cells were treated as described in the respective section. Subsequently, cells were harvested, washed twice with DPBS and lysed with NP40 lysis buffer (50 mM Tris-HCl pH 7.5-7.8, 150 mM NaCl, 0.5% NP-40, 5 mM NaF, 1 mM Na_3VO_4, 1x cOmplete protease inhibitor (Cat. No. 5056489001, Merck, Darmstadt, Germany)). After incubation on ice for 10 min, the lysate was clarified by centrifugation for 10 min at 21,000xg, 4°C.

Protein concentration was determined via BCA analysis. In this assay, Cu^{2+} ions supplied to the reaction with the reagent are reduced to Cu^{+} ions by proteins. In a consecutive reaction, Cu^{+} ions are chelated by bicinchoninic acid (BCA) which is also supplied with the reagent, resulting in a colour shift of the reaction from green to purple. Colour intensity is proportional to the amount of Cu^{+} ions available for chelation and therefore proportional to protein concentration in the sample. The coloured complex specifically absorbs light at λ=562 nm.[71] To set up the reaction, the lysate was diluted 1:10 with NP40 lysis buffer. 10 μl lysate dilution and 200 μl BCA reagent (Pierce BCA protein assay, Cat. No. 23225, Thermo Fisher Scientific, Waltham, MA, USA; reagent A and B mixed 50+1) were mixed and incubated for

30 min at 37°C. Absorption was measured at λ=562 nm (A_{562}) using a plate reader device (Infinite M200 Pro, Tecan, Männedorf, Switzerland). Seven protein standard concentrations ranging from 125 to 2,000 μg/ml as well as a blank sample were simultaneously measured with every series of samples. After subtraction of the blank value, absorption was plotted against the protein concentration of the standards. The equation of the resulting linear regression curve was used to calculate the protein concentration of the samples using the respective blank-corrected A_{562} values. For the preparation of Western blot samples, the protein amount indicated in the respective chapter was supplemented with 4x Laemmli buffer (Cat. No. 1610747, Bio-Rad, Hercules, CA, USA) and NP40 lysis buffer to make a final volume of 20 μl and a final concentration of 1x Laemmli buffer. The samples were boiled for 5 min at 95°C and subsequently applied to SDS-PAGE (see table 3.2 for gel composition). Here, proteins were separated according to their size. For size-determination of the resulting bands, pre-stained protein markers were applied to the gel (Precision Plus Protein^{TM} Dual Colour Standards, Cat. No. 1610375 and Precision Plus Protein^{TM} All Blue Prestained Protein Standards, Cat. No. 1610393, both Bio-Rad, Hercules, CA, USA). When separation was completed, proteins were transferred to a nitrocellulose membrane (0.45 μm pore size; Cat. No. 162-0115, Bio-Rad, Hercules, CA; USA) using the wet blot technique at 70 V for 2 h.

Table 3.2: **Composition of gels for SDS-PAGE**

	ddH_2O	**30% Acrylamide solution**	**Buffer**	**TMED**	**10% APS**
Resolving Gel (14%)	2.05 ml	3.5 ml	1.9 ml	75 µl	6 µl
Stacking Gel (6%)	2.7 ml	0.85 ml	1.3 ml	62.5 µl	6.3 µl

The buffers used for SDS-PAGE were composed as follows:

- *Electrophoresis Buffer*: 1x TGS buffer (25 mM Tris, 192 mM glycine, 0.1% SDS, pH 8.3; Cat. No. 1610772, Bio-Rad, Hercules, CA, USA) in water
- *Transfer Buffer*: 1x TG buffer (25 mM Tris, 1.92 M glycine, pH 8.3; Cat. No. 1610771, Bio-Rad, Hercules, CA; USA) + 20% methanol in water
- *Resolving gel buffer*: 0.4% SDS, 1.5 M Tris-HCl, pH 8.8
- *Stacking gel buffer*: 0.4% SDS, 0.5 M Tris-HCl, pH 6.8

- *TBST*: 50 mM Tris pH 8.0, 200 mM NaCl, 0.1% Tween 20

When transfer was completed, the membrane's unspecific binding sites were blocked by incubation with either 5% non-fatty dry milk (Cat. No. T145.2, Roth, Karlsruhe, Germany)/TBST or for phospho-specific antibodies in 5% bovine serum albumine (BSA; Cat. No. A6588.010; AppliChem, Darmstadt, Germany)/TBST for 1 h at room temperature.

All primary antibodies were diluted in 5% BSA/TBST. Incubation with the primary antibody was con-ducted at 4°C overnight while shaking. All primary antibodies used for this study are detailed in table 3.3.

Table 3.3: **Western blotting antibodies used for this study**

Target	**Clone**	**Species**	**Manuf.**	**Cat. No.**	**Dilution**
A. aeolicus BPL/BioID2	SS 3A5-E2	Mouse	Novus	NBP2-59941	1:500
BCL-2	124	Mouse	CST	15071	1:1000
ß-Actin	8H10D10	Mouse	CST	3700	1:1000
Caspase 3	*	Rabbit	CST	9662	1:1000
Cleaved Caspase 3		Rabbit	CST	9661	1:1000
Cleaved PARP	19F4	Mouse	CST	9546	1:1000
MARCH5	*	Rabbit	CST	19168	1:1000
MCL-1	D2W9E	Rabbit	CST	94296	1:1000
NOXA	114C307.1	Mouse	Enzo	ALX-804-408-C100	1:500

Novus: Novus Biologicals; Centennial, CO, USA
CST: Cell Signaling Technologies; Danvers, MA, USA
Enzo: Enzo Biochem Inc; Farmingdale, NY USA
* Polyclonal antibody

For detection, non-bound primary antibodies were removed by washing of the membrane three times with TBST for 5 min each. Subsequently, a horseradish-peroxidase (HRP)-coupled secondary antibody was applied to the membrane at a dilution of 1:10,000 in 0.5% BSA/TBST for one hour at room temperature. Goat-anti-rabbit-HRP (Cat. No. 111-036-003) was used for detection of primary antibodies raised in rabbit, whereas goat-anti-mouse-HRP (Cat. No. 115-036-003, both Dianova, Hamburg, Germany) was used for primary antibodies which were raised in mouse. Non-bound secondary antibodies were removed by washing of the membrane in 0.1% TBST for 3 x 5 min. For detection, equal volumes of the two components of the detection reagent (SuperSignal^{TM} West Femto Maximum Sensitivity Substrate; Cat. No. 34096, Thermo Fisher Scientific, Waltham, MA, USA) were mixed and

applied to the membrane. A chemiluminescent signal was generated by catalysation of the substrate by the secondary antibody-bound HRP. The signal was detected using the ChemiDoc^{TM} Imaging System (Bio-Rad, Hercules, CA, USA).

3.4 Mass spectrometry experiments

3.4.1 SILAC labelling

SILAC labelling (Stable Isotope Labelling of Amino Acids by Cell Culture) was first described in 2002.[72] It is accepted as one of the most accurate methods for quantitative mass spectrometry (MS) analysis. The cells were expanded in a cell culture medium containing either the natural ("light") isotopes of lysine and arginine or their respective heavier isotopes ("medium", "heavy"). See table 3.4 for the isotopes used in the respective conditions. During their cultivation in the respective medium (at least five cell doublings), the whole proteome was metabolically labelled with the respective lysine and arginine isotopes. The cells were then treated differentially. For interactome analyses, equal numbers of cells were mixes and lysed after treatment. For analysis of the ubiquitinome or phosphoproteome, the cells were lysed individually. After determination of the protein concentration, equal amounts of protein of corresponding samples were mixed. Mixing of the corresponding cells or samples crucially minimizes experimental bias since all conditions could be further treated as one sample.[73] During MS analysis, arginine and lysine isotopes of each peptide were annotated. Data were de-convoluted by assigning the results to the respective treatment conditions.

SILAC medium was composed as follows: RPMI SILAC medium (Cat. No. 283001300), 10% heat-inactivated dialyzed fetal calf serum (dFCS; Cat. No. 281001200, both Silantes, Munich, Germany), 2 mM L-Glutamine (Silantes, supplied with SILAC medium), 100 units/ml Penicillin, 100 µg/ml Steptomycin (Pen-Strep; Cat. No. 15140163, Thermo Fisher Scientific, Waltham, MA, USA).
In order to prevent arginine-to-proline conversion, which would complicate quantitation, proline was added to light, medium and heavy medium in excess (1.9 mM).

Table 3.4: **SILAC amino acids**

SILAC term	**Amino acid**	**Chem. formula**	**Manuf.**	**Cat. No.**	**Final conc. [mM]**
	L-Proline	$C^{12}{}_6H_9N^{14}O_2$	Roth	1713.2	1.9
Light	L-Arginine	$C^{12}{}_6H_{14}N^{14}{}_4O_2$	Sigma	A5006	0.126
	L-Lysine	$C^{12}{}_6H_{14}N^{14}{}_2O_2$	Sigma	L5751	0.302
Medium	L-Arginine +6	$C^{13}{}_6H_{14}N^{14}{}_4O_2$	Cambridge	CLM-2265	0.127
	L-Lysine +4	$C^{12}{}_6H_{10}D_4N^{14}{}_2O_2$	Cambridge	DLM-2640	0.306
Heavy	L-Arginine +10	$C^{13}{}_6H_{14}N^{14}{}_2N^{15}{}_2O_2$	Cambridge	CNLM-539	0.127
	L-Lysine +8	$C^{13}{}_6H_{14}N^{15}{}_2O_2$	Cambridge	CNML-291	0.3

Roth: Roth, Karlsruhe, Germany
Sigma: Sigma-Aldrich, St. Louis, MO, USA
Cambridge: Cambridge Isotope Laboratories/Eurisotop, Tewksbury, MA, USA

3.4.2 Interactome

Identification of interactors of a protein of interest was conducted using the BioID2 technique in combination with MS analysis of candidate proteins. The bait protein (protein of interest) was fused to a promiscuous bacterial biotin ligase (BioID2) and expressed in target cells. Two versions of the fusion protein were expressed in the cells in distinct experiments: biotin ligase fused to either the N-terminus or the C-terminus of the bait protein. All proteins which came into close proximity of the bait protein ($\leq$ 10 nm) were biotinylated by the biotin ligase. After treatment, the cells were lysed and biotinylated proteins were enriched using streptavidin-coated beads. Enriched proteins were eluted from the beads and analysed by MS. An overview about the BioID2 technique is depicted in figure 3.1.
In order to reveal unspecifically biotinylated proteins, an empty construct containing the biotin ligase but no bait protein, was included in the experiment. For each candidate protein identified both in fusion protein-expressing cells and in empty vector-expressing cells, a BioID2 ratio was calculated as follows:

$$BioID2\ ratio = log2\ \frac{Fusion\ protein}{Empty\ vector}$$

Only candidate proteins displaying BioID2 ratios $\geq$1 were of potential interest. It is important to keep in mind that biotinylated proteins were not necessarily direct interaction partners of the bait protein. Also indirectly interacting proteins and non-interacting proteins which were in close proximity to the bait protein were

biotinylated. Therefore, the results need careful evaluation and validation.[74]

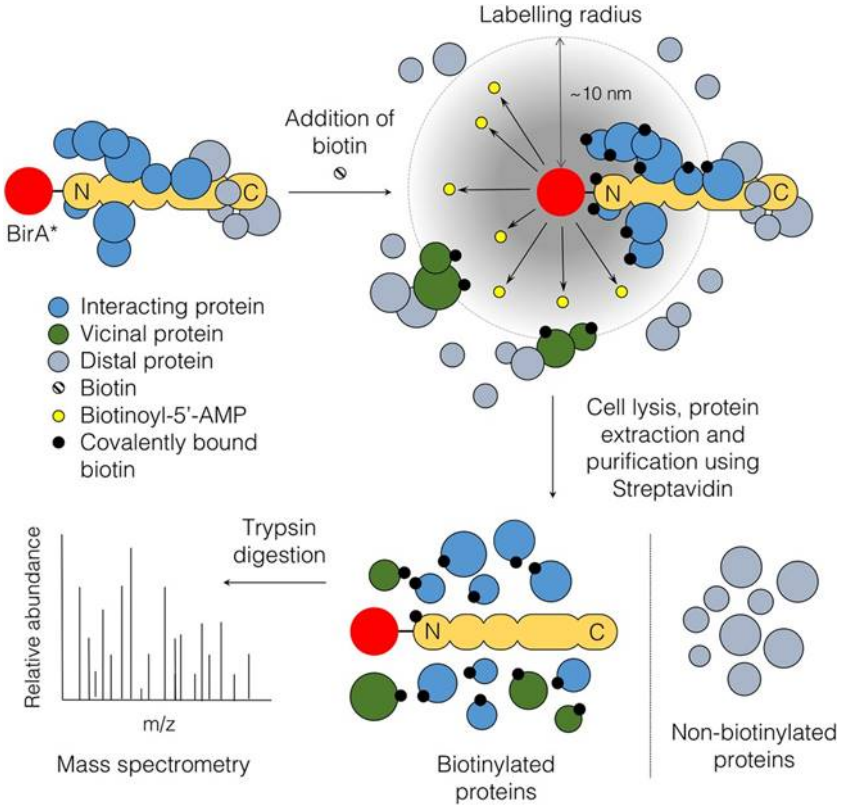

Figure 3.1: **Overview about interactome analysis using the BioID2 method.** BirA* = biotin ligase. This figure exemplarily depicts an N-terminally fused bait protein. The principle in C-terminally fused proteins is identical. Figure from[75]. Copyright obtained from John Wiley and Sons.

Cloning of BioID2 constructs

RNA isolation and reverse transcription

5x10^6 TMD8 (for cloning of SASH3 constructs) or Maver-1 (for cloning of MARCH5 constructs) cells were harvested and washed twice with DPBS. RNA isolation was conducted using the RNeasy Mini Kit (Cat. No. 74106, Qiagen, Venlo, Netherlands) according to the manufacturer's instructions. Here, cells were lysed and the lysate was applied to a silica-membrane based spin column which bound RNA. An on-column DNAse-digest was conducted using an RNase-free DNase set (Cat. No. 9254, Qiagen, Venlo, Netherlands). Subsequently, RNA was washed with an ethanol containing wash buffer and eluted from the membrane using DNase-/RNase-free ddH_2O (UltraPureTM Distilled Water, Cat. No. 10977-035, Thermo Fisher Scientific, Waltham, MA, USA). RNA content of each sample was determined using a spectral photometer (NanoDrop 2000C, Thermo Fisher Scientific, Waltham, MA, USA). RNA was stored at -80°C until further use.

Since RNA is highly susceptible to degradation, reverse transcription to DNA (copy-

DNA, cDNA) was conducted utilizing the RevertAid H Minus First strand cDNA synthesis kit (Cat. No. K1632, Thermo Fisher Scientific, Waltham, MA, USA). A volume corresponding to 250 ng purified RNA was adjusted to 11 μl with DNase-/ RNase-free ddH_2O. 1 μl random primer was added and incubated with the RNA for 5 min at 65°C. Subsequently, the reaction mix (see table 3.5) was added and mixed well. A no-template control was processed simultaneously.

Table 3.5: **Reaction mix for reverse transcription**

Component	**Volume per reaction [µl]**
5x Reaction buffer	4
RiboLock RNase inhibitor (20 U/µl)	1
RevertAid H Minus M-MuLV RT (200 U/ml)	1
10 mM dNTPs	2

Reverse transcription was conducted in a thermal cycler (T100 Thermal Cycler, Bio-Rad, Hercules, CA, USA) according to the following program:

Table 3.6: **PCR program for reverse transcription**

Step	**Temperature [°C]**	**Duration [min]**
Annealing	25	5
Synthesis	42	60
Heat-inactivation	70	5

Cloning process

By using protein of interest-specific primers which comprise a restriction enzyme motif, ligation into the likewise restriction digested BioID2 vector was enabled.
Cloning of C-terminally fused SASH3 BioID2 constructs was complicated by the presence of a BamHI restriction site in the SASH3 coding sequence. Therefore, the BioID2 vector was restriction digested with BamHI while the PCR product was restriction digested with BglII which maintains the SASH3 coding sequence integrity and produces BamHI-compatible overhangs.
In table 3.7 all primers used for cloning of BioID2 constructs with the C- or N-terminally fused protein of interest are detailed. Primers were synthesised by Sigma-Aldrich, St. Louis, MO, USA.

Table 3.7: **Primers used for cloning C- and N-terminal protein of interest fusion proteins**

Construct	Primer name	Sequence
N-terminal	MARCH5 SnaBI for	TTAGCATACGTAATGCCGGACCAAGCC
	MARCH5 XhoI rev	ATAGGCCTCGAGTTATGCTTCTTCTTG-TTCTGGATAATTCAG
	SASH3 SnaBI for	TTAGCATACGTAATGCTGCGCC-GCAAGCCCTC
	SASH3 XhoI rev	ATAGGCCTCGAGTCAAGGTGCC-CCGGCCAGGG
C-terminal	MARCH5 BamHI for	AATAAGGGATCCGCCACCATGCCGG-ACCAAGCC
	MARCH5 SnaBI rev	TTAGCATACGTATGCTTCTTCTTGT-TCTGGATAATTCAG
	SASH3 BglII for	AATAAGAGATCTGCCACCATGCTGC-GCCGCAAGCCCTC
	SASH3 SnaBI rev	TTAGCATACGTAAGGTGCCCCGGCC-AGGGAGA

Green: random nucleotides which stabilize binding of the restriction enzyme to the DNA

Red: restriction site

Underlined: Kozak sequence, enhances translation initiation.

The following PCR reaction was prepared twice per construct:

Table 3.8: **PCR reaction for cloning of C- and N-terminally fused BioID2 constructs**

Component	**Manufacturer**	**Cat. No.**	**Volume for 1x reaction**
5x Q5^{TM} reaction buffer	NEB	B9027S	10 μl
10 mM dNTPs	Thermo Fisher	R0193	1 μl
10 μM forward Primer 10 μM			2.5 μl
10 μM reverse Primer 10 μM			2.5 μl
Q5^{TM}TM High Fidelity Polymerase	NEB	M0491L	0.5 μl
DNase-free ddH_2O	Thermo Fisher	10977-035	28.5 μl

NEB: New England Biolabs, Ipswich, MA, USA
Thermo Fisher: Thermo Fisher Scientific, Waltham, MA, USA

5 μl cDNA were added to one tube, 5 μl H_2O were added to the second tube which served as H_2O control. The PCR (program see table 3.9) was subsequently run in a thermal cycler (T100 Thermal Cycler, Bio-Rad, Hercules, CA, USA). Importantly, the samples had to be put in the pre-heated machine (Hot-Start PCR).

Table 3.9: **PCR program for cloning of BioID2 constructs**

Step	**Temperature**	**Time**	
Pre-heat	98°C	15 sec	
Initial denaturation	98°C	30 sec	
Denaturation	98°C	10 sec	35 cycles
Annealing	69°C	30 sec	
Elongation	72°C	1 min	
Final elongation	72°C	2 min	
Storage	4-10°C		

After completion of the PCR program, the PCR product was applied to a 1.5% agarose/TAE gel. The bands at approx. 0.9 kb were excised and DNA was purified using the QIAquick gel extraction kit (Cat. No. 28706, Qiagen, Venlo, Netherlands). Subsequently, the respective empty BioID2 vector (N- and C-terminal fusion construct) or the purified PCR product were restriction digested at 37°C overnight according to table 3.10 and table 3.11 .

The restriction-digested vectors were dephosphorylated by addition of 2.5 μl rSAP (Cat. No. M0371, New England Biolabs, Ipswich, MA, USA) and incubation at

Table 3.10: **Restriction digestion reaction for C- and N-terminal BioID2 fusion constructs**

Component	Amount
Empty N-terminal vector OR	2 μg
Purified PCR product	Whole eluate
10x CutSmart Buffer	1x
Restriction enzyme 1	10 units
Restriction enzyme 2	10 units
DNase-free ddH_2O	Add 50 μl

Table 3.11: **Restriction enzymes for cloning of C- and N-terminal MARCH5 or SASH3 BioID2 fusion constructs**

Construct	Restriction enzyme 1	Restriction enzyme 2
N-terminal	SnaBI (Cat. No. R0130S)	XhoI (Cat. No. R0146S)
C-terminal	BamHI (Cat. No. R0136S)	SnaBI

All restriction enzymes obtained from New England Biolabs, Ipswich, MA, USA

37°C for 30 min. All samples were subjected to heat-inactivation of the restriction enzymes at 80°C for 20 min. Subsequently, buffers and inactivated restriction enzymes were removed from the reaction by using a PCR Purification kit (Cat. No. 25106, Qiagen, Venlo, Netherlands). This kit utilised a silica membrane-based spin column which binds DNA and allows washing, before it is eluted with ddH_2O. The restriction-digested and purified vectors and inserts were ligated for 3 h at room temperature according to the scheme detailed in table 3.12.

Table 3.12: **Ligation reaction for cloning of BioID2 constructs**

Component	1:3	1:5	H_2O-control
ddH_2O	13 μl	11 μl	16 μl
Empty vector	1 μl	1 μl	1 μl
Insert	3 μl	5 μl	-
T4 Ligase Buffer (supplied with T4 ligase)	2 μl	2 μl	2 μl
T4 Ligase (Cat. No. M0202L, New England Biolabs, Ipswich, MA, USA)	1 μl	1 μl	1 μl

Subsequently, the ligation reaction was transformed in *E. coli* Stbl3 and plated on LB Amp agar plates as described in section 3.2.1. The next day, mini preparations were prepared as described in section 3.2.2. Multiple clones were picked per construct. Before the plasmids were sent for sequencing, a screen for successfully cloned plasmids was performed using a test restriction digest. For this, a sample

of each purified clone was restriction digested. The restriction enzymes were chosen in order to reveal differential band pattern for empty vectors and successfully cloned constructs. Only clones which displayed the expected band pattern on an agarose/TAE gel were sent for Sanger sequencing. Midi preparations were prepared from one correct clone per construct (see section 3.2.3).

Retroviral transduction of target cells with BioID2 constructs

Approx. 16-20 h prior to transfection, 3x10^6 HEK293T cells were seeded in 10 ml complete medium per 10 cm dish.
For this method, the target cells were transduced with gibbon ape leukaemia virus (GALV)-pseudotyped retroviral particles. Per reaction, 1 μg pHIT60 (encodes retroviral gag/pol), 1 μg GALV full length vector and 4 μg of the respective BioID2 construct were added to 800 μl reduced serum medium (OptiMEMTM; Cat. No. 31985070, Thermo Fisher Scientific, Waltham, MA, USA). After mixing, 18 μl TransIT293 transfection reagent (Cat. No. MIR2705, MoBiTec, Göttingen, Germany) were added. The mixture was incubated at room temperature for 15-30 min during which the DNA was complexed by the transfection reagent in order to enable uptake by the HEK293T cells. HEK293T cells underwent a medium exchange before the transfection mixture was added dropwise to the cells and incubated for 48 h at 37°C. 48 h after transfection, viral supernatant from HEK293T cells was harvested and sterile filtered (0.45 μm pore size). 10μg/ml polybrene (Hexadimethrine bromide; Cat. No. TR-1003-G, Sigma-Aldrich, St. Louis, MO, USA) was added. 0.25x10^6 target cells were resuspended in 1 ml complete medium and added to one well of a 24 well plate. 1 ml viral supernatant was added. For transduction of larger cell numbers, multiple wells were prepared per construct. The mixture was centrifuged for 90 min at 1000xg and room temperature which promotes uptake of the viral particles by the target cells. Subsequently, supernatant was removed and replaced by complete medium. The transduced target cells were then incubated at 37°C for 48 h before transduction efficiency was determined.

Determination of transduction efficiency and enrichment of transduced cells

Mouse CD8a (Lyt2) was co-expressed with the biotin ligase fusion protein and served as selection marker. In order to monitor transduction efficiency, a sample of transduced cells was taken for flow cytometry staining of mouse CD8a. See section 3.6.1 for details about staining of cells for flow cytometry. 1 μl of an APC-conjugated anti-mouse CD8a antibody (Clone 53-6.7, Cat. No. 100712, Biolegend, San Diego,

CA, USA) was used per sample. Percentage of APC/CD8a-positive cells was determined by excitation of the fluorophore with a red laser (λ=640 nm) and detection of the signal using a 670/30 bandpass filter in a BD FACSCelesta system.
Transduced cells were enriched using mouse CD8a-coated magnetic beads. For this, cells were harvested, washed once with DPBS and resuspended in 1 ml isolation buffer (0.1% BSA, 2 mM EDTA in DPBS). One tube containing 10 μl mouse CD8a-coated magnetic beads (Cat. No. 11447D, Thermo Fisher Scientific, Waltham, MA, USA) per sample was prepared. The beads were pre-washed twice with isolation buffer utilising a magnetic rack. The resuspended cells were added to the beads and incubated for 20 min at 4°C under gentle rotation. During this time, CD8a-expressing cells were bound by the beads. For removal of CD8a-negative cells, the samples were placed in the magnetic rack. Supernatant was removed and the precipitated cells were resuspended in 1 ml isolation buffer. This way, the cells were washed three times. After the last washing step, supernatant was removed carefully and the precipitated cells were resuspended in 3 ml complete medium. Efficiency of the selection process was monitored by flow cytometry staining upon recovery of the cells. If percentage of CD8a-positive cells was still <90%, the selection process was repeated.

Validation of biotinligase-fusion protein expression

After transduced cells were enriched as described above, expression of the biotin ligase-fusion protein had to be validated. For this, a sample was taken and analysed for expression of the fusion protein by Western blotting. Empty vector-transduced cells were expected to express the biotin ligase alone. Cells transduced with the fusion protein were expected to display a double band of the target protein in Western blot: the endogenous protein at the respective height and an additional band which runs approx. 25 kDa above the endogenous protein due to fusion to the biotin ligase. Upon validation of the fusion protein expression, cells were subjected to SILAC-labelling.

Treatment and cell lysis

MARCH5 interactome

Empty vector-transduced cells were labelled with SILAC light cell culture medium, fusion protein-transduced cells were labelled with SILAC medium and heavy cell culture medium. Cells were expanded in the respective medium for at least 14 days to ensure complete protein labelling.
Upon sufficient expansion of the cells in the respective medium, $4x10^8$ cells per SILAC label were harvested and resuspended in 200 ml fresh SILAC medium of

the respective label. Approx. 16 h prior to lysis, 50 μM biotin (Cat. No. B4501-500MG, Sigma-Aldrich, St. Louis, MO, USA) were added. 6 h prior to lysis, the cells were treated as follows: heavy-labelled cells were treated with 10 nM (Jeko-1) or 0.3 nm (Maver-1) venetoclax, medium-labelled cells were treated with DMSO and light-labelled cells were left untreated. 3 h prior to lysis, each condition was split into two equal halfs. One half was treated with 10 µM MG-132 (Cat. No. S2619, SelleckChem, Houston, TX, USA), DMSO was added to the other half as a control. The combination of treatments resulting from this is detailed in figure 3.2.

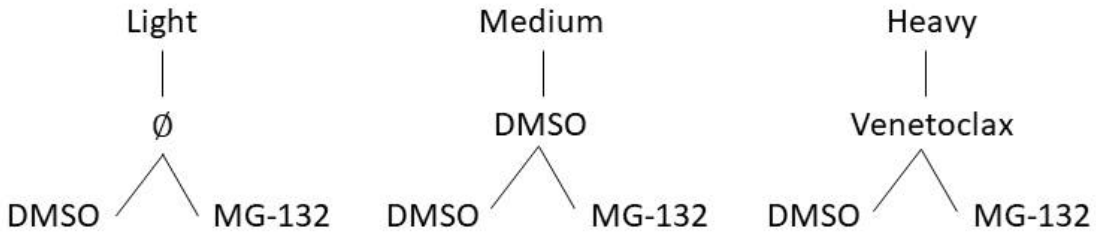

Figure 3.2: **Treatment of cells for the MARCH5 interactome**

After incubation, cell numbers of each sample were determined. A volume corresponding to 10^8 cells was harvested per sample. Light-, medium- and heavy-labelled cells were pooled, resulting in two final samples: one sample containing light-, medium- and heavy-labelled cells treated with MG-132 and a second sample with light-, medium- and heavy-labelled cells without MG-132 treatment. Each sample was lysed with 9 ml RIPA lysis buffer modified for MS (1% NP-40, 0.5% deoxycholate, 50 mM Tris, pH 7.5, 150 mM NaCl, 1 mM Na_3VO_4, 5mM NaF, 1x cOmplete EDTA-free protease inhibitor cocktail).

SASH3 interactome

For identification of SASH3 interacting proteins, empty vector transduced TMD8, Riva and SU-DHL-5 cells were labelled with SILAC light medium, SASH3 fusion protein transduced cells were labelled with SILAC heavy medium. 10^8 cells per SILAC label were resuspended in 100 ml of the respective SILAC medium und treated with 50 μM biotin for approx. 16 h. No additional treatment of the cells was conducted. Equal numbers of light- and heavy-labelled cells were harvested, mixed, washed twice with cold DPBS and lysed with 6 ml RIPA lysis buffer modified for MS (see above).

Sample preparation

After 20 min incubation on ice, the lysates were clarified by centrifugation (15,000xg, 4°C, 20 min). Meanwhile, 80 μl High capacity streptavidin agarose beads (Cat. No. 20359, Thermo Fisher Scientific, Waltham, MA, USA) per sample were pre-washed three times with RIPA lysis buffer modified for MS. Clarified lysates were added to the beads and incubated at 4°C under gentle rotation overnight. On the next day, the beads were washed three times with RIPA lysis buffer modified for MS. After the last washing step, the beads were resuspended in 50 μl 4x LDS sample buffer (Cat. No. NP0007) supplemented with 10x reducing agent (Cat. No. NP0009, both Thermo Fisher Scientific, Waltham, MA, USA) and boiled for 5 min at 95°C. Precipitated proteins were eluted from the beads during this step. Subsequently, the samples were centrifuged (300xg, 4°C, 2 min), the supernatant was transferred to a new tube and stored at -80°C until shipment for mass spectrometry analysis. The subsequent sample preparation and analysis steps were performed in the laboratory of Prof. H. Urlaub, Max Planck Institute Göttingen. Eluted proteins were separated by gel electrophoresis. The gel was stained with Coomassie blue. Each lane was cut into 20 fractions. After tryptic digestion and extraction from the gel, the resulting peptides were resuspended in sample loading buffer (2% acetonitrile and 0.05% trifluoroacetic acid) and subjected to MS measurement.

3.4.3 pYome

For analysis of differentially phosphorylated tyrosines (Y), pLKO.1-puro-GFP-sgNTC and -sgSASH3 transduced cells were expanded in SILAC light and heavy medium, respectively. 10^8 cells per condition were harvested, washed with DPBS twice and lysed with 8 M urea lysis buffer (20 mM Hepes pH 8.0, 8 M urea, 1 mM sodiumorthovanadate, 2.5 mM sodium pyrophosphate, 1 mM β-glycerophosphate).The lysates were then passed to the MS core unit. Here, equal amounts of light-and heavy-labelled proteins were pooled per cell line, trypsin-digested and tyrosine-phosphorylated peptides were enriched using immunoprecipitation (pY1000 antibody; Cat. No. 8954, Cell Signaling Technology, Danvers, MA, USA) according to the manufacturer's instructions. Enriched peptides were desalted and dried. The samples were then subjected to MS analysis using a Q Exactive HF mass spectrometer (Thermo Fisher Scientific, Waltham, MA, USA) coupled with Ultimate 3000 RSLCnano System (Dionex, Sunnyvale, CA, USA). After processing of the raw data file with MaxQuant (version 1.5.5.1), the MS spectra were searched against the UniProt human database. Further analyses were performed with Perseus (version 1.5.5.1). For this, localization probability was set to $\geq$0.75. Log2 transformed values $\geq$1 were identified as significantly regulated phosphorylation sites.

3.4.4 Ubiquitinome

Jeko-1 cells were transduced with pLKO.1-puro-GFP-sgNTC and -sgMARCH5. After puromycin selection, the cells were expanded in complete medium. Four flasks á $1.2x10^8$ cells in 100 ml complete medium were prepared. 10 nM venetoclax or DMSO as a control were added to two flasks per sgRNA respectively and incubated for 3 h. Subsequently, 10 μM MG-132 (Cat. No. S2619, Selleckchem, Houston, TX, USA) or DMSO as a control were added and incubated for another 3 h. The resulting combination of inhibitors is summarised in table 3.13. The total incubation times for venetoclax and MG-132 were 6 h and 3 h, respectively. After incubation, the cells were harvested and washed twice with cold DPBS. Subsequently, each sample was lysed separately with 10 ml 8 M urea lysis buffer. The lysates were stored at -80°C and passed to the MS laboratory. Here, each sample was labelled individually using tandem mass tags (TMT; Cat. No. 90111, Thermo Fisher Scientific, Waltham, MA, USA) according to the manufacturer's instructions which allows for simultaneous further preparation and measurement of the samples. Equal amounts of the labelled lysates were mixed and trypsin-digested. Ubiquitinated peptides were enriched using an anti-ubiquitin antibody (Cat. No. 3925, Cell Signaling Technology, Danvers, MA, USA) according to the manufacturer's instructions.

Table 3.13: **Combination of inhibitors used for ubiquitinome analysis**

Flask no.	**Venetoclax/DMSO**	**MG-132/DMSO**
1	DMSO	DMSO
2	DMSO	MG-132
3	Venetoclax	DMSO
4	Venetoclax	MG-132

3.4.5 Proteome

Differential expression levels in the individual experimental conditions interfered with conclusions about differential phosphorylation and ubiquitination levels of the respective proteins. Therefore, a global proteome was measured in parallel to the pYome, GPome and ubiquitinome samples. For this, a portion of the initial lysate was withdrawn before further manipulation and subjected to sample preparation as follows: lysates were separated by SDS-PAGE after trypsin-digestion. Subsequently, the lane was cut into individual fractions, which were then separately analysed by mass spectrometry utilising a Q Exactive HF mass spectrometer (Thermo Fisher Scientific, Waltham, MA, USA) coupled to an UltiMate 3000 Rapid Separation LC System (Dionex, Sunnyvale, CA, USA).

3.5 Quantitative gene expression analysis

3.5.1 RNA isolation and reverse transcription

RNA isolation and reverse transcription were conducted as described in section 3.4.2.

3.5.2 Quantitative real-time PCR (qRT-PCR)

Quantification of distinct transcripts (mRNA) was conducted utilizing the TaqMan^{TM} technique. Here, fluorochrome-coupled target-specific probes were used. Upon binding of the gene-specific primers, DNA amplification was enabled. During elongation of the amplicon, the probe was cleaved, which separated the fluorochrome from its quencher molecule, thereby releasing a fluorescent signal which was detected by the qPCR machine.[76] The process was conducted in consecutive cycles, analogous to conventional PCR. With every cycle, the fluorescent signal increased proportional to the abundance of the target sequence. The essential parameter to be determined was the CT value which represents the number of cycles which need to be processed until the fluorescent signal surpasses a threshold value. Since fluorescent signal and abundance of target sequence were proportional, CT value and target sequence abundance were inversely correlated. In order to relatively quantify the abundance of a specific target, Taqman probes for a house-keeping gene (e.g. GAPDH) were used. The expression of the house-keeping gene was supposed to be stable despite treatment or genetic manipulations of the cell and therefore served as internal control. Relative expression of the target mRNA was calculated according to the Livak method ($2^{-\Delta\Delta CT}$ method)[77], which compares CT values of the gene of interest to CT values of a housekeeping gene (ΔCT value) and normalizes ΔCT values of samples on ΔCT values of controls ($\Delta\Delta$CT). Finally, the relative fold gene expression level was calculated ($2^{-\Delta\Delta CT}$).

In detail, the following components were mixed per reaction: 1 μl 20x TaqMan^{TM} assay (see table 3.14), 10 μl 2x Universal TaqMan^{TM} Master Mix II with UNG (Cat. No. 4440038, Thermo Fisher Scientific, Waltham, MA, USA), 4 μl ddH_2O, 5 μl 1:5 diluted cDNA. All samples were analysed in triplicates in a 96 well plate using a qPCR machine (QuantStudio5; Thermo Fisher Scientific, Waltham, MA, USA).

Table 3.14: **TaqMan^{TM} assays used for this study**

Target	**Assay ID**
MARCH5	Hs00215155_m1
NOXA	Hs00560402_m1
MCL1	Hs03043899_m1
GAPDH	Hs02758991_g1

3.6 Flow cytometry

3.6.1 General staining procedure

In order to detect cellular proteins via flow cytometry, these proteins need to be specifically tagged with a fluorophore. For this, flurochrome-conjugated antibodies were used.
Approx. 10^6 cells were harvested per sample and washed with DPBS. Subsequently, the cells were resuspended in 300 μl FACS staining buffer (2% PenStrep, 2% FCS in DPBS). Unspecific antibody binding was prevented by addition of 3 μl human Fc receptor blocking reagent (Cat. No. 130-059-901 Miltenyi Biotech, Bergisch Gladbach, Germany) to each sample. The antibody targeting the protein of interest was added simultaneously and incubated with the sample for 15 min at 4°C while protected from light. Subsequently, the samples were washed twice with FACS staining buffer in order to remove excess antibody. After resuspension of the cells in 300 μl FACS staining buffer, the samples were analysed.

3.6.2 Apoptosis assay (Annexin V staining)

During the process of apoptosis, phosphatidylserine is exposed to the cell surface. In early stages of apoptosis, the membrane integrity is still maintained, and becomes more and more disrupted as apoptosis progresses.[78] Both features were used to determine the percentage of apoptotic cells. For this, 10^6 pLKO.1-puro-GFP-sgNTC and -sgSASH3 transduced Riva, TMD8, SU-DHL-4, SU-DHL-5 and WSU-DLCL2 cells were harvested per sample and washed twice with DPBS. After thorough removal of DPBS, the cells were resuspended in 1x Annexin binding buffer (ABB; 10 mM Hepes pH 7.4, 140 mM NaCl, 2.5 mM $CaCl_2$). 5 μl Annexin V-APC (Cat. No. 55075, BD, Franklin Lakes, NJ, USA) and 5 μl 7-Aminoactinomycin D viability staining solution (7AAD; Cat. No. 00-6993-50, Thermo Fisher Scientific, Waltham, MA, USA) were added to each sample. After careful mixing, the samples were incubated for 15 min at room-temperature while protected from light. Subsequently, 200 μl 1xABB were added to each sample which were then ready for analysis using a BD FACS LSR Fortessa system.
Cells which were treated with 2 μg/ml puromycin for 24 h served as positive control. Furthermore, single stained samples were prepared. For this, non-transduced cells and pLKO-puro-GFP-transduced cells were washed and resuspended in 1xABB. The samples were not further treated and thus served as unstained and GFP-only control, respectively. One sample with non-transduced cells was stained with 5 μl Annexin V-APC only, another sample of non-transduced cells was stained with 5 μl 7AAD only. These samples served as APC-only and 7AAD-only samples, respec-

tively. These samples serve for spectral overlap correction (compensation).
For determination of APC- and 7AAD-positive cells, only GFP-positive cells were analysed. This was achieved by applying a gating strategy in the BD FACS Diva software. Subsequently, four populations were visible, corresponding to different stages of apoptosis: double-negative cells were viable, APC-positive-7AAD-negative cells represented early apoptotic cells, double-positive cells displayed late stage apoptosis, cells which were 7AAD-positive-APC-negative were interpreted as debris.

3.7 Generation of knockout cells

3.7.1 Design of sgRNAs

The CRISPR/Cas9 system is composed of two key components: clustered regularly interspaced short palindromic repeats (CRISPR) which are short DNA sequences in each gene, and the endonuclease Cas9 (CRISPR-associated protein 9). Cas9 specifically detects CRISPR sequences and inserts a double-strand break at the respective site. Thus, Cas9 can be "programmed" to insert double-strand breaks at a specific site by providing sgRNAs that guide Cas9 to the specific site. After insertion of the double-strand break, cell-intrinsic mechanisms are initiated which serve to repair the break. Two mechanisms are capable of repairing double-strand breaks: homology directed repair (HDR) and non-homologous end-joining (NHEJ). While the first mechanism is precise but slow, the latter is quick but error-prone and thus often disrupts open reading frames. This principle is used for targeted gene knockout.[79]
Since the site of the double strand break determines the effectivity of gene knockout, several sgRNAs were designed for each gene targeted in this study. The sequences were retrieved from the Brunello library[80] and inserted into a lentiviral sgRNA transfer vector.

3.7.2 Cloning of sgRNA transfer vectors

For expression of sgRNAs, two lentiviral sgRNA transfer vectors were used: pLKO.1-puro-GFP and pLKO-neoBFP. Both vectors were kind gifts by the laboratory of Prof. Staudt (NIH, Bethesda, USA). As to be seen in figure 3.3, each sgRNA transfer vector co-expressed additional factors: pLKO.1-puro-GFP contained a puromycin resistance cassette which enabled puromycin selection of transduced cells. Additionally, EGFP was co-expressed. pLKO-neoBFP encoded a neomycin resistance cassette and BFP.

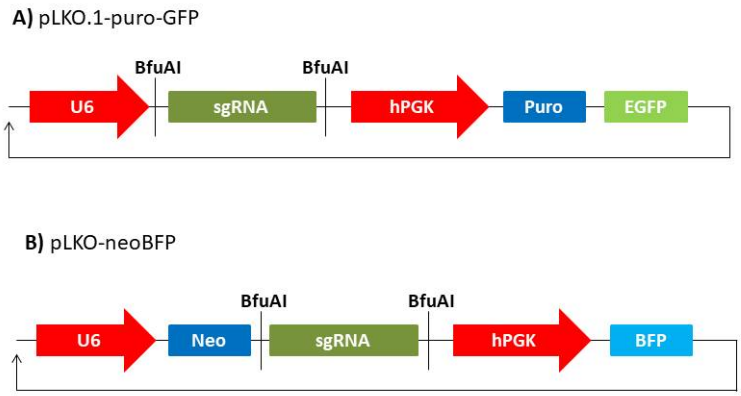

Figure 3.3: **Schematic of sgRNA transfer vectors.**
***A* pLKO-puro-GFP, *B* pLKO-neoBFP. Red arrows represent promoters, boxes represent genes.**

Table 3.15: **sgRNA sequences used for this study**

Target	**sgRNA sequence (5' → 3')**
NTC (non-targeting control)	TAAAGCAGAAGAATATACAG
MARCH5 sgRNA_2	ACCGCCAGGCCTGTCTACAACGCT
MARCH5 sgRNA_4	ACCGCTGAATGGGTGAGACCATGC
SASH3	TCAGCGAGTCGTGGTCATAG
NOXA	TCGAGTGTGCTACTCAACTC

All sgRNA sequences used for this study are detailed in table 3.15. Reverse sequences were computed and 5' overhangs were attached (ACCG for forward sequence; AAAC for reverse sequence). The resulting oligonucleotides were synthesized by Sigma Aldrich/Merck. Annealing of corresponding forward and reverse oligonucleotides was achieved by mixing 10 μM forward and 10 μM reverse oligonucleotide in DNase-free ddH_2O and boiling the mixture at 99°C for 5 min. Subsequently, the reaction was cooled to room temperature and diluted 1:200 with DNase-free ddH_2O. 3 μg of the respective backbone vector was restriction digested with 3 μl ($\equiv$ 15 units) BfuAI (Cat. No. R0701S) in NEBuffer^{TM} 3.1 (Cat. No. B7203S, both New England Biolabs, Ipswich, MA, USA) in a final volume of 50 μl at 55°C for 3 h. Subsequently, the reaction was applied to a 0.8% agarose/TAE gel. The resulting band was excised and the restriction digested vector was purified using the QIAquick gel extraction kit (Cat. No. 28706, Qiagen, Venlo, Netherlands). This kit comprises a buffer which allows resolving of the gel slice at 50°C which brings the excised DNA in solution. Subsequently, the solution is applied to a silica membrane-based spin column which binds DNA. After washing of the bound DNA, it is eluted in ddH_2O. Restriction digested vector and annealed oligonucleotides were

ligated in the following reaction:

Table 3.16: **Ligation reaction mix for cloning of lentiviral sgRNA transfer vectors**

Component	Volume
Annealed oligonucleotides	0.75 μl
10x NEB T4 ligase buffer	0.5 μl
T4 ligase (Cat. No. M0202L, New England Biolabs, Ipswich, MA; USA)	0.25 μl
Purified restriction digested vector	0.5 μl
DNase-free ddH_2O	3 μl

The reaction was incubated at room temperature for 3 h, transformed in *E. coli* Stbl3 as described in section 3.2.1 and plated on a LB Amp agar plates. The following day, mini preparations were prepared as described in section 3.2.2. Plasmids were sent for Sanger sequencing (Microsynth Seqlab) to ensure correct ligation of sgRNA sequence and vector backbone. Midi preparations were prepared from one correct clone per construct (see section 3.2.3).

3.7.3 Generation of lentiviral particles

Genetic manipulations were transferred to the target cells utilizing vesicular stomatitis virus protein G (VSV-G) pseudotyped lentiviral particles containing the respective construct. Viral particles provide the unique advantage of stably integrating their viral content into the host cell's genome. It is therefore possible to stably insert genomic manipulations into a cell which are also passed to daughter cells.

Transfection of HEK293T cells

18-24 h prior to transfection, 9x10^6 HEK293T cells were seeded in 30 ml complete medium per flask with 175 cm^2 growth area (T175 flask).
Per T175 flask, 14.4 μg psPAX (encodes lentiviral gag/pol), 4.8 μg pMD2.G (encodes VSV-G) and 19.2 μg of the respective sgRNA vector were added to 3.2 ml Reduced Serum Medium (OptiMEMTM; Cat. No. 31985070, Thermo Fisher Scientific, Waltham, MA, SUA). After thorough mixing, 115.2 μl transfection reagent (TransIT293; Cat. No. MIR2705, MoBiTec, Göttingen, Germany) were added. The mixture was incubated for 15-30 min at room temperature. During this time, the DNA components were complexed with components of the transfection reagent. Subsequently, the mixture was added dropwise to the HEK293T cells which had meanwhile undergone a medium exchange. The cells were then incubated with the transfection mixture for 24 h at 37°C. During this time, HEK293T cells incorporated

the DNA-transfection reagent complexes and initiated generation of viral particles which were then released into the supernatant.

Viral harvest and concentration

24 h after transfection, HEK293T supernatant containing lentiviral particles was collected and stored at 4°C. The transfected HEK293T cells were supplied with 30 ml fresh complete medium and incubated for another 24 h. Collection of viral supernatant and addition of medium to the cells was furthermore conducted 48 h after transfection. 72 h after transfection, viral supernatant was collected and HEK293T cells were discarded. Viral supernatant from all three collections was sterile-filtered (0.45 μm pore size) and combined with Lenti-X^{TM} concentrator (Cat. No. 631232, Takara Clontech, Mountain View, CA, USA) in a 1:4 ratio and incubated at 4°C for 30 min. During this time, viral particles were complexed by components of the Lenti-X^{TM} concentrator which allowed pelleting of the viral particles by subsequent centrifugation (1500 x g, 45 min at 4°C). After removal of the supernatant, the pellet was resuspended in 1 ml sterile DPBS, aliquoted and stored at -80°C until use.

3.7.4 Transduction of target cells

For transduction, 50 μl of concentrated virus were added to 10^6 target cells. No further manipulations were necessary, since the viral particles were able to enter the target cell via the membrane-bound low density lipoprotein (LDL)-receptor. The viral gene content (containing the construct transferring the sgRNA) was integrated into the target cell genome, transcription and translation of the encoded sequences were initiated.

3.7.5 Selection of transduced cells

For selection of pLKO.1-puro-GFP-transduced cells, 10 μg/ml puromycin (Cat. No. P8833, Thermo Fisher Scientific, Waltham, MA, USA) were added to the cell suspension. All transduced cells were resistant towards puromycin; non-transduced cells were depleted. Successful depletion of non-transduced cells was monitored by flow cytometry.
For selection of pLKO-neoBFP-transduced cells, 1 mg/ml neomycin/G418 (geneticin) could be added to the cell suspension to deplete non-transduced cells analogous to puromycin-resistant cells. Empirically, it was seen that the cells did not recover well from this treatment. Furthermore, selection of cells co-transduced with pLKO.1-puro-GFP and pLKO-neoBFP was not successful since many BFP-negative cells

remained viable. For this reasons, pLKO-neoBFP-transduced cells were subjected to FACS sorting using the BD FACSAriaIII system.

3.8 CRISPR/Cas9-based loss-of-function screen

The CRISPR/Cas9-based loss-of-function screen conducted in this study aimed to uncover genes which confer either resistance or synergy towards venetoclax treatment when knocked out. Therefore, cells were transduced with the genome-wide sgRNA Brunello library and treated with venetoclax for 14 days. Abundancy of each sgRNA was determined before and after induction of the treat-ment. From these measurements, CRISPR screen scores (CSS) were calculated. The workflow is depicted in figure 3.4

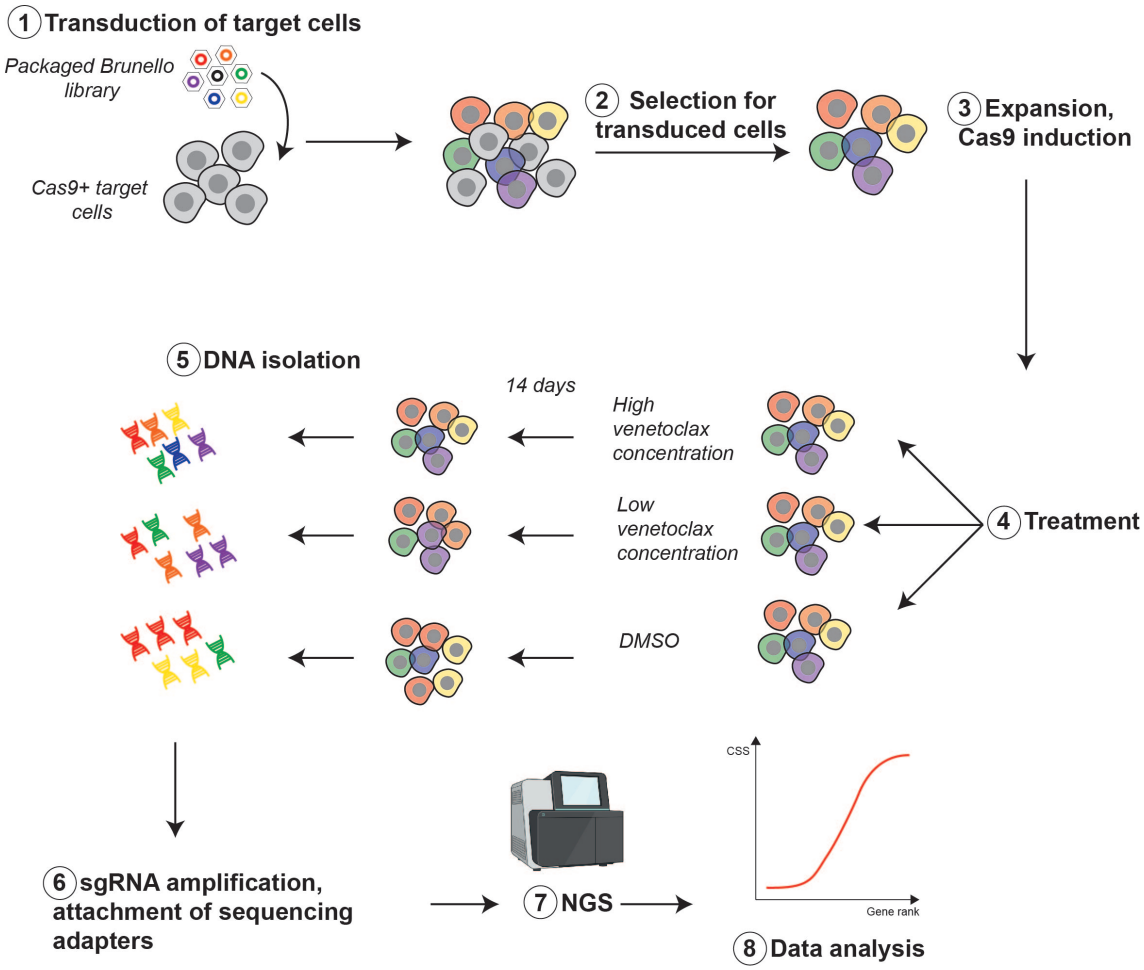

Figure 3.4: **CRISPR/Cas9-based loss-of-function screen workflow**

3.8.1 Generation of lentiviral particles and calculation of the amount of particles needed for transduction

Brunello sgRNA library was used.[80] This sgRNA library contains 3-4 independent sgRNAs per gene, which makes a total of approx. 80,000 sgRNAs targeting 20,000 genes. Non-targeting controls were also included in the library.
For this experiment it was essential that each cell was transduced by a single sgRNA. Therefore, a low multiplicity of infection (MOI) of 0.3 was aimed for. To achieve this, the amount of viral particles which would result in an MOI=0.3 had to be calculated for each target cell line and each new batch of lentiviral particles in a previous approach.
12 wells with 10^6 target cells in 3 ml complete medium each were prepared. One of the following volumes of concentrated lentiviral particles was added to three wells each: 5, 10, 20, 50, 100 μl. Two wells were left untreated. The Brunello sgRNA library utilizes the lentiGuide-Puro vector which encodes a puromycin resistance cassette. This allowed selection of transduced cells by incubating the cells with puromycin. All non-transduced cells were depleted, while only transduced cells survived. In order to determine the transduction efficiency for MOI calculation, one set of transduced cells was incubated with 5 μg/ml puromycin, while the second set served as control and was left untreated. The cells were incubated for three more days before cell viability was determined by 7AAD staining. For this, the cells were harvested, washed with DPBS and resuspended in 400 µl DPBS each. 4 μl 7AAD staining solution (Cat. No. 00-6993-50, Thermo Fisher Scientific, Waltham, MA, USA) were added and incubated with the cells for 10 min at 4°C while protected from light. Subsequently, the percentage of 7AAD negative (=viable) cells was measured by flow cytometry using the BD flow cytometer FACSCelesta equipped with a 695/40 BP filter upon excitation of the fluorochrome with λ=488 nm. From the resulting viabilities, the amount of viral particles needed to transduce the target cells with MOI=0.3 was extrapolated and projected to 2x10^8 cells.

3.8.2 Transduction of target cells

Target cells (Maver-1) were expanded to 4x10^8 in complete medium. On the day of transduction, two T175 flasks á 2x10^8 cells in 200 ml complete medium each were prepared. These represent the biological replicates R1 and R2. Each flask was separately transduced with the calculated amount of lentiviral particles containing the Brunello sgRNA library. The high cell number was necessary in order to achieve a 500x sgRNA coverage. On day three after transduction, 3 ml cell suspension were removed from each replicate and plated in three wells of a 12 well plate (1 ml per well). 5 μg/ml puromycin were added to each replicate. Subsequently, another 3 ml

of cell suspension were removed from each replicate and plated in a 12 well plate likewise. Additionally, 6 wells containing approximately $0.3x10^6$ non-transduced cells in 1 ml medium each were prepared. Puromycin was added to three wells, while the remaining three wells were left untreated. On day three of puromycin selection, cell viability was determined in the plated cells via 7AAD staining. The non-transduced cells thereby served as control. Complete depletion of non-transduced cells upon puromycin treatment had to be ensured in order to prevent falsification of the viability measurement. If non-transduced puromyin-treated cells were still viable, puromycin treatment had to be continued before further evaluation of cell viability in transduced cells could be conducted. Further processing of the CRISPR/Cas9-based loss-of-function screen was only performed if cell viability was approximately 30% which represented an MOI of 0.3.

3.8.3 Doxycyclin induction

Maver-1 cells were transduced with the pTO-Cas9 Hygro vector which employs the Tet-On system[81] which allows for targeted induction of Cas9 by application of doxycycline to the cell culture medium. Before induction of the Tet-On system, $5x10^7$ cells were removed from each replicate. The cells were pelleted and stored at -80°C for later use as day 0 sample. Cas9 expression in the remaining cells was induced with 0.25 μg/ml doxycycline. This doxycycline concentration was maintained throughout the whole subsequent process. During the following seven days, cells were expanded. Cells transduced with sgRNAs which target essential genes were depleted during this expansion period.

3.8.4 Determination of the initial venetoclax dose

Since cells containing the Brunello library were in general more sensitive to inhibitor treatment, the initial inhibitor dose used for the CRISPR/Cas9 screen had to be determined separately. For this, on day two and four an aliquot of cells was removed from each replicate and applied to a cell viability assay (see 3.1.2). Two venetoclax doses were chosen for treatment of the cells, which corresponded to approx. 50% and 70% cell viability, respectively. Treatment of the cells with the higher dose would result in outgrowth of cells transduced with sgRNAs targeting genes which rather confer resistance towards venetoclax treatment. Contrarily, treatment of the cells with the lower drug dose aimed to reveal more sensitivity-conferring genes.

3.8.5 Treatment

On the day of treatment initiation, the cells were splitted into three flasks per replicate. Each flask contained at least $5x10^7$ cells with a density of $0.5x10^6$ cells/ml. Flask 1 was treated with the lower venetoclax concentration, flask 2 with the higher concentration. Flask 3 served as control and was treated with DMSO. All flasks were incubated at 37°C. A small aliquot of cells was withdrawn from each flask. Initial cell viability was determined via 7AAD stain. During the following 14 days, a sample was taken from every flask every second day in order to determine cell viability. Drug doses were adjusted according to cell viability. For the low and high venetoclax-treated cells, a viability of 50% and 70%, respectively was intended.

3.8.6 DNA isolation

14 days after initiation of inhibitor treatment, cells were harvested and washed twice with DPBS. DNA was isolated from the cell pellets using QIAamp DNA Blood Maxi Kit (Cat. No. 51192, Qiagen, Venlo, Netherlands). Importantly, day 0 samples were now included in the process.
One 50 ml conical tube containing 1 ml protease solution was prepared per sample. Cells and DPBS were added to the protease to make a final volume of 10 ml. The samples were incubated at 70°C for 40 min. Every 10 min, the samples were mixed thoroughly to help the protease digest all proteins contained in the sample and thus lower protein contamination in the final product. After addition of 12 ml lysis buffer, the samples were inverted 15 times and thereafter vigorously shaken for 1 min. During the subsequent 30 min incubation at 70°C, the samples were mixed every 10 min. In order to precipitate DNA, 10 ml absolute ethanol (Cat. No. 24102-1L-R, Sigma Aldrich, St. Louis, MO, USA) were added per tube. Samples were mixed well. The lysates were then applied to a spin column. During the 3 min centrifugation at 2000xg at room temperature, DNA was adsorbed to the silica membrane. Flow-through was discarded. Washing of the DNA occurred by successive addition of two wash buffers and centrifugation of the columns. After the last washing step, the columns were left open in order to dry at room temperature for approx. 30 min. Subsequently, DNA elution was conducted. For this, 700 μl DNase-free ddH_2O (pre-heated to 70°C; Cat. No. 10977-035, Thermo Fisher Scientific, Waltham, MA, USA) were added to each column and incubated for 5 min. After centrifugation for 10 min at 4500xg and room-temperature, DNA content in the eluate was measured using a spectral photometer (NanoDrop 2000C, Thermo Fisher Scientific, Waltham, MA, USA). The eluate was re-loaded onto the column if DNA content was < 200ng/μl. For samples containing ≥ 200 ng/µl DNA, a second elution step with additional 700 µl ddH_2O was conducted. Final DNA content was measured in each sample.

3.8.7 Amplification of sgRNA sequences and attachment of sequencing adapters

In two consecutive PCRs, sgRNA sequences were amplified from the isolated DNA and sequencing adapters were attached which allowed for next-generation sequencing (NGS).
In a first step, the isolated genomic DNA was used as template from which sgRNA sequences were amplified. For composition of the mastermix and the PCR program, see table 3.17 and table 3.18. Importantly, each sample was processed as 24x reaction. The 25x mastermix was distributed to 24 wells of a 96 well PCR plate. 25x mastermix was prepared to make sure that each of the 24 wells contained 100 µl reaction volume. After completion of the PCR program, PCR products corresponding to the same sample were pooled. The high reaction volume was necessary in order to maintain coverage of the sgRNA library.

Table 3.17: **25x mastermix for the first PCR**

Component	**25x reaction**
10x ExTaq buffer (supplied with ExTaq polymerase)	250 μl
10 mM dNTPs (supplied with ExTaq polymerase)	200 μl
5 μM forward primer	125 μl
5 μM reverse primer	125 μl
ExTaq polymerase (Cat. No. RR001C, Takara, Mountain View, CA, USA)	37.5 μl
DNA	250 μg
ddH_2O	Add 2500 μl

Forward primer:
pLKO.1 BfuA1-F: AATGGACTATCATATGCTTACCGTAACTTGAAAGTATTTCG
Reverse primer:
pLKO.1 BfuA1-R1.3: GTAATTCTTTAGTTTGTATGTCTGTTGCTATTATG

Table 3.18: **PCR program for CRISPR/Cas9-based loss-of-function screen**

Step	**Temperature**	**Time**	
Initial denaturation	95°C	5 min	
Denaturation	94°C	30 sec	18 cycles
Annealing	65°C	30 sec	
Elongation	72°C	20 sec	
Final Elongation	72°C	5 min	
Storage	4°C	∞	

Subsequently, the PCR product obtained in the first PCR was applied to a second PCR. Here, NGS adapters were attached to the sgRNA sequences. In NGS, samples are multiplexed. For data deconvolution, the samples were barcoded on molecular level using unique combinations of forward and reverse primers (see table 3.19 and table 3.20) for each sample. For composition of the PCR mastermix, see table 3.21. The second PCR was conducted as a single reaction per sample. The PCR program for the second PCR was the same as for the first PCR (see table 3.18).

Table 3.19: **Primer sequences used for second PCR in CRISPR/Cas9-based loss-of-function screen**

Primer	Index	Sequence
D701	**CGAGTAAT**	CAAGCAGAAGACGGCATACGAGATCGAGTA-ATGTGACTGGAGTTCAGACGTGTGCTCTTC-CGATCTCTACTATTCTTTCCCCTGCACTGT
D702	**TCTCCGGA**	CAAGCAGAAGACGGCATACGAGATTCTCCG-GAGTGACTGGAGTTCAGACGTGTGCTCTTC-CGATCTCTACTATTCTTTCCCCTGCACTGT
D501	**TATAGCCT**	AATGATACGGCGACCACCGAGATCTACACT-ATAGCCTACACTCTTTCCCTACACGACGCT-CTTCCGATCTATGCATGCTCTTGTGGAAAG-GACGAAACACCG
D502	**ATAGAGGC**	AATGATACGGCGACCACCGAGATCTACACA-TAGAGGCACACTCTTTCCCTACACGACGCT-CTTCCGATCTTGCATGCAGTCTTGTGGAAA-GGACGAAACACCG
D503	**CCTATCCT**	AATGATACGGCGACCACCGAGATCTACACCC-TATCCTACACTCTTTCCCTACACGACGCTC-TTCCGATCTGCATGCATCGTCTTGTGGAAA-GGACGAAACACCG
D504	**GGCTCTGA**	AATGATACGGCGACCACCGAGATCTACACGGC-TCTGAACACTCTTTCCCTACACGACGCTCT-TCCGATCTCATGCATGACGTCTTGTGGAAA-GGACGAAACACCG

Table 3.20: **Unique primer combination in second PCR for CRISPR/Cas9-based loss-of-function screen**

Replicate	Sample	Primer reverse	Primer forward
1	Day 0	D701	D501
	DMSO		D502
	Venetoclax Low		D503
	Venetoclax High		D504
2	Day 0	D702	D501
	DMSO		D502
	Venetoclax Low		D503
	Venetoclax High		D504

Table 3.21: **Composition of reaction for second PCR in CRISPR/Cas9-based loss-of-function screen**

Component	Volume [μl]
10x buffer	10
10 mM dNTPs	8
5 μM primer forward (D50X)	5
5 μM primer reverse (D70X)	5
ExTaq polymerase	1,5
Primary PCR product	5
ddH_2O	Add 100 μl

3.8.8 Size selection

In order to purify the PCR product from non-specific products as well as excess primers and dNTPs, the specific DNA fragment was extracted via agarose gel. For this, 18 μl of the second PCR product was mixed with 10x loading dye to make a final volume of 20 μl. This mixture was applied to an E-Gel SizeSelect II 2% Agarose Gel (Cat. No. G661012, Thermo Fisher Scientific, Waltham, MA, USA) utilizing the E-Gel Power Snap Electrophoresis Device (Cat. No. G8100, Thermo Fisher Scientific, Waltham, MA, USA). A DNA ladder (E-Gel Sizing DNA ladder; Cat. No. 1048810, Thermo Fisher Scientific, Waltham, MA, USA) was used to identify the desired DNA band (375 bp). The E-Gel SizeSelect II 2% Agarose Gels allow extraction of a specific DNA band as it passes a pocket inserted in the gel. The extracted DNA was shipped to the laboratory of Prof. Staudt. NIH, Bethesda, USA where NGS was conducted.

3.8.9 NGS and CSS value calculation

In the laboratory of Prof. Staudt, the samples were quality checked and quantitated. Sequencing was conducted using the Illumina NextSeq500 system (Thermo Fisher Scientific, Waltham, MA, USA). From the raw counts of sgRNAs, CRISPR Screen Scores (CSS) were calculated. CSS values give evidence about the essentiality of a certain gene in a certain context.

3.9 Competitive growth assays

Competitive growth assays are well suited for detection of growth advantages or disadvantages upon manipulation in one or multiple genes in comparison to wild-type cells.

In a first step, target cells were transduced with a vector coding for a fluorochrome

and an sgRNA targeting the gene of interest or a non-targeting control. Transduced cells were enriched by sorting or treatment of the cells with a selection antibiotic to achieve $\geq 90\%$ transduction rate. These cells were then mixed with non-transduced cells of the same cell line in a 1:1 ratio. If an inhibitor treatment was included (see respective section), all samples were processed as duplicates. One duplicate was then resupended in complete medium containing the inhibitor, the second duplicate was resuspended in complete medium containing DMSO. If no inhibitor treatment was included, a single sample was prepared per condition and cultured in complete medium.
All samples were cultured for 14 days. Every second day, the fluorescence signal was monitored via flow cytometry. The percentage of fluorescent cells was normalised to the percentage on the day of treatment initiation (day 0) of the respective sample. An increase of fluorescent cells was expected if the knockout of the gene of interest represented a growth advantage for the cells which then outcompeted the wild-type cells. Likewise, a decrease of fluorescent cells was expected if knockout of the gene of interest represented a growth disadvantage for the cells.

The assay was also conducted with double-knockout cells as described above. Here, the two genes of interest were targeted by separate sgRNA transfer vectors which also coded for a fluorescent protein. Importantly, the vectors had to code for different fluorescent proteins, namely EGFP and BFP (encoded by pLKO.1-puro-GFP and pLKO-neoBFP, respectively). Percentage of double-positive cells was monitored over 14 days.

3.10 BH3 profiling

BH3 profiling is a method to investigate a cell's dependency on certain BCL-2 family members as well as the extent of apoptotic priming. Peptides which resemble the individual BCL-2 family members were applied to a cell suspension. Importantly, the cells were permeabilised in order to allow passage of the peptides through the membrane. Mitochondrial outer membrane permeabilisation (MOMP) as a surrogate for intrinsic apoptosis was measured by application of membrane potential-sensitive dyes.
Measurements and data analysis were performed according to protocols from the Letai laboratory[82] by Dr. K. Bojarczuk in the laboratory of Prof. Chapuy, university hospital of Göttingen.

4 Results

4.1 Role of MARCH5 in sensitisation of mantle cell lymphoma cells towards venetoclax

4.1.1 Maver-1 was highly sensitive towards BCL-2 inhibition using venetoclax

In order to identify genes/proteins which confer either resistance or sensitivity towards venetoclax upon their respective knockout, a CRISPR/Cas9-based loss-of-function screen was performed. For this, a MTT viability assay was conducted with three MCL cell lines in order to choose the most sensitive one for the planned screening experiment. Venetoclax was tested in a range of 0.61 nM – 10 µM on the MCL cell lines Jeko-1, Maver-1 and Mino. As depicted in Figure 4.1, Maver-1 was seen to be highly sensitive even to low venetoclax concentrations, with an IC_{50} of 5.59 nM. Jeko-1 cells did not display significant decrease of cell viability over a broad range of venetoclax concentrations, IC_{50} was 4.19 µM. Mino displayed an intermediate sensitivity with an IC_{50} of 863.36 nM. Based on these results, the CRISPR/Cas9-based loss-of-function screen was conducted with Maver-1 as the most sensitive cell line.

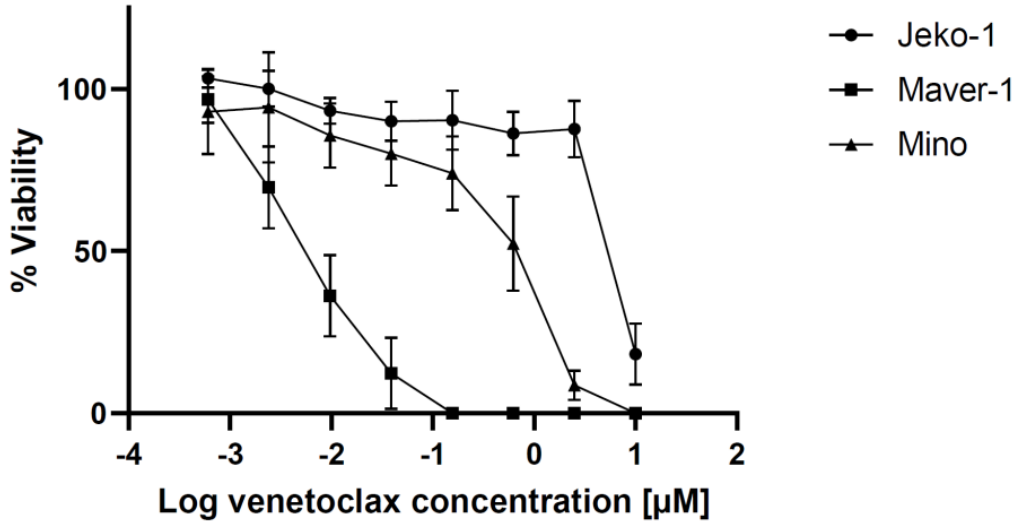

Figure 4.1: **MTT viability assay with venetoclax on Jeko-1, Maver-1 and Mino cells. Mean of 3 replicates +/- SD is depicted.**

4.1.2 Re-evaluation of Cas9 capacities in Maver-1

All cell lines used for this study were transduced with an inducible Cas9 expression vector in the collaborating laboratory of Prof. Staudt, NIH, USA. Single cell cloning and evaluation of Cas9 capacities were also conducted in this laboratory. In Figure 4.2 Cas9 expression upon induction was re-evaluated in freshly thawed cells upon arrival in the laboratory of Prof. Oellerich.

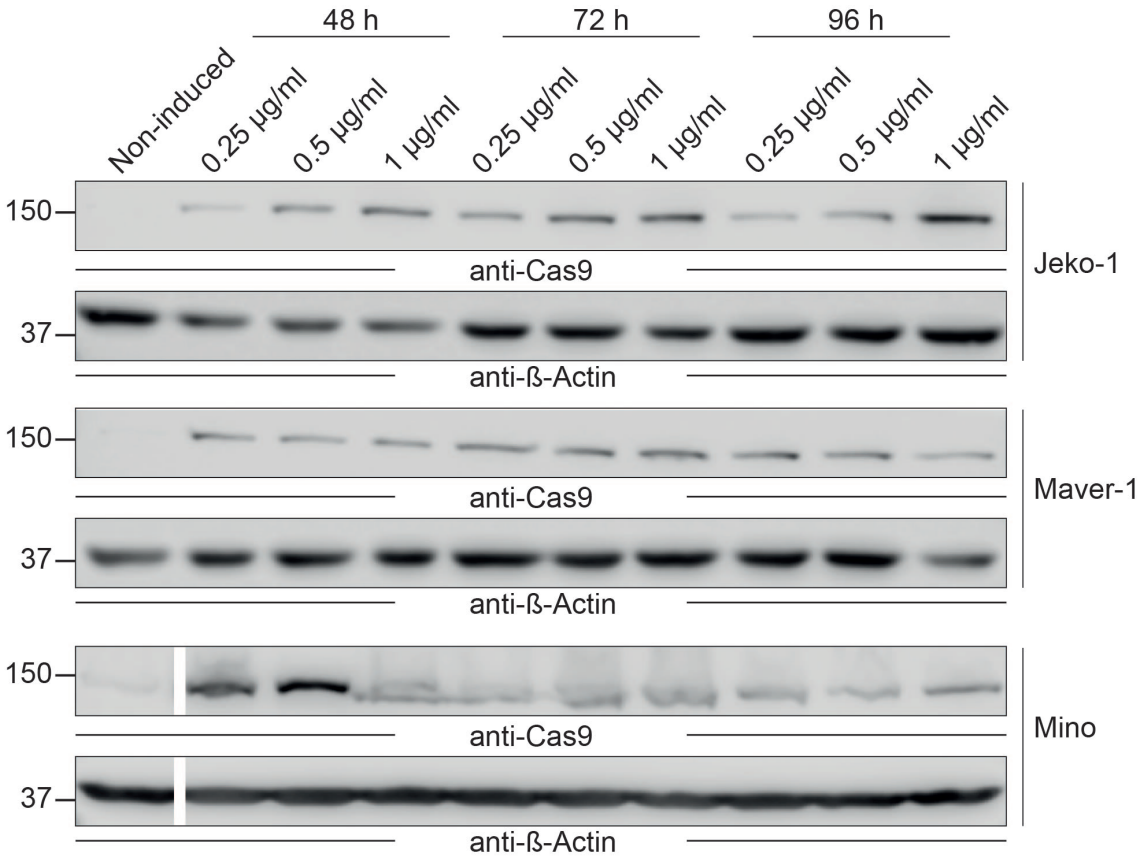

Figure 4.2: **The MCL cell lines Jeko-1, Maver-1 and Mino were transduced with an inducible Cas9 expression vector in the laboratory of Prof. Staudt. Upon arrival of the cells in the laboratory of Prof. Oellerich, Cas9 expression upon induction was re-evaluated. The cells were treated with either 0.25, 0.5 or 1 μg/ml doxycycline for 24, 72 or 96 h or were left untreated. Subsequently, the cell lysates were analysed for Cas9 expression via Western blot. β-Actin served as a loading control.**

Since the cells were passaged several times before they were cryo-preserved, Cas9 capacity of freshly thawed cells was re-evaluated in Maver-1 cells since efficient endonuclease activity was inevitable for successful completion of the CRISPR/Cas9-based loss-of-function screen.

For this, the cells were transduced with sgRNA transfer vectors targeting either the

membrane-bound intercellular adhesion molecule 1 (ICAM1, sgICAM), or coding for a non-targeting control sgRNA (sgNTC). ICAM-1 expression was analysed via flow cytometry in sgNTC- vs. sgICAM-transduced cells upon Cas9 induction. As depicted in Figure 4.3, ICAM-1 expression was decreased in sgICAM-transduced cells in comparison to sgNTC-transduced cells. This indicated proper Cas9 activity in Maver-1 cells. With this, use of Maver-1 cells for the planned CRISPR-Cas9-based loss-of-function screen was possible.

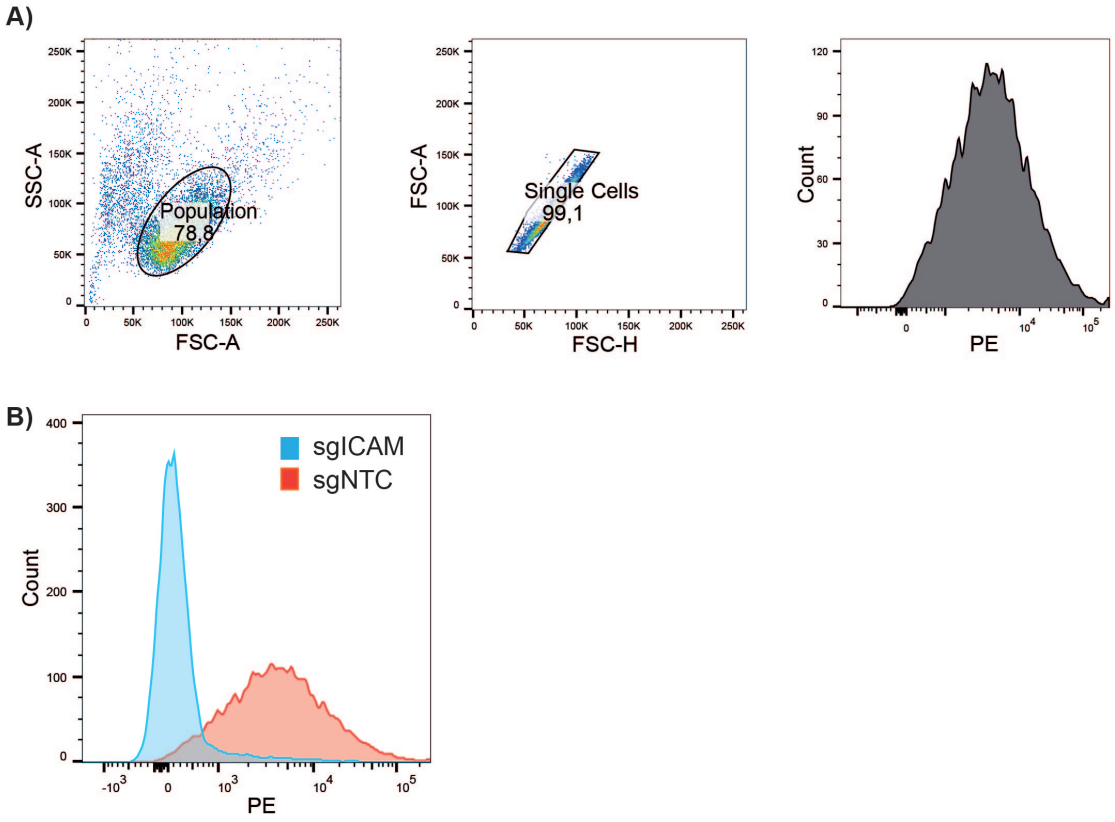

Figure 4.3: **Re-evaluation of Cas9 capacities in Maver-1 cells. Expression of ICAM-1 was analysed in pLKO.1-puro-GFP-sgNTC vs. -sgICAM transduced cells. A) FACS-gating strategy. B) Decrease of ICAM-1 expression in sgICAM-transduced cells indicates proper Cas9 activity.**

4.1.3 CRISPR/Cas9-based loss-of-function screen in Maver-1 cells under venetoclax treatment

Maver-1 cells were transduced with the Brunello library in two biological replicates, R1 and R2. After puromycin selection of transduced cells, the cells were expanded and Cas9 expression was induced. As described above, Maver-1 wild-type cells displayed a venetoclax IC_{50} value of 5.59 nM. Since cells are generally more sensitive

to inhibitor treatment upon transduction with the Brunello library, the venetoclax IC_{50} value was re-evaluated in Brunello library-transduced Maver-1 cells. For this, a sample of cells was taken on day 4 of doxycycline-induction and submitted to a MTT viability assay. This assay revealed an average venetoclax IC_{50} value of 2.65 nM for the two biological replicates. In CRISPR/Cas9-based loss-of-function screens, it is especially important to maintain the 500x sgRNA coverage. Therefore, a rather low dose was chosen for the initial venetoclax treatment, since otherwise maintenance of the 500x coverage could be impaired due to excessive cell death. The "low venetoclax" and "high venetoclax" samples were initially treated with 1 and 2 nM venetoclax, respectively. During the 14 days venetoclax treatment, cell viability was assessed every second day. It did not decrease as expected in the venetoclax-treated samples. Therefore, venetoclax doses were constantly increased; on the final day of treatment, the "low" and "high" samples were treated with 8 and 16 nM venetoclax, respectively. A considerable decrease of viability was still not observed.

Since viral transduction was used, the sgRNA sequence was stably integrated into the host cell genome. Using two consecutive PCRs, the sgRNA sequences were amplified from the DNA isolated from the cells after 14 days treatment and sequencing adapters were attached. The final PCR product was sent for sequencing, which was conducted in the laboratory of Prof. Staudt. Also data processing was performed in this laboratory. CSS values (mean value of R1 and R2) were assigned to each gene for low venetoclax, high venetoclax and DMSO treatment. CSS values were calculated from the ratio of the mean abundancy of the sgRNAs targeting a given gene after treatment in comparison to abundancy before initiation of the treatment. Generally, negative values indicate that knockout of the respective gene was a growth disadvantage for the cell, thus the respective genes were considered as essential. Positive CSS values, on the contrary, indicated that knockout of the respective gene was a growth advantage for the cell.

Besides this general consideration, there is no universal cutoff value which defines outlier CSS values. Therefore, the CSS values were plotted against their respective gene rank. As illustrated in Figure 4.4, cutoff values were manually assigned and set to -1.35 and 1.25, respectively. All CSS values $\leq$-1.35 and$\geq$1.25 were regarded as genes which upon their knockout confer sensitivity or resistance towards venetoclax, respectively.

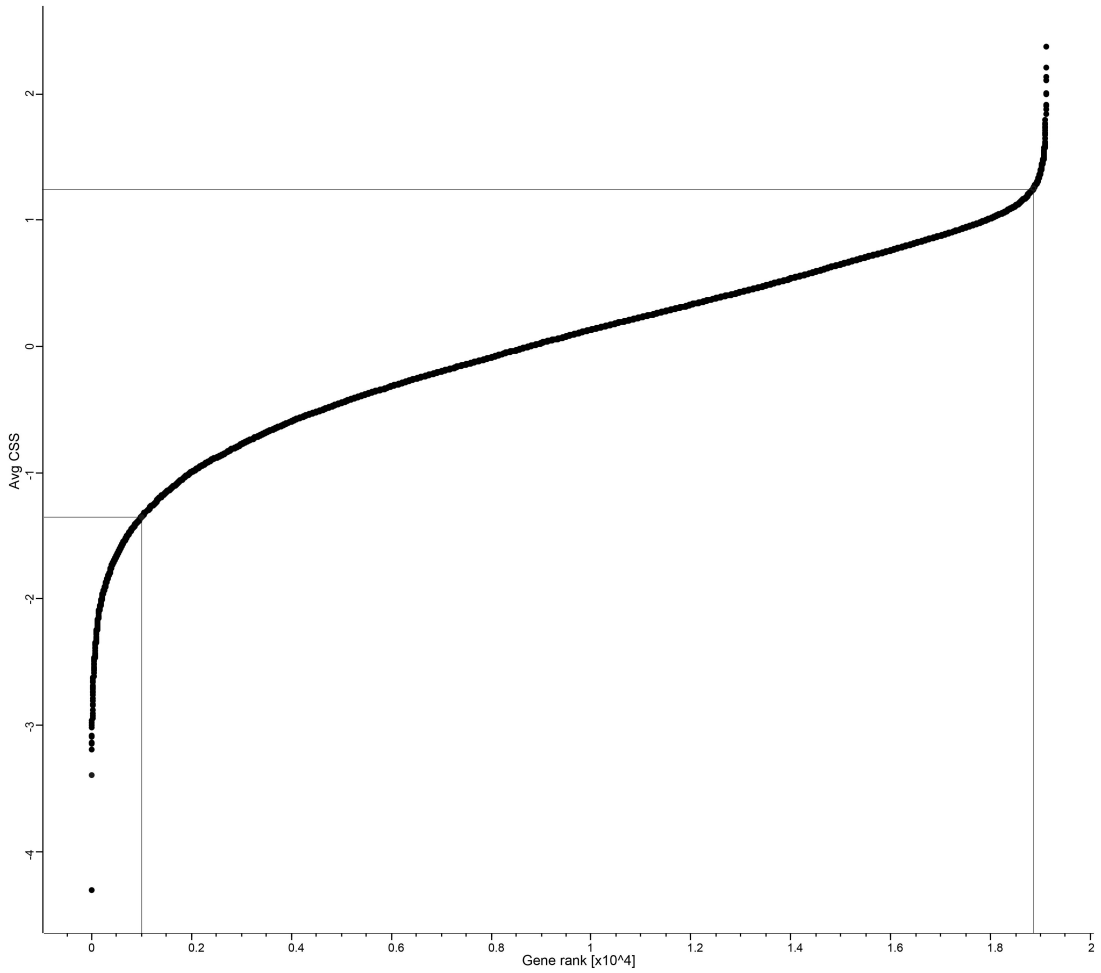

Figure 4.4: **Assignment of cutoff values for the CRISPR/Cas9-based loss-of-function screen. For each gene, the average CSS (mean of two biological replicates) was plotted against the respective gene rank. Cutoffs at -1.35 and 1.25 were set manually. Data from high venetoclax treated cells are depicted exemplarily.**

After all genes meeting the cutoff criteria were selected, Gene Set Enrichment Analysis (GSEA) was performed using the online platform MSigDB as described by[83;84]. Overlaps with Gene Ontology (GO) classifications were computed for each of the following data sets: CSS values $\leq$-1.35 or $\geq$1.25 for DMSO, low and high venetoclax treated cells each. Panessential genes were not considered in this analysis. In table 4.1, top 20 enriched GO classes for CSS values $\geq$1.25 for each data set are detailed. GO classes which occur in more than one data set are highlighted. Taken together, this table details pathways which confer resistance towards venetoclax upon knockout of their components. Interestingly, many GO classes describing metabolic processes were enriched. The two classes "GOBP_HOMEOSTATIC_-PROCESS" and "GOBP_SECRETION" are found in DMSO-treated and venetoclax low- or –high treated cells, respectively. This indicates that their enrichment did not

seem to be exclusively connected to venetoclax treatment. Knockout of components belonging to either of these GO classes generally seem to confer a growth advantage to Maver-1 cells.

Table 4.1: **GSEA of genes with CSS values $\geq$ 1.25**

#	DMSO	Low venetoclax treated cells	High venetoclax treated cells
1	GOMF_DNA_BINDING_TRANSCRIPTION_FACTOR_ACTIVITY	GOBP_ESTABLISHMENT_OF_PROTEIN_LOCALIZATION	GOBP_LIPID_METABOLIC_PROCESS
2	GOMF_SEQUENCE_SPECIFIC_DNA_BINDING	GOCC_ENDOPLASMIC_RETICULUM	GOBP_CELLULAR_LIPID_METABOLIC_PROCESS
3	GOMF_TRANSCRIPTION_REGULATOR_ACTIVITY	GOBP_INTRACELLULAR_TRANSPORT	GOBP_ORGANOPHOSPHATE_METABOLIC_PROCESS
4	GOCC_GOLGI_APPARATUS	GOBP_CELLULAR_MACROMOLECULE_LOCALIZATION	GOBP_INTRACELLULAR_TRANSPORT
5	GOBP_SENSORY_ORGAN_DEVELOPMENT	GOBP_INTRACELLULAR_PROTEIN_TRANSPORT	GOCC_ENDOPLASMIC_RETICULUM
6	GOMF_CIS_REGULATORY_REGION_SEQUENCE_SPECIFIC_DNA_BINDING	GOBP_HOMEOSTATIC_PROCESS	GOBP_PHOSPHOLIPID_METABOLIC_PROCESS
7	GOMF_CALCIUM_ION_BINDING	GOMF_ENZYME_BINDING	GOBP_LIPID_BIOSYNTHETIC_PROCESS
8	GOBP_HOMEOSTATIC_PROCESS	GOBP_CELL_ACTIVATION	GOBP_INTRACELLULAR_PROTEIN_TRANSPORT
9	GOBP_TRANSMEMBRANE_TRANSPORT	GOBP_REGULATION_OF_CELLULAR_LOCALIZATION	GOBP_IMMUNE_SYSTEM_DEVELOPMENT
10	GOBP_DEVELOPMENTAL_PROCESS_INVOLVED_IN_REPRODUCTION	GOBP_CELLULAR_HOMEOSTASIS	GOBP_CELLULAR_MACROMOLECULE_LOCALIZATION
11	GOMF_SIGNALING_RECEPTOR_BINDING	GOBP_MACROMOLECULE_CATABOLIC_PROCESS	GOBP_ESTABLISHMENT_OF_PROTEIN_LOCALIZATION
12	GOBP_REGULATION_OF_PROTEIN_PHOSPHORYLATION	GOMF_PROTEIN_HETERODIMERIZATION_ACTIVITY	GOBP_SMALL_MOLECULE_METABOLIC_PROCESS
13	GOMF_TRANSPORTER_ACTIVITY	GOCC_DNA_PACKAGING_COMPLEX	GOBP_REGULATION_OF_IMMUNE_SYSTEM_PROCESS
14	GOMF_ION_TRANSMEMBRANE_TRANSPORTER_ACTIVITY	GOBP_REGULATION_OF_IMMUNE_SYSTEM_PROCESS	GOBP_CELL_SURFACE_RECEPTOR_SIGNALING_PATHWAY_INVOLVED_IN_CELL_CELL_SIGNALING
15	GOBP_SECRETION	GOBP_NEGATIVE_REGULATION_OF_GENE_EXPRESSION_EPIGENETIC	GOBP_RESPONSE_TO_BIOTIC_STIMULUS
16	GOBP_CELL_CELL_SIGNALING	GOBP_PHOSPHATIDIC_ACID_METABOLIC_PROCESS	GOBP_REGULATION_OF_CELLULAR_LOCALIZATION
17	GOCC_INTRINSIC_COMPONENT_OF_PLASMA_MEMBRANE	GOBP_REGULATION_OF_METAL_ION_TRANSPORT	GOBP_RESPONSE_TO_DRUG
18	GOBP_CATION_TRANSPORT	GOBP_IMMUNE_SYSTEM_DEVELOPMENT	GOBP_SECRETION
19	GOBP_ANIMAL_ORGAN_MORPHOGENESIS	GOBP_CHEMICAL_HOMEOSTASIS	GOCC_ORGANELLE_SUBCOMPARTMENT
20	GOBP_REGULATION_OF_PHOSPHORUS_METABOLIC_PROCESS	GOBP_POSITIVE_REGULATION_OF_SIGNALING	GOBP_ORGANOPHOSPHATE_BIOSYNTHETIC_PROCESS

GOMF= GO Molecular Function; GOBP= GO Biological Process; GOCC= GO Cellular Component. Yellow= Enriched in DMSO and Low venetoclax treated cells. Green=Enriched in DMSO and High venetoclax treated cells. Orange= Enriched in Low and High venetoclax treated cells.

GSEA was likewise performed with CSS values $\leq$-1.35 of all data sets in order to identify enriched GO classes. The results are given in table 4.2. In comparison with CSS values $\geq$1.25, less GO classes were found in more than one data set with CSS values $\leq$-1.35. Since no overlapping GO classes were found in DMSO-treated and venetoclax-treated cells, the enriched GO classes of venetoclax-treated cells seemed to be specifically connected to BCL-2 inhibition. Enriched GO classes in DMSO-treated cells generally represent pathways which can be considered as indispensable for Maver-1 cells. The extent to which enrichment of GO classes in venetoclax-treated cells were connected to BCL-2 inhibition should be examined in another set of experiments. However, genes belonging to the regulation of the intrinsic apoptotic pathway were not found to be enriched.

Table 4.2: **GSEA of genes with CSS values ≤ -1.35**

#	DMSO	Low venetoclax treated cells	High venetoclax treated cells
1	GOMF_RNA_BINDING	GOCC_MICROTUBULE_CYTOSKELETON	GOMF_IDENTICAL_PROTEIN_BINDING
2	GOCC_RIBONUCLEOPROTEIN_COMPLEX	GOBP_NEUROGENESIS	GOBP_POSITIVE_REGULATION_OF_NUCLEOBASE_CONTAINING_COMPOUND_METABOLIC_PROCESS
3	GOCC_RIBOSOMAL_SUBUNIT	GOBP_CELL_PROJECTION_ORGANIZATION	GOCC_ORGANELLE_SUBCOMPARTMENT
4	GOBP_NUCLEAR_TRANSCRIBED_MRNA_CATABOLIC_PROCESS_NONSENSE_MEDIATED_DECAY	GOBP_ORGANOPHOSPHATE_METABOLIC_PROCESS	GOBP_PROTEOLYSIS
5	GOCC_CYTOSOLIC_RIBOSOME	GOBP_POSITIVE_REGULATION_OF_MOLECULAR_FUNCTION	GOBP_SMALL_MOLECULE_METABOLIC_PROCESS
6	GOBP_TRANSLATIONAL_INITIATION	GOBP_POSITIVE_REGULATION_OF_NUCLEOBASE_CONTAINING_COMPOUND_METABOLIC_PROCESS	GOMF_SEQUENCE_SPECIFIC_DNA_BINDING
7	GOBP_ORGANONITROGEN_COMPOUND_BIOSYNTHETIC_PROCESS	GOCC_MICROTUBULE_ORGANIZING_CENTER	GOCC_MICROTUBULE_CYTOSKELETON
8	GOMF_STRUCTURAL_CONSTITUENT_OF_RIBOSOME	GOBP_SMALL_MOLECULE_METABOLIC_PROCESS	GOCC_NEURON_PROJECTION
9	GOCC_RIBOSOME	GOMF_ENZYME_BINDING	GOBP_HOMEOSTATIC_PROCESS
10	GOBP_COTRANSLATIONAL_PROTEIN_TARGETING_TO_MEMBRANE	GOBP_LIPID_METABOLIC_PROCESS	GOCC_PLASMA_MEMBRANE_REGION
11	GOBP_ESTABLISHMENT_OF_PROTEIN_LOCALIZATION_TO_ENDOPLASMIC_RETICULUM	GOCC_ENDOPLASMIC_RETICULUM	GOMF_TRANSCRIPTION_REGULATOR_ACTIVITY
12	GOBP_PEPTIDE_BIOSYNTHETIC_PROCESS	GOBP_POSITIVE_REGULATION_OF_SIGNALING	GOBP_POSITIVE_REGULATION_OF_MULTICELLULAR_ORGANISMAL_PROCESS
13	GOBP_VIRAL_GENE_EXPRESSION	GOCC_SUPRAMOLECULAR_COMPLEX	GOBP_LIPID_METABOLIC_PROCESS
14	GOBP_NUCLEAR_TRANSCRIBED_MRNA_CATABOLIC_PROCESS	GOBP_CELL_CYCLE_PROCESS	GOMF_CIS_REGULATORY_REGION_SEQUENCE_SPECIFIC_DNA_BINDING
15	GOBP_PROTEIN_LOCALIZATION_TO_ENDOPLASMIC_RETICULUM	GOBP_REGULATION_OF_PROTEIN_MODIFICATION_PROCESS	GOCC_ENDOPLASMIC_RETICULUM
16	GOBP_AMIDE_BIOSYNTHETIC_PROCESS	GOBP_POSITIVE_REGULATION_OF_BIOSYNTHETIC_PROCESS	GOBP_APOPTOTIC_PROCESS
17	GOBP_MRNA_METABOLIC_PROCESS	GOBP_MACROMOLECULE_CATABOLIC_PROCESS	GOBP_REGULATION_OF_TRANSPORT
18	GOBP_PEPTIDE_METABOLIC_PROCESS	GOBP_POSITIVE_REGULATION_OF_CATALYTIC_ACTIVITY	GOBP_CARBOHYDRATE_DERIVATIVE_METABOLIC_PROCESS
19	GOBP_RNA_CATABOLIC_PROCESS	GOBP_CELLULAR_MACROMOLECULE_CATABOLIC_PROCESS	GOBP_CELL_CYCLE
20	GOBP_CELLULAR_AMIDE_METABOLIC_PROCESS	GOBP_CELL_CYCLE	GOMF_DNA_BINDING_TRANSCRIPTION_FACTOR_ACTIVITY

GOMF= GO Molecular Function; GOBP= GO Biological Process; GOCC= GO Cellular Component. Orange= Enriched in Low and High venetoclax treated cells.

Besides enriched pathways, also individual genes were examined. The top 10 genes with negative CSS values are listed in table 4.3. A list of panessential genes was provided by the laboratory of Prof. Staudt. Genes which were panessential according to this list were not included into the analysis. However, some of the genes which were essential for DMSO-treated Maver-1 cells were panessential genes according to the database depmap.org (for example RPS8 and RPL35). Therefore, it was important to analyse candidate genes in detail before subsequent experiments were planned.

Genes which appeared in more than one data set are highlighted in orange. These are *SLN*, *PKN2*, *PDK3*, *ZNF573*, *P2RX5* and *MARCH5*. The functions of the corresponding proteins are listed in table 4.4. The proteins corresponding to these genes do not seem to be functionally linked to each other.

Furthermore, top 50 genes were searched for genes belonging to the BCL-2 family. In Low venetoclax treated cells, *BCL2L1* was found among the top 50 genes with negative CSS value. *PMAIP1* and *BAX* were found among the top 50 genes with positive CSS value.

Table 4.3: **Top 10 genes with negative CSS values for DMSO, low and high venetoclax treated cells, respectively. Mean CSS values from two biological replicates are given. Genes which appear in low and high venetoclax treated cells are highlighted in orange.**

DMSO		Low venetoclax treated		High venetoclax treated	
Gene	**CSS**	**Gene**	**CSS**	**Gene**	**CSS**
RPS26	-5.07	*SLN*	-3.82	*PKN2*	-4.303
CDK4	-4.87	*TRAF3*	-3.568	*MARCH5*	-3.395
RPS8	-4.713	*OR10V1*	-3.541	*P2RX5*	-3.193
RPL35	-4.509	*PKN2*	-3.506	*GPRIN1*	-3.145
RPS15	-4.431	*GPR78*	-3.506	*SLN*	-3.141
COX17	-4.372	*PDK3*	-3.404	*OTUD7A*	-3.078
EEF1A1	-4.124	*ZNF573*	-3.216	*PDK3*	-3.018
POU2AF1	-4.121	*FAM134C*	-3.064	*MAP3K13*	-2.998
POLR2J	-3.949	*P2RX5*	-3.035	*GEMIN6*	-2.977
WASH1	-3.891	*MARCH5*	-2.999	*ZNF573*	-2.96

Table 4.4: **Protein functions of corresponding genes which are among the top 10 genes with negative CSS values in both low and high venetoclax treated cells.**

Gene	Protein name	Protein function
SLN	Sarcolipin	Component of sarcoplasmic reticulum, catalyses ATP-dependent Ca2+ transport
PKN2	Protein Kinase N2	Serine/threonine-protein kinase and Rho/Rac effector protein
PDK3	Pyruvate Dehydrogenase 3	Component of pyruvate dehydrogenase complex
ZNF573	Zinc Finger Protein 573	Transcriptional regulation
P2RX5	Purinergic Receptor P2X 5	ATP receptor and ligand-gated ion channel
MARCH5	Membrane Associated Ring-CH-Type Finger 5	Mitochondrial E3 ubiquitin ligase

Top 10 individual genes with positive CSS values for each data set were analysed likewise. As detailed in table 4.5, *ATP1B3* (Na^+/K^+ and H^+/K^+ ATPase), *CRACR2B* (plays a role in store-operated Ca^{2+} entry) and *NBL1* (possible candidate as a tumour suppressor gene of neuroblastoma) appeared in both low and high venetoclax treated cells.

Table 4.5: **Top 10 genes with positive CSS values for DMSO, low and high venetoclax treated cells, respectively. Mean CSS values of two biological replicates are given. Genes which appear in more than one data set are highlighted in orange.**

DMSO		Low venetoclax treated		High venetoclax treated	
Gene	**CSS**	**Gene**	**CSS**	**Gene**	**CSS**
GPR107	2.328	*ATP1B3*	2.486	*ATP1B3*	2.373
MYO6	2.054	*EMC7*	2.458	*CRACR2B*	2.208
MEX3C	1.992	*CRACR2B*	2.401	*LCP1*	2.137
HYPM	1.977	*VCPIP1*	2.256	*CDH7*	2.003
ZNF879	1.963	*NBL1*	2.053	*NBL1*	1.997
SHROOM4	1.955	*GPATCH8*	2.046	*ZNF622*	1.905
ATP8B4	1.952	*METTL23*	1.998	*CHURC1*	1.883
HGC6.3	1.931	*FAM72C*	1.947	*PGM2L1*	1.878
GK2	1.880	*AGPAT2*	1.930	*NDUFC2-KCTD14*	1.840
ERGIC1	1.871	*ZC3H7B*	1.901	*POLR3E*	1.799

A brief literature research revealed few studies which investigated MARCH5 as a potential regulator of intrinsic apoptosis, as it was linked to regulation of a MCL-1/NOXA axis. This finding fitted into the context of venetoclax as a BCL-2 specific inhibitor. None of the other genes which were found in both low and high venetoclax treated cells displayed such a connection to BCL-2. It was therefore reasonable to examine MARCH5 in further experiments.

4.1.4 Validation of venetoclax sensitisation of MCL cells upon MARCH5 knockout

In order to validate the findings from the CRISPR/Cas9-based loss-of-function screen, the four sgRNA sequences targeting MARCH5 provided in the Brunello library were cloned into the pLKO.1-puro-GFP vector. Cells were transduced with all four constructs as well as a non-targeting control (sgNTC). Efficiency of MARCH5 knockout was evaluated for each construct. Transduction with sgMARCH5_2 and sgMARCH5_4 revealed the best MARCH5 knockouts. These two sgRNA sequences were therefore used for further knockout experiments.
A competitive growth assay was performed with Maver-1 cells transduced with pLKO.1-puro-GFP-sgNTC, -sgMARCH5_2 and –sgMARCH5_4. Transduced and non-transduced cells were co-cultured in complete medium containing either DMSO or 0.3 nM venetoclax over 14 days while the percentage of GFP-positive cells was monitored every second day. This assay was additionally performed in Jeko-1 and Mino cells, which were treated with either DMSO or 10 nM venetoclax. As depicted in Figure 4.5, MARCH5 knockout seemed to bear a growth disadvantage for the tested cells. The growth disadvantage was even more pronounced when MARCH5-depleted cells were additionally treated with venetoclax, which indicates sensitisation towards venetoclax treatment upon MARCH5 deletion. Interestingly, this also applied to Jeko-1, even though these cells were more resistant towards venetoclax than Maver-1 and Mino in their respective wild-type form.

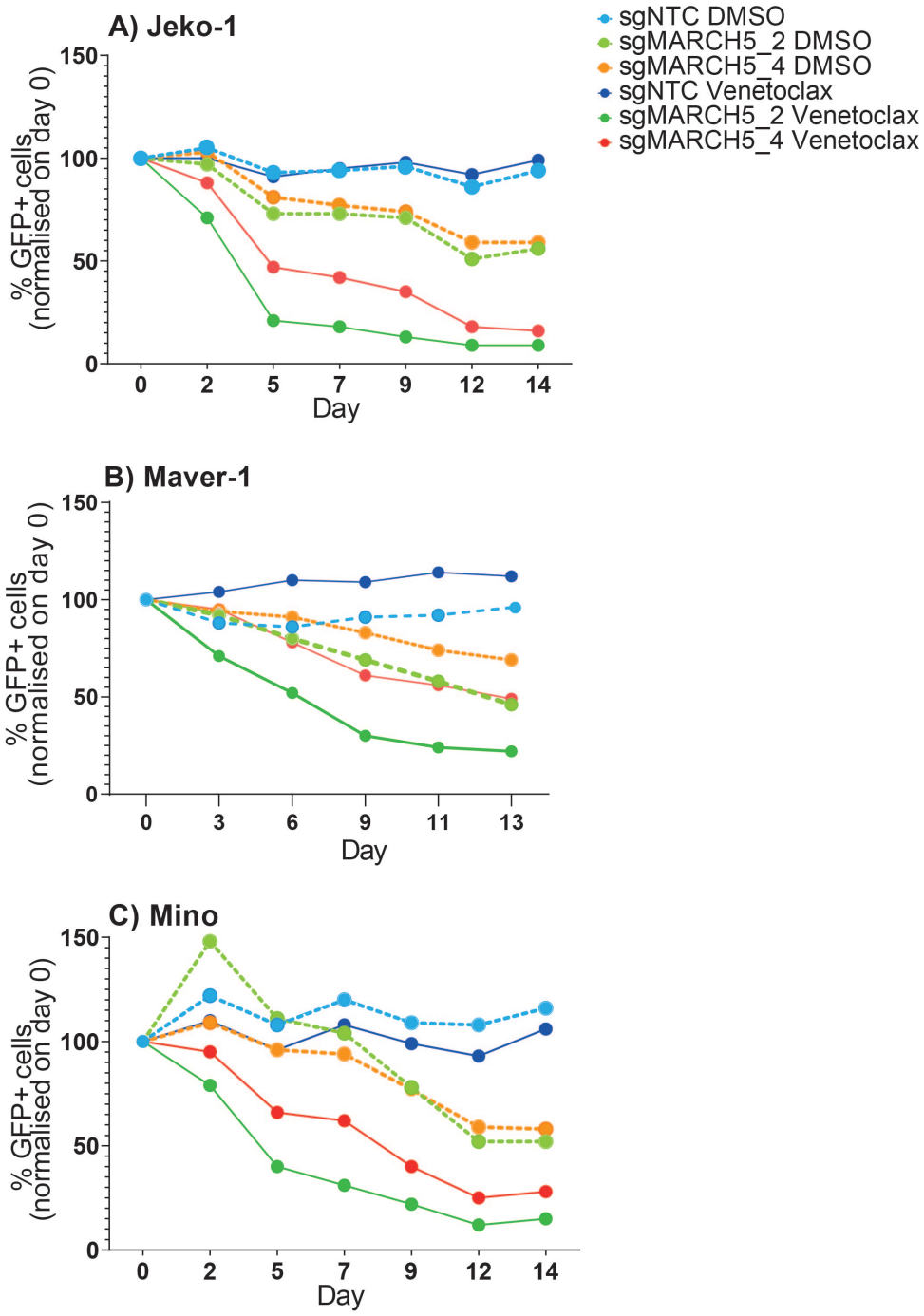

Figure 4.5: **MCL cell lines were sensitised towards venetoclax upon MARCH5 knockout. Jeko-1 (A), Maver-1 (B) and Mino (C) cells were transduced with pLKO-puro-GFP-sgNTC or two constructs targeting MARCH5 (pLKO-puro-GFP-sgMARCH5_2, -sgMARCH5_4) and co-cultured with wild-type cells in complete medium containing either DMSO or venetoclax. Percentage of GFP$^+$ cells was monitored over 14 (Maver-1 13) days. One representative experiment of three biological replicates per cell line is depicted.**

4.1.5 Activation of caspase activity upon MARCH5 knockout

A growth disadvantage of MARCH5-depleted cells in comparison to wild-type cells was observed in the competitive growth assay, especially under venetoclax treatment. This phenomenon could be attributed to either impaired proliferation or induction of apoptosis. In order to address this question, Jeko-1, Maver-1 and Mino cells were treated with either DMSO, 0.3 nM (Maver-1) or 10 nM (Jeko-1, Mino) venetoclax for 6 h and analysed via Western blot subsequently. Caspase 3 is an executioner caspase which upon cleavage contributes to execution of cellular destruction. Poly-(ADP-ribose)-polymerase (PARP) is a direct target of caspase 3. Cleavage of these proteins indicates activation of apoptosis. As depicted in Figure 4.6, caspase 3 and PARP were both cleaved upon MARCH5 depletion, and the proportion of cleaved protein was further increased upon additional venetoclax treatment. This finding verified that cells undergo apoptosis upon MARCH5 depletion, which was even more induced upon additional venetoclax treatment.

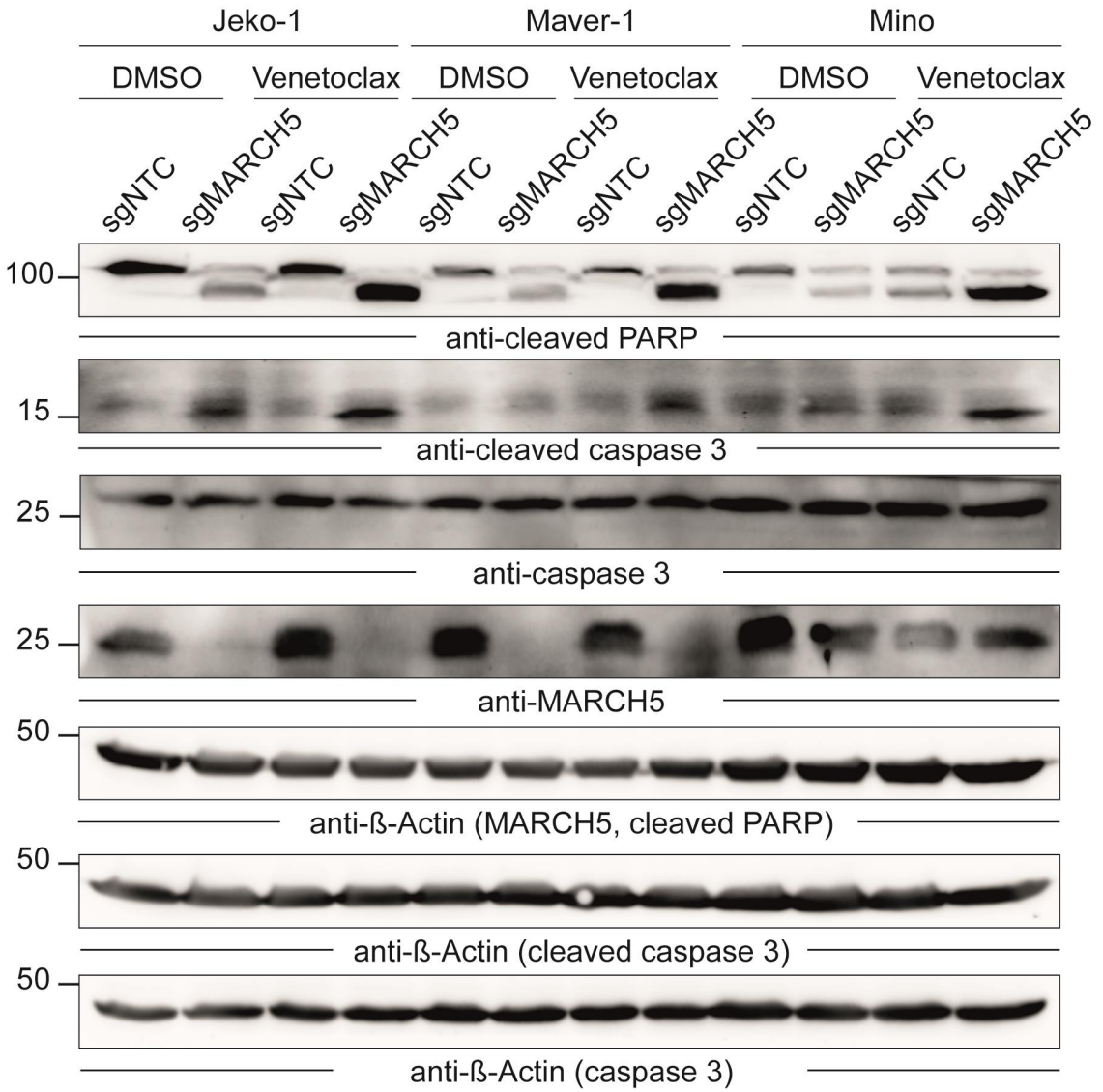

Figure 4.6: **Apoptosis was induced in MCL cell lines upon MARCH5 depletion and additional venetoclax treatment. pLKO.1-puro-GFP-sgNTC- and -sgMARCH5-transduced Jeko-1, Maver-1 and Mino cells were treated with either DMSO or venetoclax for 6 h. Subsequently, levels of cleaved PARP, cleaved caspase 3 and total caspase 3 levels were analysed via Western blot. The antibody used to detect cleaved PARP bound to both cleaved and full length PARP, which led to the appearance of a double band on the Western blot. The upper band belongs to full length PARP, the lower one to cleaved PARP. β-Actin served as loading control. One representative Western blot of two biological replicates is shown.**

4.1.6 Verification of BCL-2-dependency of MARCH5-depleted cells using BH3 profiling

Jeko-1 and Maver-1 cells were transduced with pLKO.1-puro-GFP-sgNTC and -sgMARCH5_2. The dependency of these cells towards individual BCL-2 family members was evaluated utilizing BH3 profiling. This method measures cytochrome c release upon treatment of the cells with peptides mimicking pro-apoptotic BCL-2 family proteins. The measurements were conducted by Dr. K. Bojarczuk in the laboratory of Prof. Chapuy at the university hospital in Göttingen.
Two positive controls were included in this assay: BIM is a control for the capability of the tested cells to generally undergo BAX/BAK-dependent apoptosis. Cytochrome c release levels should reach 90-100% upon application of BIM, otherwise the tested cells are deficient of intrinsic apoptosis. Alamethicin is a positive control for the assay itself, as it induces cytochrome c release independent of BAX/BAK. BAD peptide targets BCL-2 and BCL-XL; HRK targets BCL-XL only. Therefore BCL-2 dependency can be extrapolated by subtracting HRK response from BAD response. MS1 targets MCL-1. PUMA peptide serves as control for general apoptotic priming of a cell. Furthermore, venetoclax (ABT-199) was applied to the cells in the indicated concentrations for one hour.
The results for BH3 profiling of pLKO.1-puro-GFP-sgNTC- and -sgMARCH5-transduced Jeko-1 and Maver-1 cells are shown in Figure 4.7.

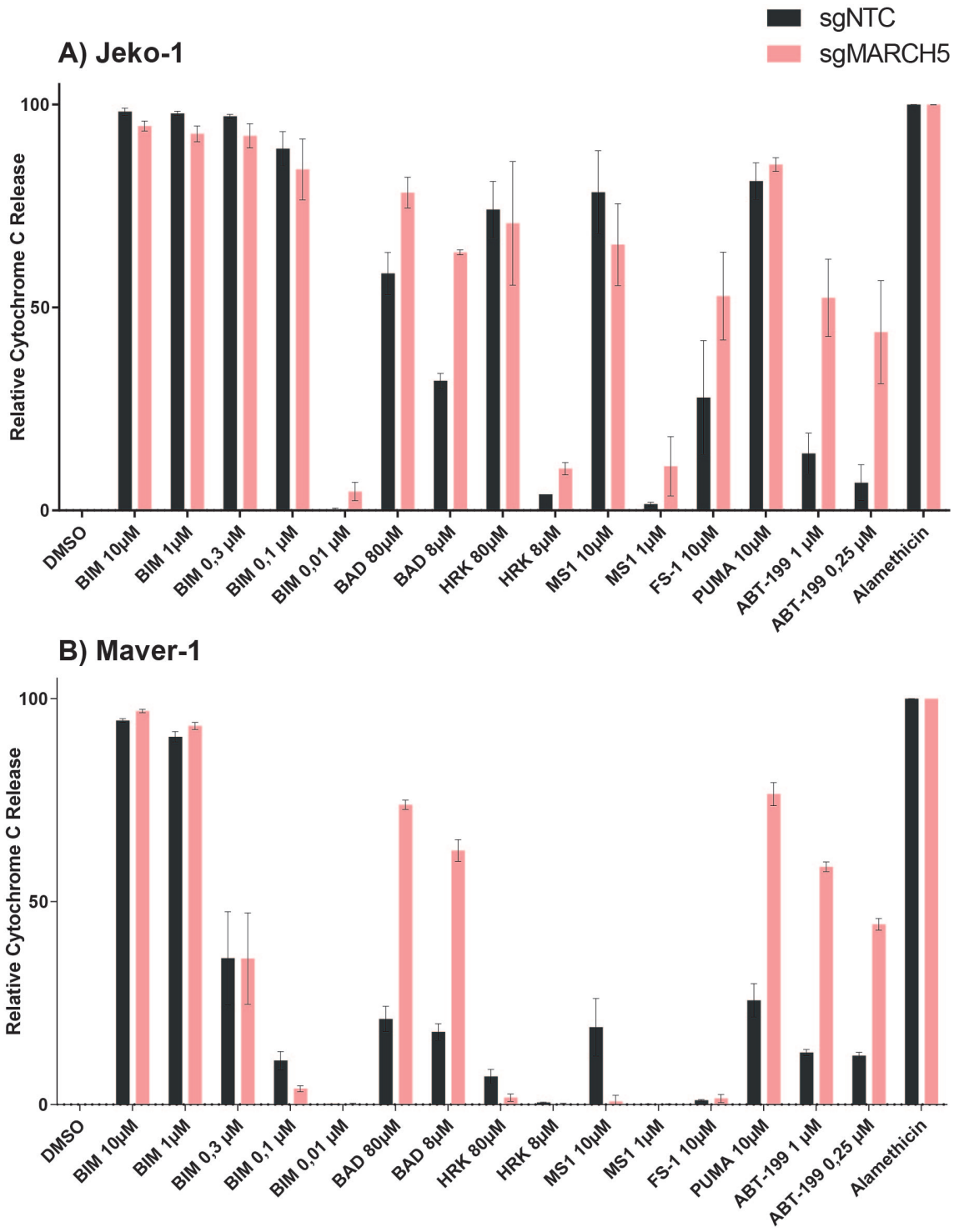

Figure 4.7: **pLKO.1-puro-sgNTC or -sgMARCH5_2 transduced Jeko-1 (A) and Maver-1 (B) cells were subjected to BH3 profiling. Mean of 4 technical replicates +/- SD is shown. MARCH5 depleted cells (red bar) were sensitised towards BCL-2 inhibition in comparison to control cells (black bar).**

Generally, Jeko-1 and Maver-1 both were capable of undergoing intrinsic apoptosis, since cytochrome c release levels reached 90-100% upon application of BIM peptide. Also the alamethicin assay control resulted in high cytochrome c release. Maver-1 clearly showed increased BCL-2 dependency upon MARCH5 depletion, since the level of cytochrome c release was enhanced upon application of BAD but not HRK peptide. In Jeko-1 on the other hand, response to HRK peptide was much higher than in Maver-1 cells. The response remained unaltered upon MARCH5 knockout. Response to BAD was increased upon MARCH5 knockout, which indicated BCL-2 dependency of MARCH5-depleted Jeko-1 cells. Concerning dependency on MCL-1, Jeko-1 displayed high responsiveness to MS1 peptide. However, MS1 was applied in two concentrations (10 and 1 µM, respectively). Upon application of 10 µM, MARCH5-depleted cells seemed to be slightly less sensitive to MCL1 inhibition, while this effect was inversed upon application of the lower concentration of MS1 peptide. Maver-1 cells displayed a low response of pLKO.1-puro-GFP-sgNTC-transduced cells upon application of 10 µM MS1 peptide while all other conditions did not provoke cytochrome c release. Interpretation of MCL-1 dependency of these two cell lines therefore was inconclusive. Cytochrome c release levels upon application of PUMA peptide represents general apoptotic priming of the cells. Jeko-1 cells displayed a high level of general priming, which remained unaltered upon MARCH5 knockout. General priming of Maver-1 on the other hand was low in pLKO.1-puro-GFP-sgNTC-transduced cells and was increased upon MARCH5 depletion.
Taken together, both Jeko-1 and Maver-1 were sensitised towards BCL-2 inhibition upon MARCH5 knockout which confirmed the findings from the CRISPR/Cas9-based loss-of-function screen and the competitive growth assay.
BH3 profiling was furthermore conducted with Mino cells (data not shown). These cells displayed an extraordinary high response towards application of BAD peptide even without depletion of MARCH5. Sensitisation towards BCL-2 inhibition could therefore not be evaluated in these cells.

4.1.7 MARCH5-depleted cells displayed enhanced levels of MCL-1 and NOXA protein

In order to examine a possible functional connection between MARCH5, MCL-1 and NOXA (as proposed by other studies), Jeko-1, Maver-1 and Mino were transduced with pLKO.1-puro-sgNTC or sgMARCH5_2 and treated with either DMSO as a control or 0.3 (Maver-1) or 10 nM (Jeko-1, Mino) venetoclax for 6 h. The lysates were analysed for MCL-1, NOXA, MARCH5 and BCL-2 expression via Western blot. As to be seen in Figure 4.8, MCL cell lines displayed MCL-1 and NOXA

upregulation upon MARCH5 knockout. MCL-1 and NOXA levels were not altered upon application of venetoclax. Interestingly, levels of BCL-2, the direct target of venetoclax, remained unchanged upon either knockout of MARCH5 or treatment of the cells with venetoclax.

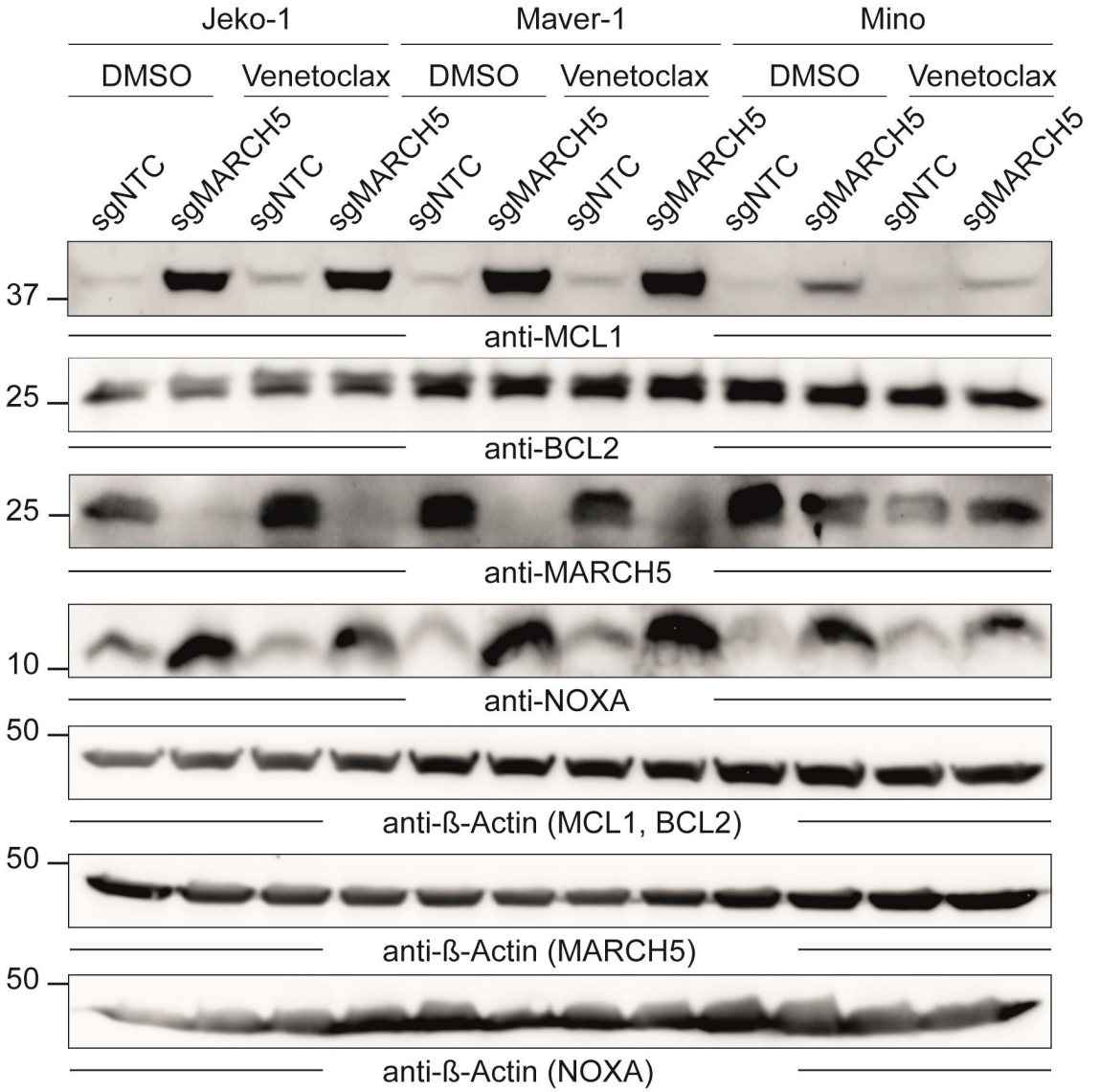

Figure 4.8: **MCL-1 and NOXA levels were increased upon MARCH5 knockout. pLKO.1-puro-GFP-sgNTC- and sgMARCH5-transduced Jeko-1, Maver-1 and Mino cells were treated with either DMSO or venetoclax for 6 h and subsequently analysed via Western blot. In all tested cell lines, MCL-1 and NOXA levels were increased upon MARCH5 knockout. Levels of these proteins were independent of venetoclax treatment. BCL-2 levels remained unchanged by either MARCH5 knockout or BCL-2 inhibition. β-actin served as loading control. One representative Western blot of three biological replicates is shown.**

To address the question whether upregulation of MCL-1 and NOXA levels was due to transcriptional regulation or due to protein stabilisation, Jeko-1, Maver-1 and Mino cells were transduced with pLKO.1-puro-GFP-sgNTC and -sgMARCH5_ 2 and treated with either DMSO or venetoclax (Jeko-1 and Mino 10 nM, Maver-1 0.3 nM) for 6 h. Subsequently, RNA was isolated from the cells and reversely transcribed to cDNA. Expression levels of *MCL1*, *PMAIP1* (encoding NOXA), and *MARCH5* were evaluated via qRT-PCR. Figure 4.9 illustrates that levels of *MCL1* and *PMAIP1* display certain minor variations but overall remain stable upon *MARCH5* knockout. This indicates that increased protein levels of MCL-1 and NOXA upon MARCH5 knockout might be due to stabilisation by post-translational modifications.

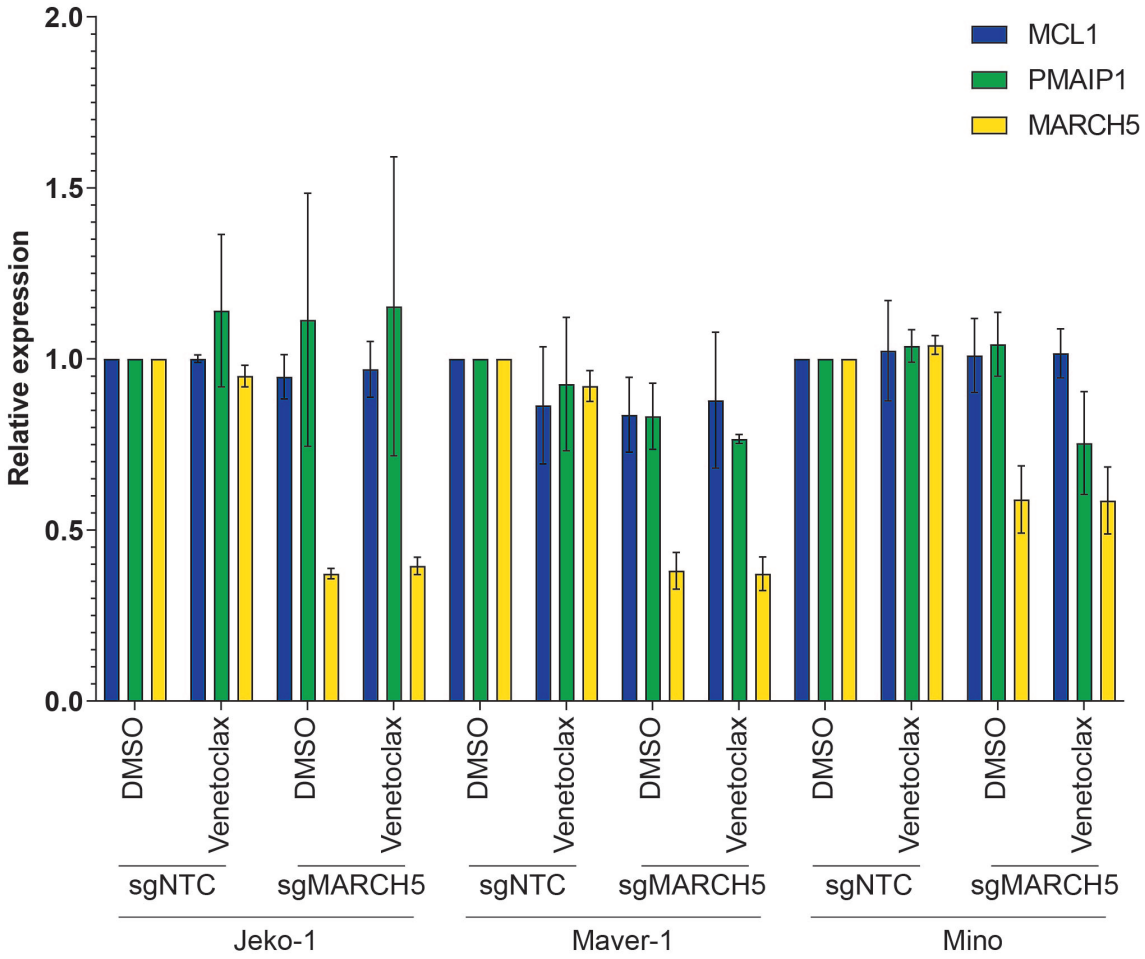

Figure 4.9: **Expression levels of *MCL1* and *PMAIP1* (encoding NOXA) remained stable upon *MARCH5* knockout. qRT-PCR analysis of pLKO.1-puro-GFP-sgNTC or -sgMARCH5 transduced Jeko-1, Maver-1 and Mino cells upon treatment with either DMSO or venetoclax (Jeko-1, Mino 10 nM; Maver-1 0.3 nM) for 6 h. Expression levels of *MCL1*, *PMAIP1*, *MARCH5* and *GAPDH* were analysed. ΔΔCT values (relative expression levels) for *MCL1*, *PMAIP1* and *MARCH5* were calculated by normalisation of the respective ΔCT values on *GAPDH* expression in pLKO.1-puro-sgNTC-transduced, DMSO-treated cells of the respective cell line. Mean of 3 biological replicates +/- SD is shown.**

4.1.8 Simultaneous depletion of MARCH5 and NOXA partly reversed effects of MARCH5 knockout

After fundamental characteristics of MARCH5-depleted cells were evaluated, the exact mechanism of BCL-2 sensitisation was aimed to be addressed. NOXA as a pro-apoptotic protein was considered to play a major role in this mechanism. It was hypothesised that effects of MARCH5 depletion could be reversed upon simultaneous knockout of NOXA. This hypothesis was tested in a competitive growth assay

with MARCH5 and NOXA double-knockout Jeko-1 and Maver-1 cells with venetoclax or DMSO treatment. For this, cells were transduced with two sgRNA transfer vectors (pLKO.1-puro-GFP/pLKO-neoBFP) targeting MARCH5, NOXA or a non-targeting control. In this manner, four conditions were created: a pure control (NTC/NTC), a pure MARCH5 knockout (MARCH5/NTC), a pure NOXA knockout (NTC/NOXA) and a MARCH5-NOXA double-knockout (MARCH5/NOXA). Results of the competitive growth assays are shown in Figure 4.10. For both cell lines, treatment of MARCH5-depleted cells (MARCH5/NTC) with venetoclax resulted in a fast and severe growth disadvantage. Under DMSO treatment, the growth disadvantage was less pronounced. These findings correspond to the findings in Figure 4.5. A partial rescue effect could be observed when Jeko-1 or Maver-1 cells were treated with venetoclax upon MARCH5 and NOXA double-knockout.

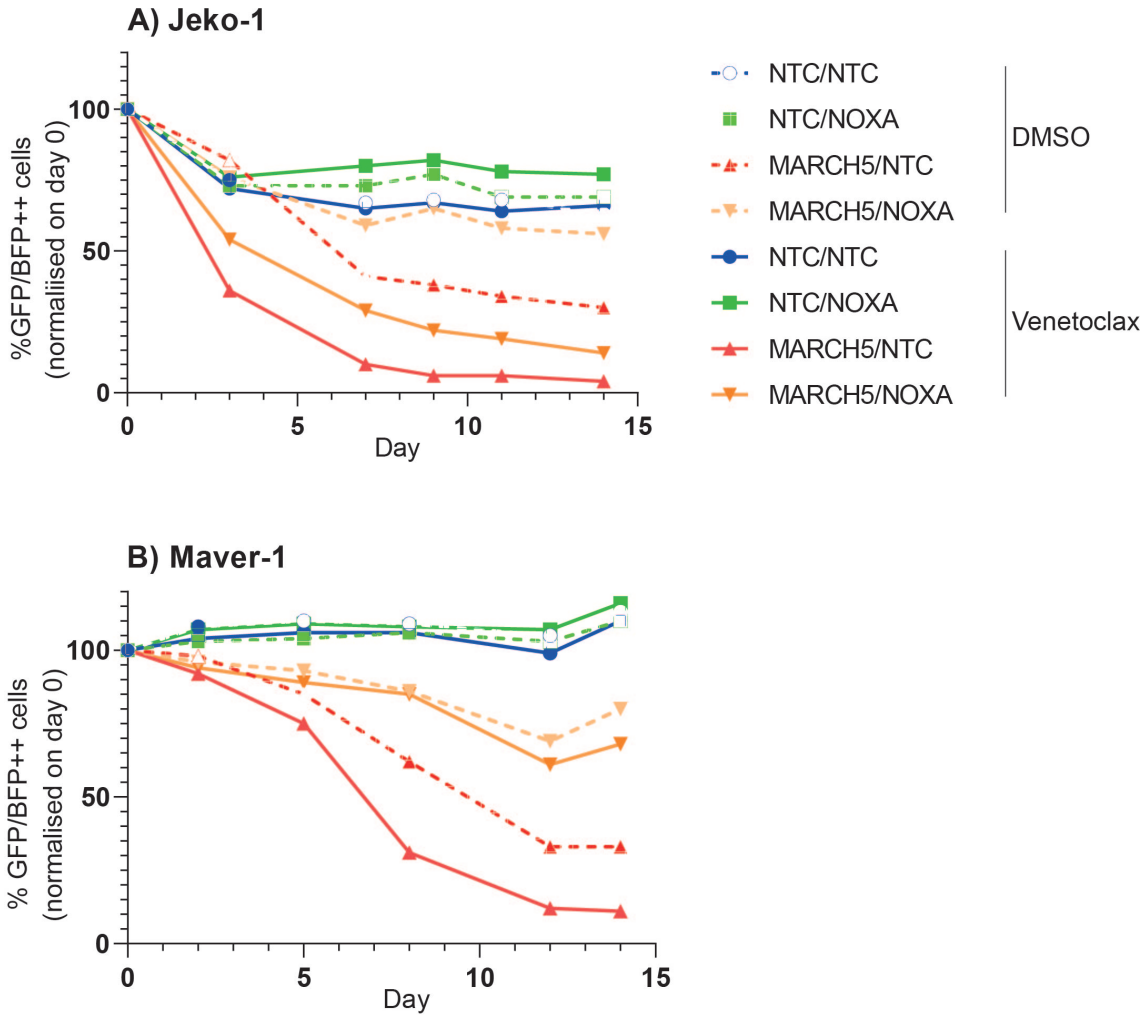

Figure 4.10: **Additional NOXA knockout partly reverted BCL-2 sensitisation upon MARCH5 depletion. Competitive growth assay of Jeko-1 and Maver-1 cells transduced with combinations of sgMARCH5, sgNOXA and sgNTC and additional DMSO or venetoclax (Jeko-1 10 nM; Maver-1 0.3 nM) treatment. One representative result of two biological replicates is shown.**

4.1.9 Analysis of MARCH5-interacting proteins

The BioID2 method is a valuable tool to find possible interactors of a protein of interest. To this end, the protein of interest (MARCH5) was fused to a biotin ligase. The fusion protein or the empty vector was expressed in the target cells. The empty vector-transduced cells served as a negative control. All proteins which came into close proximity of MARCH5 were biotinylated by the biotin ligase. Biotinylated proteins were enriched using streptavidin-coated beads and subsequently analysed via mass spectrometry.

Following transduction and selection for transduced Jeko-1 and Maver-1 cells, empty vector-transduced cells were labelled with SILAC light medium; MARCH5-fusion protein transduced cells were labelled with SILAC medium and heavy cell culture medium. Light-labelled cells were left untreated, medium-labelled cells were treated with DMSO as a control and heavy-labelled cells were treated with 10 nM (Jeko-1) or 0.3 nM (Maver-1) venetoclax for 6 h. Additionally, each condition was divided into two approaches: one was treated with the proteasome inhibitor MG-132 while the other one was left untreated. Two separate IPs were performed and analysed via mass spectrometry.
Noticeably, the MG-132 treated cells yielded much less MARCH5-interacting proteins. The following results therefore are based on the non-MG-132 treated cells.
One major aim of this experiment was to validate the interaction between MARCH5, MCL-1 and NOXA. Since a MARCH5 IP failed to be established, this interaction needed to be validated using an alternative method. In Maver-1 cells, MCL-1 was identified as a MARCH5-interacting protein. In Jeko-1 cells, this interaction was not identified. NOXA was not identified in any of the samples. NOXA is a very small protein with a mass of 6 kDa, which yields only two tryptic peptides. Therefore, NOXA is especially difficult to identify via mass spectrometry. Absence of NOXA in the MARCH5 interactome might therefore be a measurement artefact.
Besides MCL-1, four more BCL-2 family proteins were identified as MARCH5 interactors in Maver-1 cells: BIM (encoded by *BCL2L11*), BCL2L13, BAX and BCL-2. These proteins were only identified in Maver-1 but not in Jeko-1 cells. Additionally, some of the known MARCH5 interactors were identified, such as MFF, Drp-1 (encoded by *DNM1L*), MAVS. This finding confirmed the effectivity of the BioID2 method. In Figure 4.11, MARCH5-interacting BCL-2 family proteins and known interactors which were identified in Maver-1 cells are depicted.

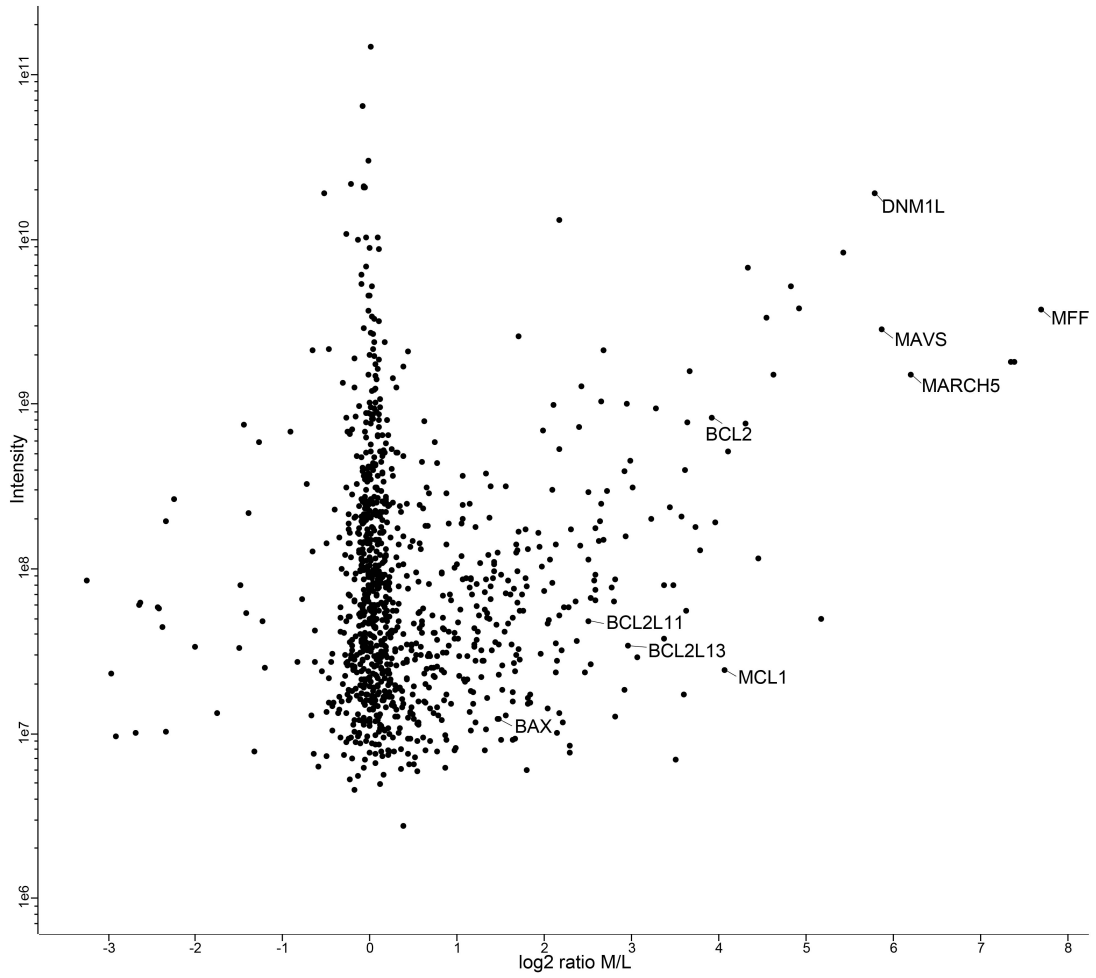

Figure 4.11: **MARCH5 interactome in Maver-1 cells. BioID2 empty vector transduced cells were labelled with SILAC light cell culture medium, BioID2-MARCH5 construct transduced cells were SILAC medium and heavy labelled. Light labelled cells were left untreated, medium labelled cells were treated with DMSO, and heavy labelled cells were treated with 0.3 nM venetoclax for 6 h. Biotinylated proteins were immunoprecipitated and analysed by mass spectrometry. BCL-2 family proteins as well as known MARCH5 interacting proteins are marked.**

In order to obtain an overview about potential networks between MARCH5 interacting proteins, a STRING analysis using the online platform string-db.org was conducted. For this, only proteins with log2 ratios ≥ 1 were analysed. In the STRING analysis, the minimum interaction score was set to 0.4 (medium).

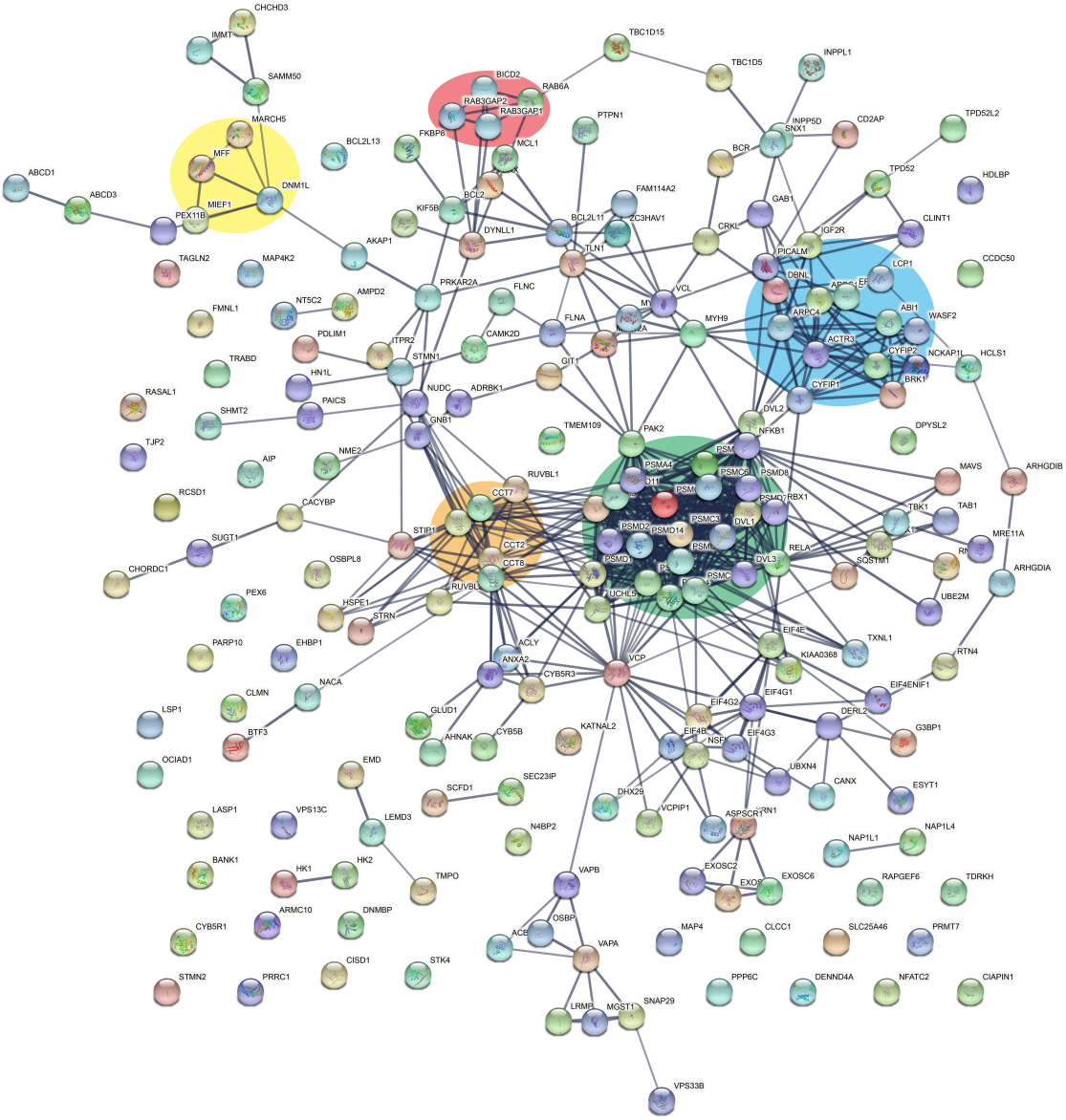

Figure 4.12: **STRING analysis of MARCH5-interacting proteins identified in DMSO-treated Maver-1 cells using the online tool string-db.org. Only proteins with a log2 ratio of $\leq$1 were subjected to this analysis. The minimum interaction score was set to a confidence of 0.4 (medium confidence). Five potential functional clusters are marked in either yellow, red, blue, green or orange.**

As to be seen in Figure 4.12, five potential functional clusters were found:

- Yellow cluster: proteins such as MARCH5 itself, MFF and DNM1L. These proteins regulate mitochondrial morphology.
- Red cluster: BICD2, RAB3GAP2, RAB3GAP1 and RAB6A. In this cluster, proteins which activate Rab GTPases are found.
- Blue cluster: proteins such as ARPC4, ACTR3, BRK1 and DBNL. These

proteins are involved in actin polymerisation.

- Green cluster: proteins such as PSMD8, PSMC6, PSMD14 and PSMA4. These are components of the 26S proteasome.
- Orange cluster: proteins such as CCT7, CCT2, CCT8. These proteins belong to a molecular chaperone.

Rab GTPases (red cluster) and actin polymerisation (blue cluster) are again functionally linked to the regulation of vesicle trafficking.

The same analysis was performed for venetoclax treated Maver-1 cells as well as DMSO and venetoclax treated Jeko-1 cells (data not shown). Here, the same pattern of clusters was observed.

4.1.10 Analysis of MARCH5-dependent ubiquitination

Many potential MARCH5-interacting proteins were identified in the MARCH5 interactome. However, the BioID2 method is not suitable to define proteins which are effectively ubiquitinated by MARCH5. In order to address this question, an ubiquitinome analysis utilising the TMT method was conducted. For this, Jeko-1 cells were transduced with pLKO.1-puro-GFP-sgNTC or -sgMARCH5_2 and treated with DMSO or 10 nM venetoclax for 6 h. Additionally, each condition was split into two halves, one half was left untreated, while the other half was treated with 10 μM MG-132 for 3 h. Cells were lysed with urea lysis buffer and submitted to the mass spectrometry unit.
Log2 fold changes of ubiquitination were calculated and normalised to pLKO.1-puro-GFP-sgNTC-transduced cells. Cutoff values for significantly up- or downregulated ubiquitination were set to 0.5 and -0.5, respectively. In total, approx. 10,500 ubiquitination sites were identified. For both DMSO- and venetoclax-treated cells, approx. 10% of the identified ubiquitination sites were significantly downregulated and approx. 17% were significantly upregulated.
Regulation of BCL-2 family proteins was of special interest in this experiment. In table 4.6, all BCL-2 family proteins identified in the ubiquitinome analysis are given. Several ubiquitination sites in MCL-1 and one site each for NOXA (*PMAIP1*), BCL2A1 and BCL2L13 were identified. One of three ubiquitination sites in MCL-1 (K238) was significantly less ubiquitinated in MG-132 and MG-132 + venetoclax-treated cells. NOXA ubiquitination was significantly downregulated in DMSO-, MG-132- and MG-132 + venetoclax-treated cells. BCL2A1 and BCL2L13 ubiquitination remained unchanged.

Table 4.6: **MARCH5-dependent ubiquitination of BCL-2 family proteins. Red marked values indicate changes of ubiquitination below cut-off value (-0.5). Mean log2 fold change values, normalised on similarly treated pLKO.1-puro-GFP-sgNTC-transduced Jeko-1 cells are given.**

Ubiq. site	sgMARCH5 DMSO	sgMARCH5 MG132	sgMARCH5 venetoclax	sgMARCH5 venetoclax MG-132
MCL1 K234	-0.29	-0.08	-0.29	-0.29
MCL1 K279	-0.26	-0.3	-0.29	-0.26
MCL1 K238	-0.45	-0.78	-0.26	-0.9
PMAIP1 K48	-0.62	-1.28	-0.23	-0.69
BCL2A1 K53	-0.02	-0.17	-0.13	0.32
BCL2L13 K116	-0.19	0.31	0.14	0.06

As a next step, the functional impact of MARCH5 depletion with or without additional venetoclax treatment was analysed. For this, GSEA was conducted. In order to concentrate on proteins which were ubiquitinated in a MARCH5-dependent manner, only proteins which were significantly less ubiquitinated in MARCH5-depleted cells were included in this analysis. Significantly upregulated ubiquitination was regarded as a compensatory mechanism, which was apparently not MARCH5-dependent. In Figure 4.13, gene sets which were enriched in both DMSO- and venetoclax-treated cells are detailed. For each class, -Log10 p-values are given. Notably, -Log10 p-values are increased for venetoclax-treated cells for most of the gene sets.

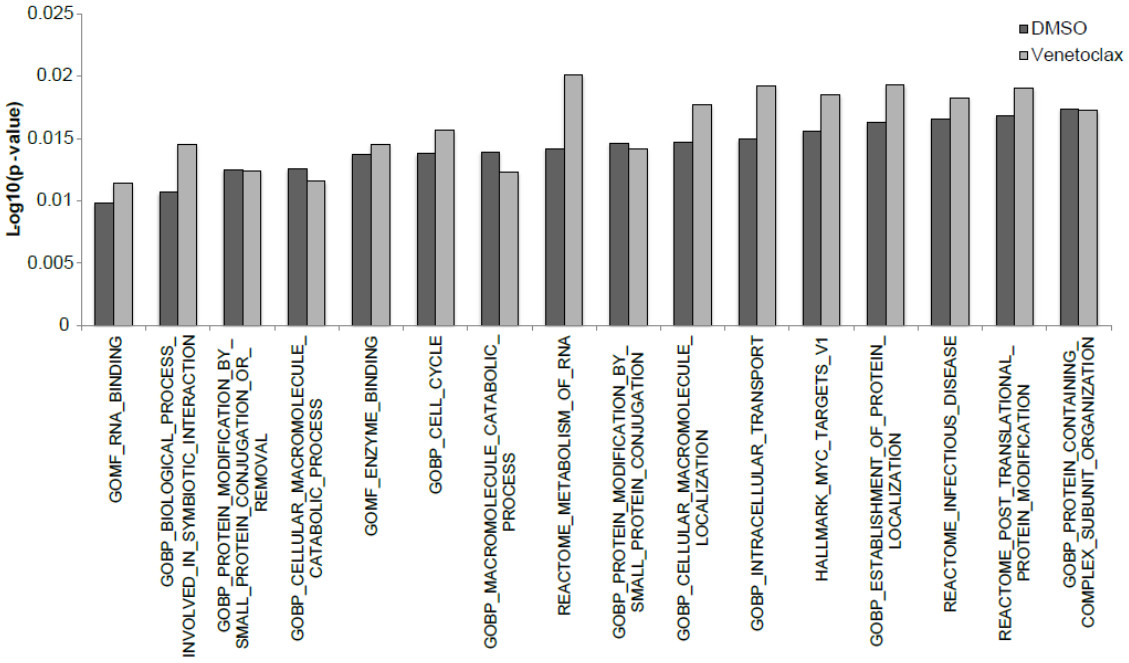

Figure 4.13: **Gene sets enriched in DMSO- and venetoclax-treated MARCH5-depleted Jeko-1 cells. GSEA was conducted for all significantly less ubiquitinated sites in DMSO- and venetoclax-treated cells. All gene sets which were enriched in both treatments are given with their respective Log10 p-value.**

Overall, gene sets which were enriched in DMSO- and venetoclax-treated cells can be allocated to the following contexts:

- RNA metabolism
- Posttranslational modifications
- Intracellular transport, metabolism and localisation of (macro-) molecules
- Cell cycle regulation

Additionally, some gene sets were enriched in DMSO- or venetoclax-treated cells only, indicating that the respective pathway was exclusively targeted by the respective treatment.

Gene sets which were enriched in DMSO- but not in venetoclax-treated cells:

- REACTOME_CELL_CYCLE
- REACTOME_CELL_CYCLE_MITOTIC
- REACTOME_CELLULAR_RESPONSES_TO_EXTERNAL_STIMULI

Gene sets which were enriched in venetoclax-treated cells only:

- GOBP_CELLULAR_PROTEIN_CATABOLIC_PROCESS
- GOBP_PROTEIN_CATABOLIC_PROCESS
- GOBP_REGULATION_OF_CATABOLIC_PROCESS
- GOBP_MODIFICATION_DEPENDENT_MACROMOLECULE_CATABOLIC_PROCESS

In DMSO-treated cells, there was a clear focus on cell cycle regulation, while in venetoclax-treated cells, mainly catabolic processes, probably proteasomal degradation, was regulated.
Finally, integration of interactome data and the ubiquitinome analyses was conducted (see Figure 4.14) The cutoff values defined in the respective sections were applied. Noticeable, the set of MARCH5-interacting proteins is not fully overlapping with the set of proteins identified in the ubiquitinome analysis. Therefore, the results of this data integration need to be carefully evaluated. MARCH5-interacting proteins which showed increased ubiquitination did not seem to be functionally connected to each other. MARCH5-interacting proteins which displayed decreased ubiquitination upon MARCH5 depletion on the other hand, seemed to be functionally connected to a certain extend. Here, some components of the 26S proteasome (for example PSMA3, PSMC6) could be found, additionally some ATPases such as RUVBL1 and RUVBL2. Components involved in vesicular trafficking which were identified in the MARCH5 interactome did not seem to be regulated in their ubiquitination.

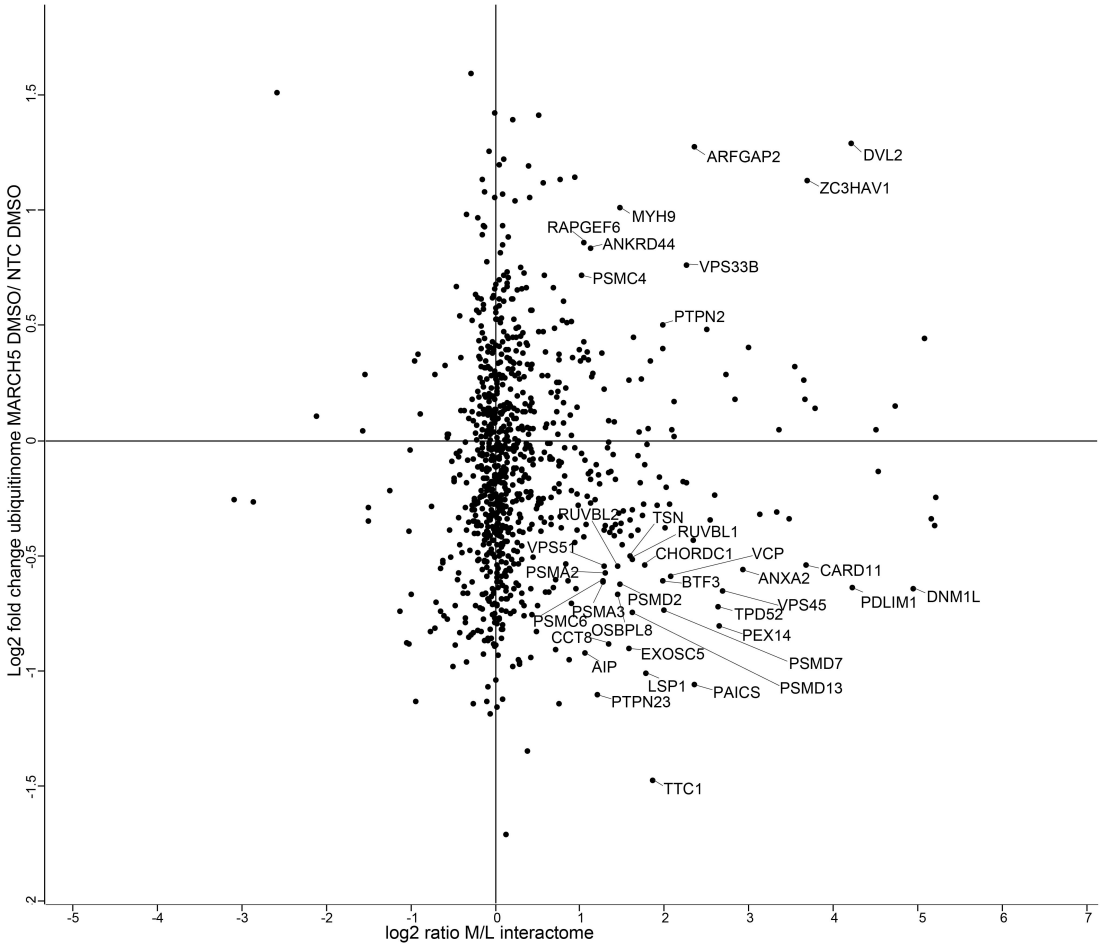

Figure 4.14: **Integration of data from MARCH5-dependent ubiquitinome and interactome analysis. All MARCH5-interacting proteins (cutoff value = 1) were mapped against the changes in ubiquitination (cutoff values 0.5 and -0.5 for significant up- and downregulation of ubiquitination, respectively).**

4.2 Role of SASH3 in DLBCL BCR signalling

4.2.1 Identification of genes with differential essentiality in ABC- and GCB-DLBC cell lines

The exact mode of BCR signalling in GCB-DLBCL cells to date is incompletely understood. The second part of the present study aimed to gain a refined view on differential BCR signalling in ABC- and GCB-DLBCL cells and to find potential new therapeutic targets within this pathway.

The collaborating laboratory of Prof. Staudt, NIH, USA, recently conducted a genome-wide loss-of-function CRISPR/Cas9 screen in a set of DLBCL cell lines, which revealed a new signalling mode in a specific subset of ABC-DLBCL cells[21]. The complete data set is published and was used as basis for a separate analysis. The genome-wide loss-of-function CRISPR/Cas9 screen was conducted in four ABC-DLBCL cell lines (HBL1, TMD8, U2932, HLY1) and four GCB-DLBCL cell lines (DOHH2, SU-DHL-4, SU-DHL-5, WSU-DLCL2). In order to identify genes which are essential for GCB-DLBCL cell lines but no for ABC-DLBCL cell lines, the mean CSS value for each gene within each DBCL subtype was calculated. Mean CSS values of ABC-DLBCL cell lines were plotted against mean CSS values of GCB-DLBCL cell lines (see Figure 4.15).

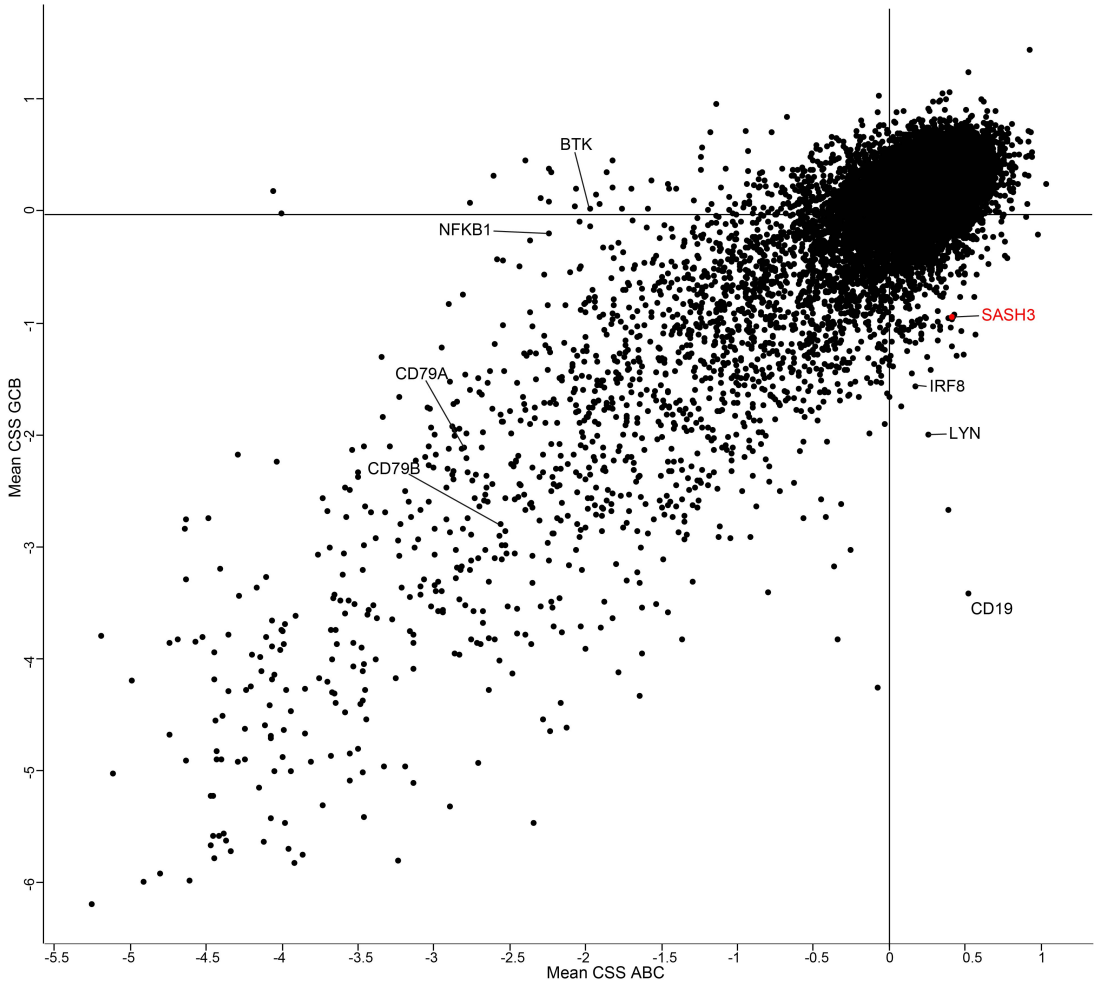

Figure 4.15: **Mean CSS values of ABC-DLBCL vs. GCB-DLBCL cell lines. Data from a genome-wide loss-of-function screen conducted by Phelan *et al.*[21] were re-analysed.**

The essentiality of certain genes which were detected in the re-analysis of the CRISPR/Cas9-based loss-of-function screen validated this analysis:

- *BTK* was found to be essential for ABC-DLBCL cell lines but not for GCB-DLBCL cell lines, which is in line with the response of the respective DLBCL subgroup to BTK inhibition with ibrutinib.

- *NFKB1* as a component of the NF-κB signalling pathway was essential for ABC-DLBC cell lines but not for GCB-DLBCL cell lines. This finding is in line with the general concept of NF-κB dependency of ABC- but not GCB-DLBCL cells.

- *CD79A* and *CD79B* were essential for both ABC- and GCB-DLBCL cell lines as the BCR is generally regarded as providing a survival signal for B-cells.

Among the genes which were essential for GCB- but not for ABC-DLBCL cells, *CD19* and *LYN* were found. GCB-DLBCL cells are known to be dependent on these two factors.
Finally, SASH3 was chosen to be examined in more detail for the following reasons:

- SASH3 has been described to be involved in TCR signalling. Since TCR and BCR signalling share common features, it was assumed that SASH3 could also play a role in BCR signalling.
- SASH3 was described as a potential adapter protein, which are common elements in the BCR signalling pathway.

4.2.2 SASH3 was essential for GCB- but not for ABC-DLBCL cell lines

In order to validate the findings from the CRISPR/Cas9-based loss-of-function screen conducted by Phelan *et al.*, four sgRNA sequences targeting SASH3 (sgSASH3_1 - _4) as provided in the Brunello library were cloned into the pLKO.1-puro-GFP vector. The best SASH3 knockout was seen for sgSASH3_1-transduced cells. This construct was therefore used for further analyses. Two ABC-DLBCL cell lines (TMD8 and Riva) and three GCB-DLBCL cell lines (DOHH2, SU-DHL-5 and WSU-DLCL2) were transduced with pLKO.1-puro-GFP-sgSASH3_1 or a non-targeting control (-sgNTC) and subjected to a competitive growth assay. As depicted in Figure 4.16, SASH3 was not essential for both ABC-DLBCL cell lines. From the three tested GCB-DLBCL cell lines, DOHH2 and SU-DHL-5 revealed dependency on SASH3.

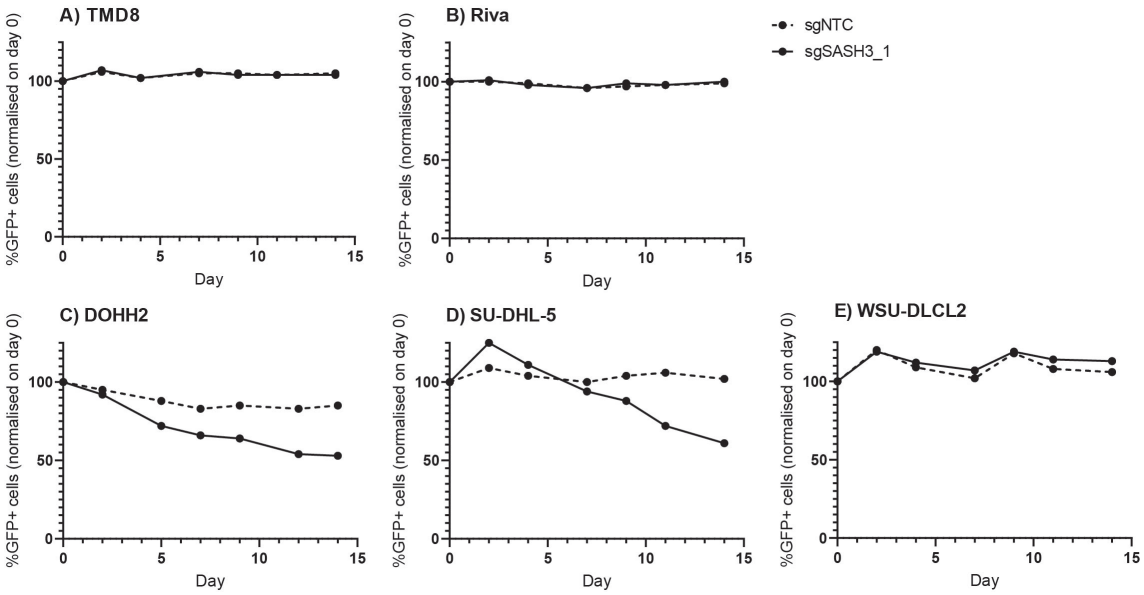

Figure 4.16: **Competitive growth assay with pLKO.1-puro-GFP-sgNTC or -sgSASH3_1-transduced TMD8 (A), Riva (B), DOHH2 (C), SU-DHL-5 (D) and WSU-DLCL2 (E) cells. Two of the GCB-DLBCL cell lines (DOHH2 and SU-DHL-5) were dependent on SASH3 but none of the ABC-DLBCL cell lines.**

4.2.3 Knockout of SASH3 increased the apoptosis levels in DLBCL cell lines

Annexin V staining was used to address the question whether apoptosis was the underlying mechanism for the growth disadvantage of SASH3-depleted GCB-DLBCL cells. For this, TMD8, Riva, SU-DHL-4, SU-DHL-5 and WSU-DLCL2 cells were transduced with pLKO.1-puro-GFP-sgNTC or -sgSASH3. Puromycin selection was omitted, since apoptosis levels may have been falsified by this treatment. Applying the gating strategy as depicted in Figure 4.17A, only GFP-positive cells were included in subsequent analyses. Percentages of apoptotic cells are illustrated in Figure 4.17B. Interestingly, all of the tested cell lines displayed increased levels of apoptotic cells upon knockout of SASH3.

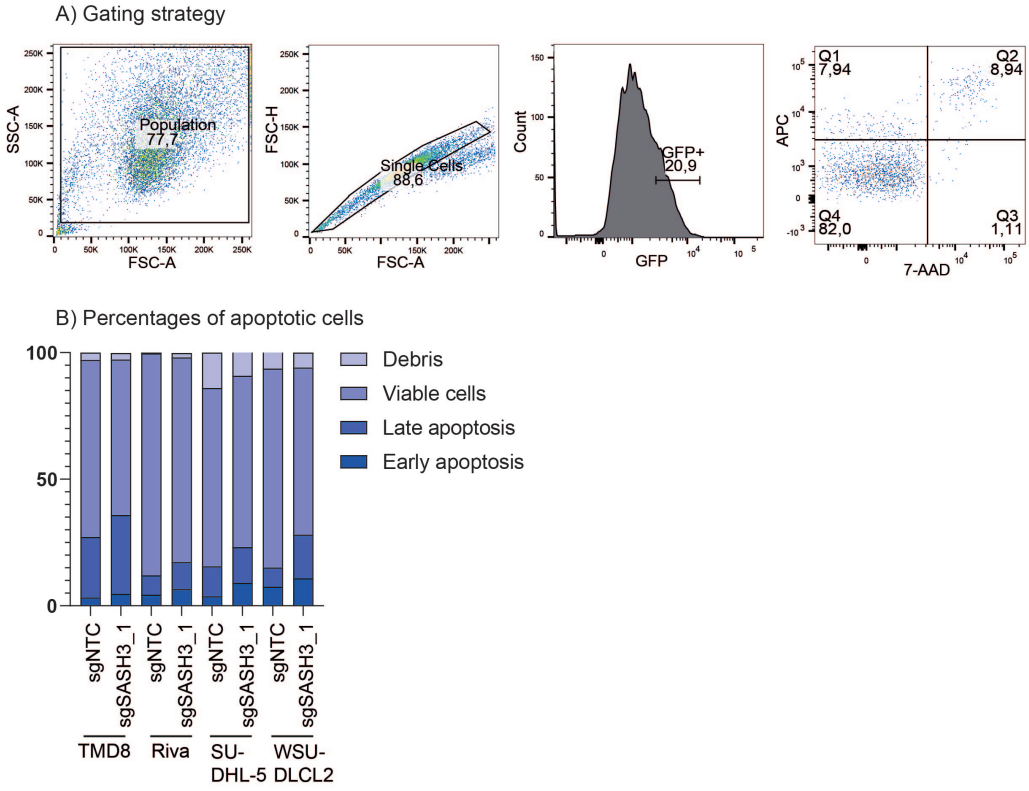

Figure 4.17: **Levels of apoptotic cells were increased in SASH3-depleted ABC- and GCB-DLBCL cell lines. Freshly pLKO.1-puro-GFP-sgNTC- or –sgSASH3_1-transduced TMD8, Riva, SU-DHL-5 and WSU-DLCL2 cells were stained with Annexin V-APC and 7-AAD and analysed by flow cytometry. A) Gating strategy which only included GFP$^+$ cells in order to omit puromycin selection of transduced cells. APC (Annexin V expression) is plotted against the viability marker 7-AAD which generates four quadrants: Q1 = Early apoptosis; Q2 = Late apoptosis; Q3 = Debris; Q4 = Viable cells. Gating of Riva sgNTC-transduced cells are depicted as an example. B) Percentages of cells in each quadrant are depicted in the bar diagram. SASH3 depletion led to increased levels of apoptosis in each cell line.**

4.2.4 Analysis of SASH3-interacting proteins and their respective essentiality

Since SASH3 displayed differential essentiality for ABC- and GCB-DLBCL cell lines, differential interaction partners were expected in these two entities. To address this, a BioID2-based interactome analysis for SASH3 in TMD8 and SU-DHL-5 was conducted. Both cell lines were transduced with N- and C-terminally tagged BioID2-

SASH3 constructs. The following results are based on the C-terminal tagged BioID2 construct, since it revealed more interaction partners than the N-terminal construct. All proteins which displayed a log2 fold chance value of ≥1 were regarded to be significantly enriched and thus further analysed.

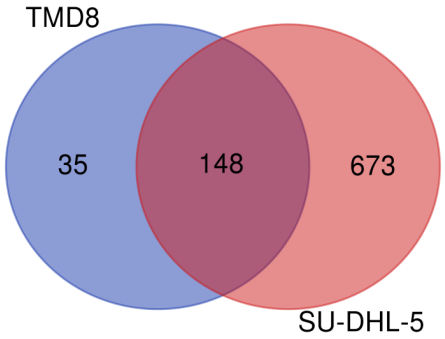

Figure 4.18: **TMD8 and SU-DHL-5 cells display a considerable number of common SASH3-interacting proteins. A BioID2-based SASH3 interactome analysis was conducted in TMD8 and SU-DHL-5 cells. Proteins which displayed a log2 fold change ratio ≥ 1 were regarded to be significantly enriched. The amount of overlapping proteins enriched in both cell lines was analysed using a Venn diagram.**

Figure 4.18 depicts the number of overlapping interaction partners for TMD8 and SU-DHL5. Of note, much more interaction partners were identified in SU-DHL-5 than in TMD8. A considerable amount of proteins was identified as SASH3 interactors in both cell lines. The proteins which were identified as SASH3 interactors in TMD8 only, in SU-DHL-5 only and the overlapping proteins were subjected to GSEA. Table 4.7 illustrates the GO classes which were enriched for each category. Notably, several GO classes were enriched in both cell lines. Mainly GO classes referring to cytoskeletal and cell adhesion processes were enriched.

Table 4.7: **GO classes which are enriched among SASH3 interacting proteins in either SU-DHL-5 and TMD8, TMD8 only or SU-DHL-5 only.**

#	TMD8 and SU-DHL-5	TMD8 only	SU-DHL-5 only
1	GOMF_CADHERIN_BINDING	GOMF_CELL_ADHESION_MOLECULE_BINDING	GOBP_INTRACELLULAR_TRANSPORT
2	GOMF_CELL_ADHESION_MOLECULE_BINDING	GOMF_CADHERIN_BINDING	GOMF_CADHERIN_BINDING
3	GOBP_REGULATION_OF_ORGANELLE_ ORGANIZATION	GOMF_RNA_BINDING	GOBP_ESTABLISHMENT_OF_PROTEIN_ LOCALIZATION
4	GOBP_POSITIVE_REGULATION_OF_CELLULAR_ COMPONENT_ORGANIZATION	GOMF_ENZYME_BINDING	GOMF_CELL_ADHESION_MOLECULE_BINDING
5	GOBP_PROTEIN_CONTAINING_COMPLEX_ SUBUNIT_ORGANIZSATION	GOCC_ANCHORING_JUNCTION	GOMF_ENZYME_BINDING
6	GOBP_REGULATION_OF_CELLULAR_ COMPONENT_BIOGENESIS	GOCC_CELL_SUBSTRATE_JUNCTION	GOBP_CELLULAR_MACROMOLECULE_ LOCALIZATION
7	GOBP_IMMUNE_EFFECTOR_PROCESS	GOBP_PROTEIN_CONTAINING_COMPLEX_ SUBUNIT_ORGANIZATION	GOBP_CELL_CYCLE
8	GOCC_SUPRAMOLECULAR_COMPLEX	GOCC_SUPRAMOLECULAR_COMPLEX	GOMF_ENZYME_REGULATOR_ACTIVITY
9	GOMF_CYTOSKELETAL_PROTEIN_BINDING	GOBP_INTRACELLULAR_TRANSPORT	GOBP_CYTOSKELETON_ORGANIZATION
10	GOMF_PROTEIN_CONTAINING_COMPLEX_ BINDING	GOBP_NEGATIVE_REGULATION_OF_INTRINSIC_ APOPTOTIC_SIGNALING_PATHWAY	GOBP_POSITIVE_REGULATION_OF_MOLECULAR_ FUNCTION

Despite the fact that BCR signalling was not identified as an enriched GO class in the interactome, still many proteins related to BCR signalling were identified in the BioID2 experiment when the list of enriched proteins was individually reviewed. These were especially many crucial factors of proximal BCR signalling, such as SYK, BTK and PLCγ2, and secondly factors of downstream signalling pathways such as NF-κB and MAPK signalling. It was especially surprising to find proteins related to NF-κB signalling in the GCB-DLBCL cell line SU-DHL-5, since this DLBCL subtype is generally considered not to be dependent on NF-κB signalling.
In a separate analysis, proteins identified in the interactome were matched with the respective CSS value from the CRISPR/Cas9-based loss-of-function screen conducted by Phelan *et al.* This analysis aimed to shed more light on the actual dependencies of cell lines on SASH3-interacting proteins. Notably, the detailed comparison between dependencies in the ABC- and GCB-DLBCL cell line needed careful evaluation, since not all proteins were identified in both cell lines. In Figure 4.19, proteins identified in TMD8 were matched with the respective CSS values. Interestingly, the identified proteins/genes seem to be divided in three major groups, referring to their respective CSS value. Two proteins/genes displayed a CSS value of approx. 1, indicating that TMD8 cells have growth advantage upon knockout of the respective gene. These were namely *TBK1* and *INPP5D*. The latter (*INPP5D*, encoding SHIP1) is a known negative regulator of BCR signalling. Secondly, a group of genes/proteins presented with a CSS value of approx. 0, indicating that a knockout of the respective gene does not affect proliferation of TMD8 cells. Mainly proteins belonging to the MAPK signalling pathway but also SASH3 itself were located here. Finally, proteins/genes related to proximal BCR signalling, such as BLNK, SYK and BTK displayed a CSS value $\leq$1, indicating strong dependency of TMD8 cells on proximal BCR signalling.

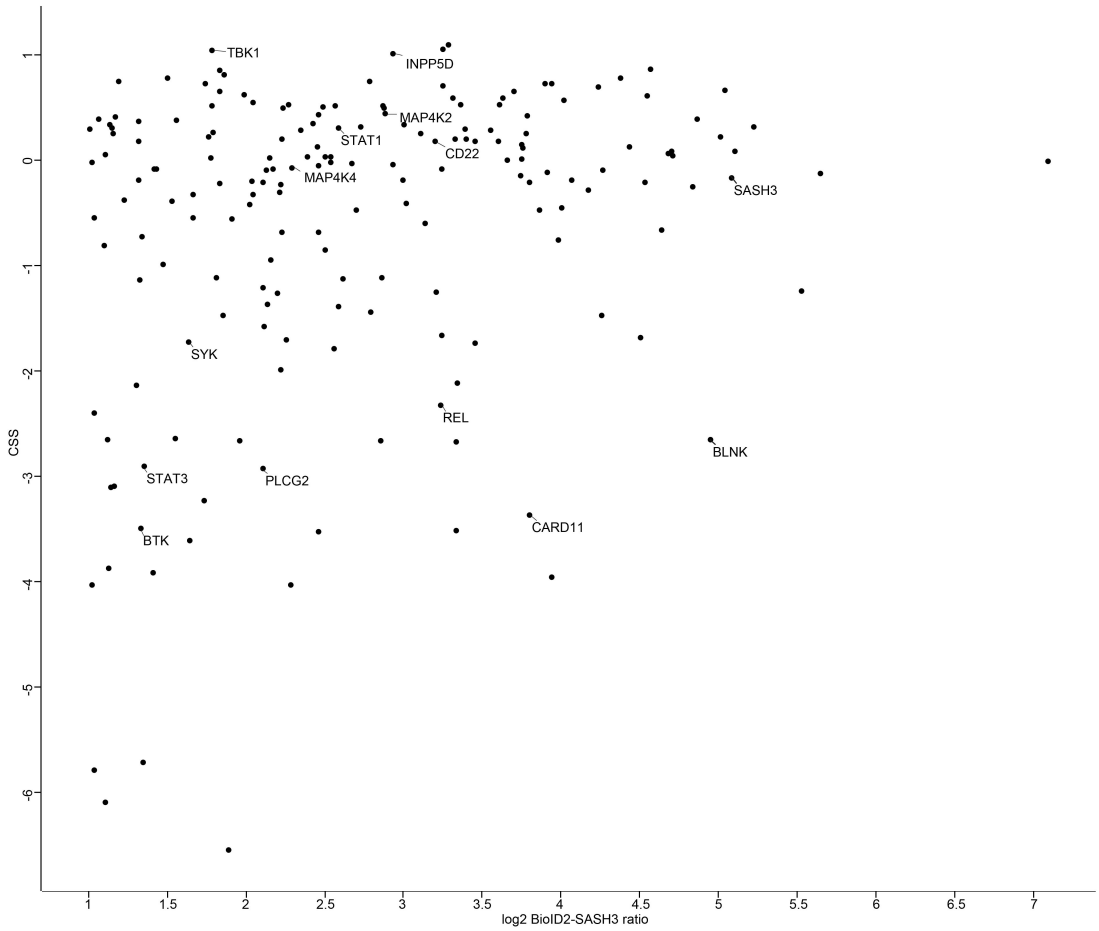

Figure 4.19: **Proteins related to proximal BCR signalling interact with SASH3 and are essential for TMD8 cells. SASH3-interacting proteins identified in TMD8 cells were matched with their respective CSS value retrieved from the CRISPR/Cas9-based loss-of-function screen conducted by Phelan *et al.***

In Figure 4.20, CSS values were matched with SASH3-interacting proteins which were identified in SU-DHL-5 cells. According to this illustration, most of the SASH3-interacting genes/proteins which were identified to be essential for TMD8 cells could be found in a cluster with CSS values of approx. 0. These genes/proteins did not seem to be relevant for the GCB-DLBCL cell line SU-DHL-5 but still seemed to interact with SASH3. A small group of genes/proteins which seemed to interact with SASH3 in SU-DHL-5 cells displayed CSS values $\leq$-1, which indicated dependency of SU-DHL-5 cells on the following factors:

- SYK: this gene/protein was also identified as SASH3-interacting and essential gene/protein in TMD8 cells.
- LYN and CSK are two SRC family kinases which are relevant for proximal BCR signalling. These genes/proteins seemed to be essential for SU-DHL-5

cells. However, a comparison to essentiality in TMD8 cells was not possible, since these proteins were not identified in the SASH3-interactome in TMD8 cells.

- PIK3C3 and PIK3CD, two factors belonging to PI3K signalling seemed to be essential for SU DHL 5 cells. The known dependency of GCB-DLBCL cell on PI3K signalling renders this finding plausible.
- NFKB2 and RELB are members of the NF-κB signalling pathway. Dependency of SU-DHL-5 on these factors was surprising, since GCB-DLBCL cells are generally known to be independent of NF-κB signalling.
- CD22 was identified in TMD8 cells as well but displayed a CSS value of approx. 0 in this cell line. SU-DHL-5 cells on the contrary seemed to be dependent on this factor.

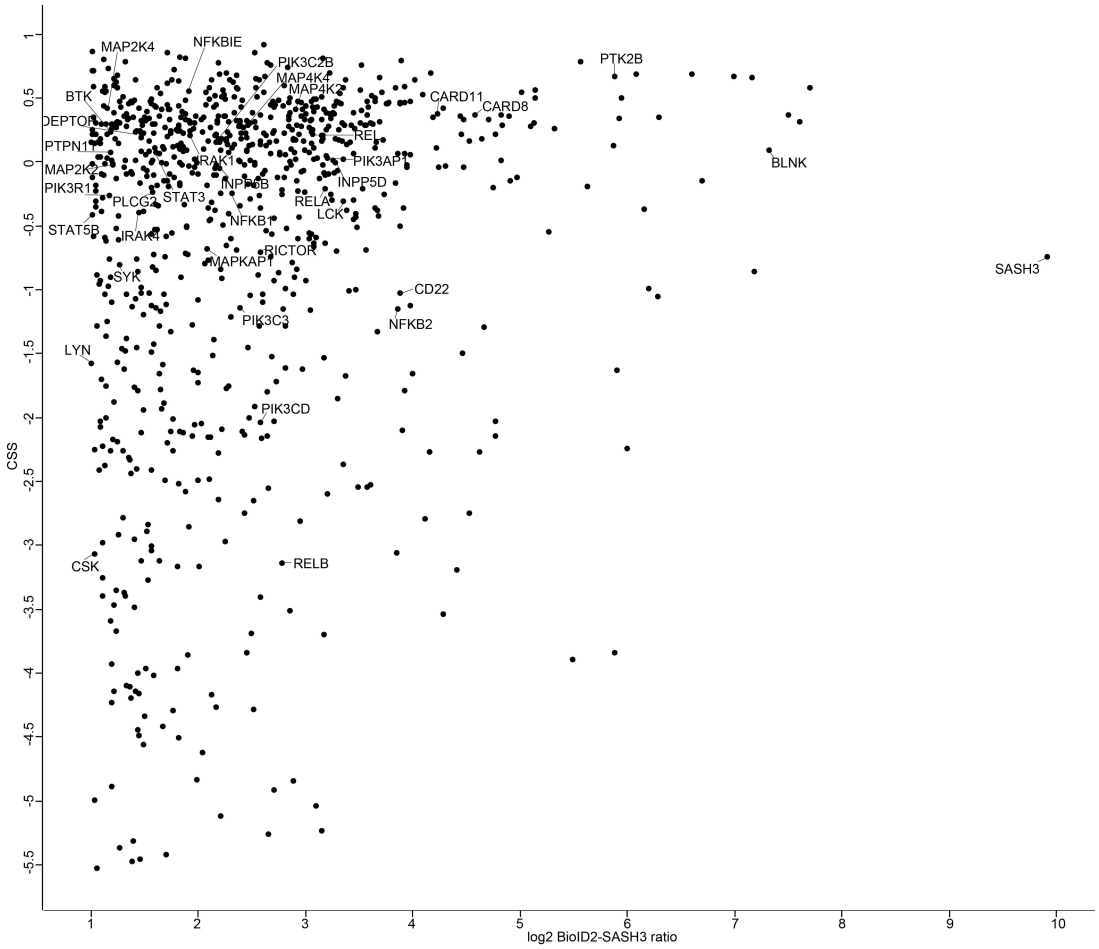

Figure 4.20: **SU-DHL-5 cells depend on another set of BCR signalling-related factors than TMD8. SASH3-interacting proteins in SU-DHL-5 cells were matched with their respective CSS values retrieved from the CRISPR/Cas9-based loss-of-function screen conducted by Phelan *et al.* Several genes/proteins were identified in both TMD8 and SU-DHL-5 cells but partly showed differential essentialities in these two cell lines.**

4.2.5 Investigation of phosphoproteomic changes in ABC- and GCB-DLBCL cell lines upon SASH3 knockout

In order to investigate SASH3-dependent BCR signalling in more detail, a global phosphoproteome was conducted in control (pLKO.1-puro-GFP-sgNTC-transduced) and SASH3-depleted (pLKO.1-puro-GFP-sgSASH3-transduced) cells. Log2 fold change ratios of -1 and +1 were chosen as cutoff value for significant down- or upregulation of phosphorylation, respectively.

Unfortunately, most of the proteins identified in the global phosphoproteome displayed log2 fold changes of approx. 0 and were therefore not considered to be significantly changed in their phosphorylation. Among the few proteins which displayed

log2 fold changes ≥1 or ≤-1, no proteins belonging to the BCR signalling pathway were identified in SU-DHL-5 cells. In TMD8 cells, only three proteins belonging to the BCR signalling pathway were significantly higher phosphorylated upon SASH3 knockout. These were NFKB1, PTK2BA and PRKCD (data not shown).

Since many proteins belonging to the BCR signalling pathways are tyrosine-phosphorylated upon (in-)activation, a tyrosine phosphoproteome (pYome) analysis was performed in a next step. For this, pLKO.1-puro-GFP-sgNTC and –sgSASH3_1-transduced SU-DHL-5 and Riva cells were used. Since Riva cells displayed a higher amount of BCR-related SASH3-interacting proteins in the interactome (data not shown), this cell line was chosen as a representative cell line in pYome analysis. -1 and +1 were again chosen as cutoff values for significantly phosphorylated proteins. In both cell lines approx. 2% and 1% of the identified phosphorylation sites were significantly down- and upregulated, respectively.

Many proteins involved in BCR signalling were identified in the pYome analysis. However, very few proteins displayed log2 fold changes >1 or <-1 indicating significant changes of phosphorylation upon SASH3 knockout. For both cell lines, DOK1 Y296 and PI3KCD T935 were significantly higher phosphorylated; PTPN11 Y279 was significantly less phosphorylated upon SASH3 knockout. For Riva, LYN Y306 was additionally found to be significantly less phosphorylated.

In order to define proteins which were differentially phosphorylated upon SASH3 knockout, log2 fold change values for Riva were plotted against log2 fold change values for SU-DHL-5 (see Figure 4.21). Proteins with a difference of ≥0.5 between Riva and SU-DHL-5 were labelled. For this analysis, also proteins with individual log2 fold changes below the cutoff values were considered.

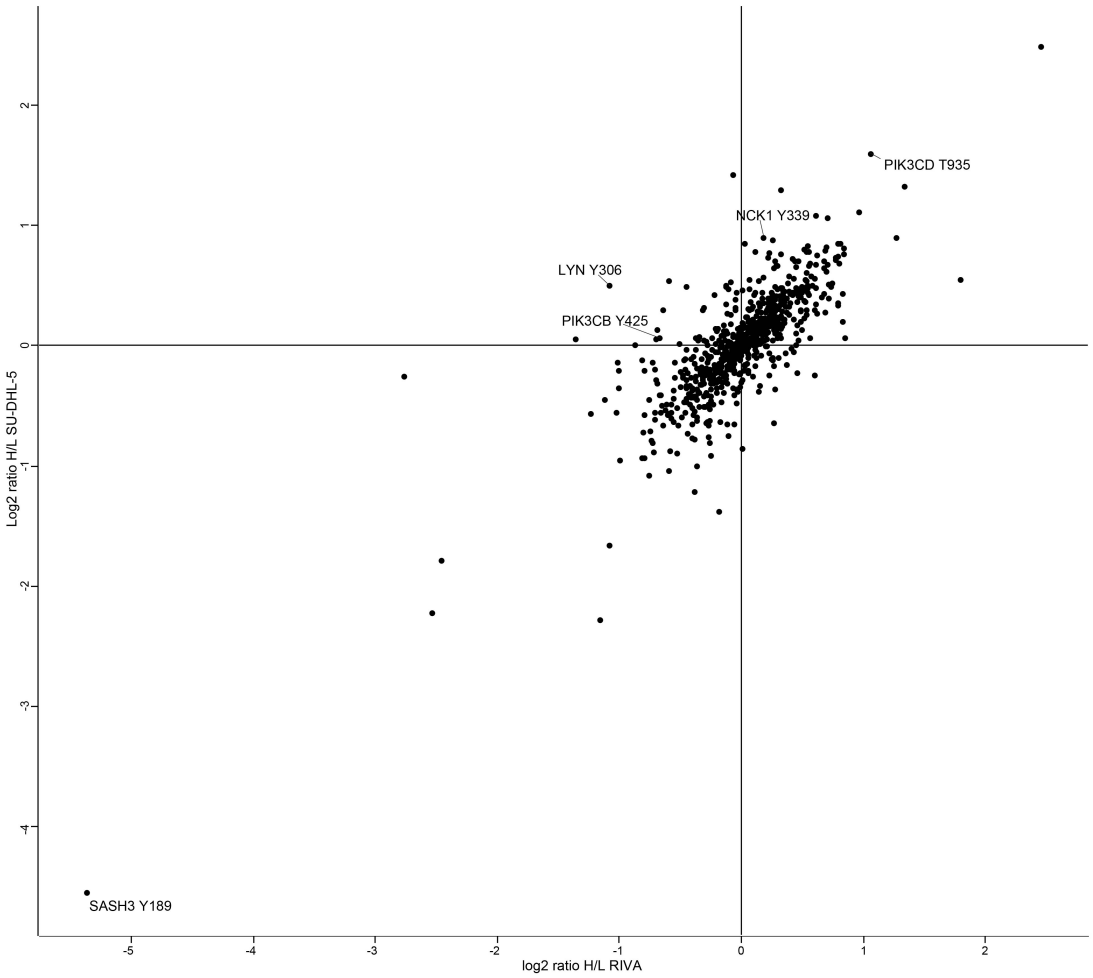

Figure 4.21: **Differential phosphorylation of proteins and the respective phosphosites in Riva and SU-DHL-5 cells upon SASH3 knockout, normalised on pLKO.1-puro-GFP-sgNTC-transduced cells. Proteins with a log2 fold change difference between Riva and SU-DHL-5 >0.5 are labelled.**

Besides SASH3 itself, four phosphosites were found to be differentially phosphorylated upon SASH3 knockout: LYN Y306, PIK3CB Y425, NCK1 Y339 and PIK3CD T935.

Proteins such as BLNK, CARD11 and members of the NF-κB signalling pathway were found to be interacting with SASH3. Interestingly, their respective phosphorylation was not found to be significantly altered upon SASH3 knockout. Thus, the respective interaction could be an indirect one.

5 Discussion

5.1 Role of MARCH5 in the regulation of intrinsic apoptosis in mantle cell lymphoma

Venetoclax is a promising therapeutic option for MCL but still it could not overcome the incurability of this disease. Therefore, additional therapeutic targets which could enhance venetoclax effectivity are needed. To this end, a CRISPR/Cas9-based loss-of-function screen was conducted in the MCL cell line Maver-1 in order to identify genes which confer either sensitivity or resistance towards venetoclax upon their respective knockout. MARCH5 was identified as one of the top hits conferring sensitivity. In targeted approaches, the underlying mechanism was examined.

Besides the sensitisation towards venetoclax, upregulation of MCL-1 and NOXA protein levels were observed in MARCH5-depleted MCL cells. These findings are in line with studies from Djajawi *et al.* and Haschka *et al.* ([46;47]) who described the same phenotype in a number of epithelial cancer entities. Furthermore, Djajawi *et al.* postulated that MARCH5 cooperates with UBE2K and MTCH2 to regulate the MCL-1-NOXA axis. They observed MCL-1 and NOXA upregulation in MARCH5- as well as in UBE2K- and MTCH2-depleted cells. In the interactome analysis conducted in the present study, both proteins were not identified as MARCH5 interactors in the MCL cell lines Jeko-1 and Maver-1. According to the data from the initial CRISPR/Cas9-based loss-of-function screen, UBE2K was found to be essential for Maver-1 under venetoclax but not under DMSO treatment. This effect was not observed for MTCH2 on the other hand. Therefore, the mechanism postulated by Djajawi *et al.* does not seem to apply to MCL cells. A possibility to further address this would be to examine MCL-1 and NOXA protein levels in UBE2K- and MTCH2-depleted cells. The mechanism described by Djajawi *et al.* would finally be disapproved in MCL cells if MCL-1 and NOXA protein levels were not altered upon UBE2K and MTCH2 knockout.

This could additionally be proved by examination of MCL-1 and NOXA protein levels which are not expected to be upregulated in UBE2K- and MTCH2-depleted cells.

5.1.1 MCL-1/NOXA-MARCH5 interaction needs to be validated

Upregulation of the BCL-2 family proteins MCL-1 and NOXA as well as sensitisation towards BCL-2 inhibition of MARCH5-depleted cells suggest that MARCH5 is involved in the regulation of the intrinsic apoptotic pathway. It was hypothesised that MARCH5 regulates NOXA turnover via ubiquitination. Upon MARCH5 knockout, NOXA would be stabilised and eventually trigger intrinsic apoptosis. To validate this hypothesis, it was important to confirm the MARCH5-dependent NOXA ubiquitination as it was already escribed by Haschka *et al.* in other cancer entities.[47] In the interactome analysis, NOXA was not identified. Due to the small size of NOXA, this could have been a technical artefact, since NOXA yields only two tryptic peptides and is therefore hard to detect in MS analyses. Unfortunately, an alternative approach to validate the MARCH5-NOXA interaction using an antibody-based Co-IP technique failed since it could not be established properly in the present study. A MARCH5 pulldown with subsequent analysis of NOXA interaction via Western blot was tested as well as the reversed approach (detection of MARCH5 interaction upon NOXA pulldown). Possibly this was due to low frequency of MARCH5-NOXA complexes which were then hard to detect on a Western blot basis. The validation of MARCH5-NOXA interactions should be prioritised in further studies. Besides the BioID2 and the Co-IP technique, proximity-ligation assays could be used to address this question.

In the ubiquitinome analysis of MARCH5-depleted Jeko-1 cells, decreased NOXA K48 ubiquitination was identified. This site was described as a target for ubiquitination by the E3 ubiquitin ligase CHIP upon DNA damage. Subsequently, NOXA was subjected to lysosomal degradation in this process.[85] MARCH5-dependent NOXA K48 ubiqutination should be validated in subsequent experiments, for example using a Tandem ubiquitin biding entities (TUBEs)-based Western blot or site-directed mutagenesis which disrupts ubiquitination capacities of NOXA K48. Furthermore, NOXA degradation via the lysosomal pathway could be examined, for example using cellular imaging. In this context also MCL-1-MARCH5 interactions need to be validated. MCL-1 was identified as MARCH5-interacting protein in the interactome analysis. Additionally, the ubiquitinome analysis revealed decreased MCL-1 ubiquitination upon MARCH5 knockout. MARCH5-dependent ubiquitination of both MCL-1 and NOXA was also described in the study by Haschka *et al.* Still, MARCH5-dependent ubiquitination of MCL-1 and NOXA should be validated, e.g. using a TUBE IP.

Without the above mentioned validation experiments, which would confirm MARCH5-dependent ubiquitination of both MCL-1 and NOXA in MCL cells, two more sce-

narios are conceivable for the upregulation of MCL-1 in MARCH5-depleted cells. Firstly, MCL-1 upregulation could be a compensatory mechanism. When NOXA is stabilised in MARCH5-depleted cells, MCL-1 as a direct NOXA-interactor could be upregulated as a cellular mechanism to prevent apoptosis. Since both MCL-1 and NOXA are regulated on protein level only, a mechanism for MCL-1 upregulation could be based on posttranslational modifications. This would possibly involve further proteins, such as MULE which is an E3 ubiquitin ligase known to target MCL-1.[86] Secondly, elevated levels of NOXA have higher MCL-1 binding capacities. MCL-1 could therefore be stabilized by binding to NOXA, thus MCL-1 protein levels are increased.

Another important factor which would shed more light on the MARCH5-dependent regulation of intrinsic apoptosis is the timely sequence of MCL-1 and NOXA upregulation. If both proteins were simultaneously upregulated upon MARCH5 knockout, this would indicate equal dependence of NOXA and MCL-1 on MARCH5. If one protein was upregulated immediately upon MARCH5 knockout and upregulation of the other protein was delayed, this could indicate MARCH5-dependency of the immediately upregulated protein and a compensatory mechanism which leads to upregulation of the second protein.

5.1.2 NOXA as a possible key component in induction of intrinsic apoptosis upon MARCH5 knockout

In order to further investigate the role of NOXA in the MARCH5-dependent mechanism, a competitive growth assay in MARCH5/NOXA double knockout cells was conducted. As expected, BCL-2 sensitisation was partly reverted in these cells. This finding is in line with the study from Subramanian *et al.*[48] The authors found that the human colorectal cancer cell line HCT116 was sensitised to ABT737, a combined BCL-2, BCL-XL and BCL-W inhibitor when MARCH5 was depleted. This effect was reverted in MARCH5-NOXA co-deleted cells.

Of note, NOXA is a strong pro-apoptotic protein. Cells are likely to display reduced rates of apoptosis when NOXA is deleted. Therefore, a central role of NOXA in the MARCH5-dependent mechanism needs to be carefully evaluated. To address this question, the competitive growth assay could be repeated using co-deletion of MARCH5 and pro-apoptotic proteins other than NOXA. If reversion of BCL-2 sensitisation was only detectable in MARCH5-NOXA co-deleted cells, a prominent role for NOXA would be evident. However, Subramanian *et al.* indeed observed reversion of ABT737 sensitisation in MARCH5-NOXA but not in MARCH5-BIM co-deleted cells. They furthermore postulated a direct role of NOXA in the inactivation of MCL-1 which eventually leads to cell death.

Notably, NOXA is known to be regulated in a p53-dependent manner.[87] An alternative hypothesis is therefore an involvement of p53 in the hypothesised MARCH5-NOXA axis. Importantly, p53 protein levels are regulated by an E3 ubiquitin ligase, MDM2. MARCH5-dependent regulation of p53 or MDM2 could be hypothesised, but neither MDM2 nor p53 were identified as MARCH5-interacting proteins. Furthermore, these proteins were not identified in the ubiquitinome analysis. A MARCH5-dependent regulation of p53 is therefore unlikely. However, an involvement of p53 in the upregulation of NOXA is not disproved by this finding. p53 is known to be mutated in many cancer cells. This is also true for the MCL cell lines used in the present study. Maver-1 and Mino each display a distinct *TP53* point mutation, while *TP53* is deleted in Jeko-1 cells[88]. Since NOXA was seen to be upregulated in Maver-1, Mino and also in the *TP53*-deleted Jeko-1 cells, a p53-dependent regulation of NOXA is unlikely. This assumption is in line with Subramanian *et al.*[48] who postulated a novel p53-independent upregulation of NOXA in MARCH5-depleted cells.

5.1.3 BCL-2 family members might have additional roles

The above described findings indicate that loss of MARCH5 leads to NOXA-dependent cell death. As observed in the competitive growth assay, MARCH5 knockout alone is a growth disadvantage for MCL cells. But why are MARCH5-depleted cells highly sensitised towards BCL-2 inhibition? According to the BH3 profiling results, the mechanism distinctly involves sensitisation to BCL-2 inhibition. Sensitisation towards BCL-XL inhibition or others was not observed. A direct link between MARCH5 and BCL-2 sensitisation is still missing. In Maver-1 cells, BCL-2 was identified as MARCH5-interacting protein in the interactome studies, but BCL-2 ubiquitination was not significantly altered upon MARCH5 knockout.

Focussing on BCL-2 family members other than MCL-1 and NOXA, it was observed that BCL-2, BCL2L11 (BIM) and BCL2L13 (BCL-Rambo) were identified as MARCH5-interacting proteins in Maver-1 but not in Jeko-1 cells. BAX was the only additional BCL-2 family protein which was identified as MARCH5-interactor in both Jeko-1 and Maver-1. This finding points out a possible additional role for BAX in the underlying mechanism; secondly, it emphasises the differences between the MCL cell lines.

Additional roles of BCL-2 family proteins other than regulation of intrinsic apoptosis might be involved in the MARCH5-dependent mechanism. MARCH5 was initially identified as a regulator of proteins involved in mitochondrial dynamics regulation, such as Drp-1 and MFN2. A review by Autret and Martin[89] suggests that BCL-2 family members might also be involved in mitochondrial dynamics and ques-

tion whether regulation of mitochondrial dynamics and regulation of intrinsic apoptosis are distinct functions or whether these two components are principally belonging together. During apoptosis, mitochondria undergo fission, therefore a connection between mitochondrial dynamics and the apoptotic machinery is reasonable. The review furthermore hypothesises that BAX and BAK may be involved in the regulation of mitochondrial dynamics. With this, a new hypothesis is conceivable: in addition to the known role of MARCH5 as an upstream regulator of Drp-1, MFN2 and other proteins controlling mitochondrial dynamics, MARCH5 might also regulate BAX which in turn is involved in mitochondrial dynamics during intrinsic apoptosis. This could furthermore explain why MARCH5 appears to be involved in two pathways, namely regulation of mitochondrial dynamics and intrinsic apoptosis, which seemingly are completely distinct mechanisms. To verify this hypothesis, several experiments should be conducted. In order to validate a role of BAX in mitochondrial dynamics, changes in mitochondrial morphology in BAX-depleted cells in comparison to control cells should be examined. Additionally, BAX-interacting proteins could be defined using the BioID2 technique. Enrichment of BAX-interacting proteins which are known to be involved in mitochondrial dynamics would be a valuable hint towards an additional role of BAX in this pathway. Finally, the same experiments could be repeated with other BCL-2 family members. Especially BCL-2 would be interesting.

Additionally, Chong *et al.* reviewed non-canonical roles of BCL-2 proteins. Virtually each BCL-2 family member has been found to have additional roles besides regulating intrinsic apoptosis. Regulation of Ca^{2+} and redox homeostasis and inflammation are processes which many BCL-2 proteins seem to interact with.[90] In this context, mitochondria-ER contact sites should be discussed. These are involved in Ca^{2+} homeostasis, reactive oxygen species (ROS) production and others, thus being likely to involve BCL-2 family protein non-canonical functions. Furthermore, MFN2 and Drp-1 were linked to mitochondria-ER contact sites.[91] Thus, indirect regulation of processes linked to mitochondria-ER contact sites by MARCH5 is conceivable. To address this question, measurement of Ca^{2+} or ROS levels in MARCH5-depleted cells could give more insight whether this hypothesis is plausible. Localisation of MARCH5 in mitochondria-ER contact sites could furthermore be validated using fluorescence microscopy.

Moreover, in the MARCH5 interactome studies, enrichment of proteins being involved in vesicular transport has been observed. Vesicular transport could be another process connected to MARCH5 involvement in mitochondria-ER contact sites. Furthermore, proteins regulating the cell cycle were enriched in the ubiquitinome analysis. Also concerning cell cycle regulation, BCL-2 family proteins have been assumed to play a dual role here.[92] An experiment which could give first basic insights

into MARCH5-dependent cell cycle regulation is a BrdU-based analysis in control versus MARCH5-depleted cells. Differential percentages of cells in each cell cycle phase would indicate a role for MARCH5 in cell cycle regulation.

5.1.4 Summary and future perspectives

With the new hypotheses described above, MARCH5 is put into a broader cellular context. However, there are still some issues which do not fit into the concept. Firstly, it is still unclear why MARCH5-depleted cells are sensitised to BCL-2 inhibition. Several mechanisms of how MARCH5 depletion could induce apoptosis are conceivable, but sensitisation towards BCL-2 inhibition can so far not be explained. Secondly, so far the topology of MARCH5-dependent ubiquitin chains has not been examined, yet. K48 linkage seems plausible, especially in the context of MARCH5-dependent regulation of NOXA turnover. However, also K63 linkage seems possible, in particular with regard to a potential role of MARCH5 in vesicular trafficking. Knowing the exact type of ubiquitin linkage conferred by MARCH5 would give more insight into possible downstream mechanisms.
Taken together, with MARCH5, a new factor conferring sensitivity towards venetoclax upon its knockout in MCL cells was discovered. The present study illustrates that the MARCH5-dependent MCL-1-NOXA axis which was already described in other cancer entities also applies to MCL cells. Additionally, a potential role for NOXA was examined. Mass spectrometry-based experiments aimed to uncover so far unknown MARCH5-interacting proteins and proteins which are ubiquitinated in a MARCH5-dependent manner. The latter indicated a potential correlation between MARCH5 and other cellular pathways such as vesicle transport or cell cycle regulation.
Especially with regard to Jeko-1 cells which displayed low sensitivity towards venetoclax in the wild-type state but were highly sensitised to venetoclax when MARCH5 was knocked out, MARCH5 becomes an interesting therapeutic option. Venetoclax resistant cancer cells could simultaneously be treated with a MARCH5 inhibitor. Drugability of MARCH5 needs to be validated in andvance. Alternatively, MARCH5 protein expression could be abrogated using molecular tools such as aptamers. Importantly, all cellular pathways which are dependent on MARCH5 need to be elucidated before a MARCH5 inhibitor could be applied. As described above, many pathways may be affected by MARCH5 inhibition, which enhances the chances for adverse effects.

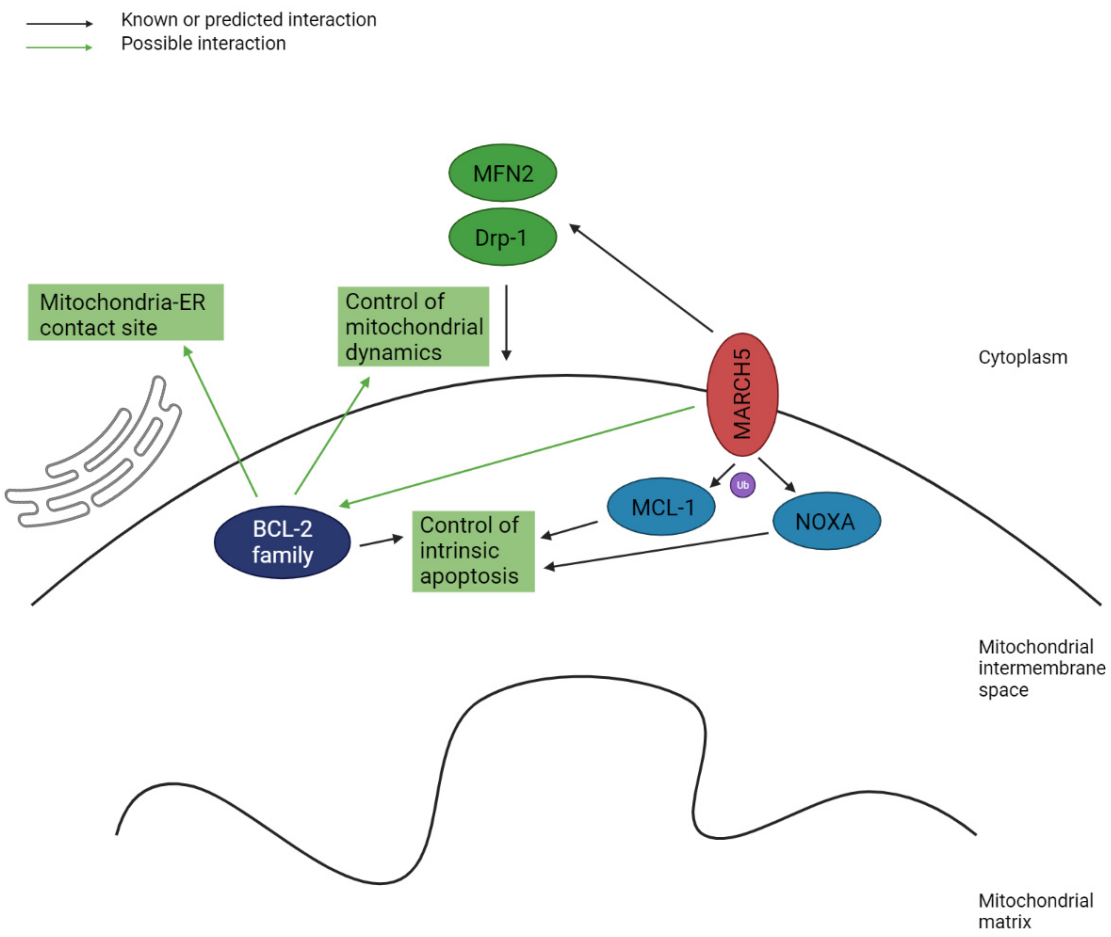

Figure 5.1: **Overview about known and possible interactions and downstream processes which are dependent on MARCH5 and BCL-2 family proteins. MARCH5 ubiquitinates MCL-1 and NOXA which in turn regulate intrinsic apoptosis. Furthermore, mitochondrial dynamics are regulated by proteins such as Drp-1 and MFN2 which in turn are target to MARCH5-dependent regulation. MARCH5-dependent regulation of further BCR-2 family members is suggested, which in turn additionally regulate mitochondrial dynamics and processes at the mitochondria-ER contact site. Figure created with Biorender.com.**

5.2 Role of SASH3 in BCR signalling in DLBCL cells

In this part of the study, BCR signalling as an important oncogenic pathway was examined in DLBCL cells. To date, several differences between ABC- and GCB-DLBCL cells have been elucidated, but there are still many unknown factors. SASH3 was discovered as an essential protein for GCB-DLBCL cells when CRISPR/Cas9-based screening data from ABC- and GCB-DLBCL cell lines were compared. SASH3

was shown to be involved in TCR signalling.[33] Due to the analogy between TCR and BCR signalling, it seemed reasonable that SASH3 is also involved in BCR signalling.

5.2.1 Definition of a possible SASH3 signalling mechanism based on the SASH3 homologue HACS1

HACS1 (also termed SLy2) displays high sequence similarity to SASH3. In contrast to SASH3, HACS1 has already been investigated in B-cells. The following mechanism has been proposed: HACS1 expression is enhanced upon BCR ligation in a PI3K/PKC-dependent manner. Non-phosphorylated HACS1 is located in the nucleus, where it is part of a complex regulating gene transcription. Phosphorylated HACS1 is restricted to the cytoplasmic compartment, where it is bound to 14-3-3 proteins and participates in negative regulation of BCR signalling and cytoskeletal reorganisation. Furthermore, HACS1 has been shown to interact with NF-κB proteins.[93]

The mechanism described for HACS1 in B-cells shares high similarity with the role of SASH3 in T-cells. Here, the dual role in the cytoplasmic and the nuclear compartment is of high importance, too. In the nucleus, SASH3 seems to interact with the transcription factor Forkhead box protein O 1 (FOXO1). In the cytoplasm, SASH3 is phosphorylated upon TCR signalling activation. Here a PI3K/PKC-dependent mechanism is suggested as well. As described for HACS1, phosphorylated SASH3 is restricted to the cytoplasmic compartment, where it is also bound to 14-3-3 proteins. Overall, SASH3 is proposed to be involved in gene transcription regulation and cell cycle inhibition in T-cells.[33]

The signalling mechanisms described for HACS1 and SASH3 are in line with the findings from the present study. Here, interaction with members of the PI3K and the NF-κB signalling pathways was observed. However, interaction with FOXO1 or other members of the FOXO transcription factor family has not been observed. In this context, experimental conditions are of special importance. When investigating proteins which occur in the cytoplasmic and the nuclear compartment, it needs to be ensured that the lysis buffer used for the respective study is capable of disrupting the nuclear membrane. With the use of RIPA lysis buffer in the interactome experiments, this was ensured. Absence of FOXO proteins in the interactome therefore is in contrast to previous findings for SASH3 and HACS1.

14-3-3 proteins (encoded by *YWHAB*, *YWHAG*, *YWHAQ* and others) were described to bind and retain SASH3 and HACS1 in the cytoplasmic compartment. In the interactome analysis in the present study, many 14-3-3 proteins were indeed identified, but neither of them displayed a log2 fold change >1, indicating that these proteins do not significantly interact with SASH3 in the tested cell lines. These find-

ings should be validated using a method such as co-IP.
HACS1 and SASH3 have been described to participate in negative regulation of BCR and TCR signalling, respectively. This opposes the findings from the current study. If SASH3 was a negative regulator of BCR signalling, knockout of SASH3 would yield a growth advantage for the respective cells. Since the opposite was observed, a differential mechanism seems to underlie SASH3 signalling in GCB-DLBCL cells. Besides the overall SASH3 interactome, this study aimed to define SASH3 downstream targets. For this, phosphoproteome analyses were conducted in the present study. Unfortunately, no BCR signalling-related proteins were identified in the global phosphoproteome and very few ones in the pYome experiment. The proteins identified in the pYome should again be studied in more detail. For example, Western blot analysis for phosphorylation of the respective potential targets in SASH3 knockout and control cells could be conducted.

5.2.2 Differential essentialities of SASH3-interacting proteins in ABC- and GCB-DLBCL cell lines

After SASH3 was discovered to be of differential essentiality for ABC- and GCB-DLBCL cells, it was assumed that the SASH3 interactome could provide evidence for these differences. Surprisingly, the spectrum of SASH3-interacting proteins was quite similar in ABC- and GCB-DLBCL cells. It was especially surprising to find many factors of NF-κB signalling as SASH3 interactors in GCB-DLBCL cells, since this entity is known to be independent of the NF-κB pathway. Plotting of the SASH3 interacting proteins against their respective CSS value shed more light on this phenomenon. It was observed that the individual BCR signalling components are of differential essentiality in ABC- and GCB-DLBCL cells. PI3K signalling seems to play a major role in SASH3 signalling. GCB-DLBCL cells are highly dependent on PI3K signalling but little is known about the exact downstream mechanisms. SASH3 might be an integral part of PI3K signalling regulation, since knockout of SASH3 is toxic for GCB-DLBCL cells. In further experiments, e.g. via Western blot, PI3K signalling outcome should be examined in SASH3 depleted and control cells. If PI3K signalling is disabled upon SASH3 knockout, this would be evidence for a crucial role of SASH3 in PI3K signalling and hence the SASH3 dependence of GCB-DLBCL cells.
Furthermore, CD22 was observed to be of differential essentiality for ABC- and GCB-DLBCL cells. While TMD8 cells did not depend on this protein, knockout of CD22 was toxic for SU-DHL-5 cells. With respect to the data obtained from Phelan *et al.* ([21]), CD22 knockout was toxic only for SU-DHL-5 cells, but not for any of the other tested GCB-DLBCL cell lines. Therefore, CD22 cannot be regarded as a

general factor which might explain the differential essentiality of SASH3 in ABC- and GCB-DLBCL cells.

5.2.3 Summary and future perspectives

Taken together, the SASH3 studies added novel knowledge to two fields:

- SASH3 was so far not studied in B-cells, therefore the SASH3 interactome analysis was novel to both SASH3 and B-cell biology.
- In DLBCL biology, SASH3 was so far not known to be an essential factor exclusively to GCB-DLBCL cells.

A role of SASH3 in BCR signalling was hypothesised, since it is involved in the related TCR signalling pathway. Also interaction with members of the NF-κB signalling pathway was anticipated to a certain extent, based on the findings for the SASH3 homologue HACS1. But the interaction with proximal BCR signalling components was surprising and suggests that SASH3 might play a dual role in B-cells. This finding should be validated and investigated in more detail. Also shuttling between nuclear and cytoplasmic compartment, as it was described for HACS1, should be investigated.
A challenging task which would elucidate much of the SASH3-dependent mechanism in DLBCL cells would be the definition of kinases upstream of SASH3. Astoul *et al.* proposed a PI3K-/PKC-dependent mechanism for SASH3 S27 phosphorylation.[94] This is in line with the findings from the interactome studies, since many proteins from the PI3K family have been observed to interact with SASH3. In order to validate these findings, Co-IP studies could be conducted, furthermore SASH3 phosphorylation upon knockout of specific PI3K family members could be examined. In addition to the studies concerning the exact mechanism of SASH3 involvement in BCR signalling, the overall outcome of SASH3 signalling should be examined. In the present study, apoptosis levels in SASH3 depleted and control ABC- and GCB-DLBCL cells were investigated. Elevated levels of apoptosis were observed upon SASH3 knockout. This was in line with the expectations for GCB-DLBCL cells, but highly unexpected in ABC-DLBCL cells since they were not dependent on SASH3 in the CRISPR/Cas9-based loss-of-function seen and in the competitive growth assay. Repetition of the Annexin V staining and additional analysis of markers for apoptosis (such as cleaved PARP and cleaved caspase 3) should be conducted in order to validate this finding. Secondly, it should be determined whether gene transcription is regulated in a SASH3-dependent mechanism. Since many members of the NF-κB signalling pathway were found to interact with SASH3, expression levels of NF-κB target genes could be examined via qRT-PCR in SASH3 knockout

and control cells. The outcomes of this experiment would be especially interesting in GCB-DLBCL cells, which are known to be independent of NF-κB signalling but some components of this signalling pathway still appeared in the SASH3 interactome.

The exclusive essentiality of SASH3 in GCB-DLBCL cells could be exploited as a new therapeutic option for this DLBCL entity. Since SASH3 does not possess enzymatic activity, inhibition of this protein using a small molecule inhibitor will not be possible. Therefore, other possibilities to inhibit SASH3 need to be evaluated, for example abrogation of the protein expression via antisense oligonucleotides. However, as with MARCH5, the exact signalling mechanism needs to be elucidated first in order to prevent adverse events of SASH3 inhibition.

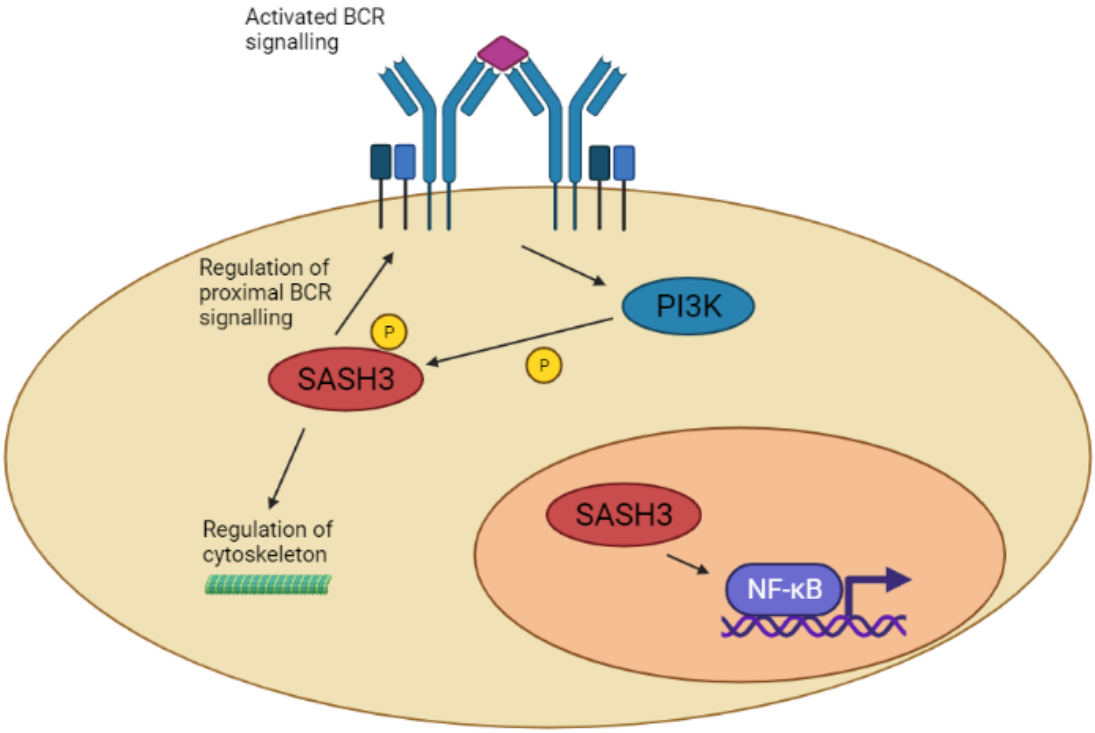

Figure 5.2: **Overview about proposed SASH3 mechanism of action. Upon BCR signalling activation, SASH3 is phosphorylated in a PI3K-dependent manner. Phosphorylated SASH3 then regulates proximal BCR signalling as well as cytoskeletal remodelling. Non-phosphorylated SASH3 translocates into the nucleus where it regulates NF-κB-dependent gene transcription. Figure created with Biorender.com.**

6 Appendix

Schriftliche Erklärung

Ich erkläre ehrenwörtlich, dass ich die dem Fachbereich Medizin der Johann Wolfgang Goethe-Universität Frankfurt am Main zur Promotionsprüfung eingereichte Dissertation mit dem Titel

Roles of MARCH5 and SASH3 in oncogenic signalling in B-cell Non-Hodgkin lymphoma

in dem Universitätsklinikum Frankfurt, Zentrum der Inneren Medizin, Medizinische Klinik 2, unter Betreuung und Anleitung von Prof. Dr. Thomas Oellerich mit Unterstützung durch Dr. Carmen Döbele ohne sonstige Hilfe selbst durchgeführt und bei der Abfassung der Arbeit keine anderen als die in der Dissertation angeführten Hilfsmittel benutzt habe. Darüber hinaus versichere ich, nicht die Hilfe einer kommerziellen Promotionsvermittlung in Anspruch genommen zu haben.

Ich habe bisher an keiner in- oder ausländischen Universität ein Gesuch um Zulassung zur Promotion eingereicht*. Die vorliegende Arbeit wurde bisher nicht als Dissertation eingereicht.

Vorliegende Ergebnisse der Arbeit wurden (oder werden) in folgendem Publikationsorgan veröffentlicht:

—

(Ort, Datum) (Unterschrift)

∗) im Falle des Nichtzutreffens entfernen

Danksagung

Lebenslauf

(Ort, Datum) (Unterschrift)

Bibliography

[1] Shankland KR, Armitage JO, Hancock BW. Non-Hodgkin lymphoma *Lancet.* 2012;380:848–857.

[2] Shaffer AL, Young RM, Staudt LM. Pathogenesis of human B cell lymphomas *Annu Rev Immunol.* 2012;30:565–610.

[3] Lenz G, Staudt LM. Aggressive lymphomas *The New England journal of medicine.* 2010;362:1417–1429.

[4] Ghielmini M, Zucca E. How I treat mantle cell lymphoma *Blood.* 2009;114:1469–1476.

[5] Jain P, Wang M. Mantle cell lymphoma: 2019 update on the diagnosis, pathogenesis, prognostication, and management *Am J Hematol.* 2019;94:710–725.

[6] Swerdlow SH, Campo E, Pileri SA, et al. The 2016 revision of the World Health Organization classification of lymphoid neoplasms *Blood.* 2016;127:2375–2390.

[7] Vogt N, Dai B, Erdmann T, Berdel WE, Lenz G. The molecular pathogenesis of mantle cell lymphoma *Leuk Lymphoma.* 2017;58:1530–1537.

[8] Vegliante MC, Palomero J, Pérez-Galán P, et al. SOX11 regulates PAX5 expression and blocks terminal B-cell differentiation in aggressive mantle cell lymphoma *Blood.* 2013;121:2175–2185.

[9] Liu Y, Barta SK. Diffuse large B-cell lymphoma: 2019 update on diagnosis, risk stratification, and treatment *Am J Hematol.* 2019;94:604–616.

[10] Alizadeh AA, Eisen MB, Davis RE, et al. Distinct types of diffuse large B-cell lymphoma identified by gene expression profiling *Nature.* 2000;403:503–511.

[11] Schmitz R, Wright GW, Huang DW, et al. Genetics and Pathogenesis of Diffuse Large B-Cell Lymphoma *N Engl J Med.* 2018;378:1396–1407.

[12] Chapuy B, Stewart C, Dunford AJ, et al. Molecular subtypes of diffuse large B cell lymphoma are associated with distinct pathogenic mechanisms and outcomes 2018.

[13] Kondo M. Lymphoid and myeloid lineage commitment in multipotent hematopoietic progenitors *Immunol Rev.* 2010;238:37–46.

[14] Gellert M. V(D)J recombination: RAG proteins, repair factors, and regulation *Annu Rev Biochem.* 2002:101–132.

[15] Murphy K, Weaver C. *Janeway Immunologie.* Berlin, Heidelberg: Springer Berlin Heidelberg 2018.

[16] LeBien TW, Tedder TF. B lymphocytes: how they develop and function *Blood.* 2008;112:1570–1580.

[17] Dal Porto JM, Gauld SB, Merrell KT, Mills D, Pugh-Bernard AE, Cambier J. B cell antigen receptor signaling 101 *Mol Immunol.* 2004;41:599–613.

[18] Young RM, Staudt LM. Targeting pathological B cell receptor signalling in lymphoid malignancies *Nature Rev Drug Discov.* 2013;12:229–243.

[19] Davis RE, Ngo VN, Lenz G, et al. Chronic active B-cell-receptor signalling in diffuse large B-cell lymphoma *Nature.* 2010;463:88–92.

[20] Young RM, Phelan JD, Wilson WH, Staudt LM. Pathogenic B-cell receptor signaling in lymphoid malignancies: New insights to improve treatment *Immunol Rev.* 2019;291:190–213.

[21] Phelan JD, Young RM, Webster DE, et al. A multiprotein supercomplex controlling oncogenic signalling in lymphoma *Nature.* 2018;560:387–391.

[22] Havranek O, Xu J, Köhrer S, et al. Tonic B-cell receptor signaling in diffuse large B-cell lymphoma *Blood.* 2017;130:995–1006.

[23] Wang ML, Rule S, Martin P, et al. Targeting BTK with ibrutinib in relapsed or refractory mantle-cell lymphoma *N Engl J Med.* 2013;369:507–516.

[24] Wen T, Wang J, Shi Y, Qian H, Liu P. Inhibitors targeting Bruton's tyrosine kinase in cancers: drug development advances *Leukemia.* 2021;35:312–332.

[25] Hershkovitz-Rokah O, Pulver D, Lenz G, Shpilberg O. Ibrutinib resistance in mantle cell lymphoma: clinical, molecular and treatment aspects *Br J Haematol.* 2018;181:306–319.

[26] Burger JA, Wiestner A. Targeting B cell receptor signalling in cancer: preclinical and clinical advances *Nat Rev Cancer.* 2018;18:148–167.

[27] Jerkeman M, Hallek M, Dreyling M, Thieblemont C, Kimby E, Staudt L. Targeting of B-cell receptor signalling in B-cell malignancies *J Intern Med.* 2017;282:415–428.

[28] Beer S, Simins AB, Schuster A, Holzmann B. Molecular cloning and characterization of a novel SH3 protein (SLY) preferentially expressed in lymphoid cells *Biochim Biophys Acta.* 2001;1520:89–93.

[29] Kaneko T, Li L, Li Shawn SC. The SH3 domain - a family of versatile peptide- and protein-recognition modules

[30] Kim CA, Bowie JU. SAM domains: uniform structure, diversity of function *Trends Biochem Sci.* 2003;28:625–628.

[31] Beer S, Scheikl T, Reis B, Hüser N, Pfeffer K, Holzmann B. Impaired immune responses and prolonged allograft survival in Sly1 mutant mice *Mol Cell Biol.* 2005;25:9646–9660.

[32] Reis B, Pfeffer K, Beer-Hammer S. The orphan adapter protein SLY1 as a novel anti-apoptotic protein required for thymocyte development *BMC Immunol.* 2009;10:38.

[33] Schäll D, Schmitt F, Reis B, Brandt S, Beer-Hammer S. SLy1 regulates T-cell proliferation during Listeria monocytogenes infection in a Foxo1-dependent manner *Eur J Immunol.* 2015;45:3087–3097.

[34] Arefanian S, Schäll D, Chang S, et al. Deficiency of the adaptor protein SLy1 results in a natural killer cell ribosomopathy affecting tumor clearance *Oncoimmunology.* 2016;5:e1238543.

[35] Hershko A, Ciechanover A. The ubiquitin system *Annu Rev Biochem.* 1998;67:425–479.

[36] Pohl C, Dikic I. Cellular quality control by the ubiquitin-proteasome system and autophagy *Science.* 2019;366:818–822.

[37] Yang Y, Staudt LM. Protein ubiquitination in lymphoid malignancies *Immunol Rev.* 2015;263:240–256.

[38] Komander D, Rape M. The ubiquitin code *Ann Rev Biochem.* 2012;81:203–229.

[39] Kwon YT, Ciechanover A. The Ubiquitin Code in the Ubiquitin-Proteasome System and Autophagy *Trends Biochem Sci.* 2017;42:873–886.

[40] Wang D, Ma L, Wang B, Liu J, Wei W. E3 ubiquitin ligases in cancer and implications for therapies *Cancer Metastasis Rev.* 2017;36:683–702.

[41] Nandi D, Tahiliani P, Kumar A, Chandu D. The ubiquitin-proteasome system *J Biosci.* 2006;31:137–155.

[42] Di Costanzo A, Del Gaudio N, Conte L, Altucci L. The Ubiquitin Proteasome System in Hematological Malignancies: New Insight into Its Functional Role and Therapeutic Options *Cancers (Basel).* 2020;12.

[43] Yonashiro R, Ishido S, Kyo S, et al. A novel mitochondrial ubiquitin ligase plays a critical role in mitochondrial dynamics *EMBO J.* 2006;25:3618–3626.

[44] Karbowski M, Neutzner A, Youle RJ. The mitochondrial E3 ubiquitin ligase MARCH5 is required for Drp1 dependent mitochondrial division *J Cell Biol.* 2007;178:71–84.

[45] Park YY, Lee S, Karbowski M, Neutzner A, Youle RJ, Cho H. Loss of MARCH5 mitochondrial E3 ubiquitin ligase induces cellular senescence through dynamin-related protein 1 and mitofusin 1 *J Cell Sci.* 2010;123:619–626.

[46] Djajawi TM, Liu L, Gong JNn, et al. MARCH5 requires MTCH2 to coordinate proteasomal turnover of the MCL1:NOXA complex *Cell Death Differ.* 2020.

[47] Haschka MD, Karbon G, Soratroi C, O'Neill KL, Luo X, Villunger A. MARCH5-dependent degradation of MCL1/NOXA complexes defines susceptibility to antimitotic drug treatment *Cell Death Differ.* 2020.

[48] Subramanian A, Andronache A, Li YC, Wade M. Inhibition of MARCH5 ubiquitin ligase abrogates MCL1-dependent resistance to BH3 mimetics via NOXA *Oncotarget.* 2016;7:15986–16002.

[49] Shiiba I, Takeda K, Nagashima S, Yanagi S. Overview of Mitochondrial E3 Ubiquitin Ligase MITOL/MARCH5 from Molecular Mechanisms to Diseases *Int J Mol Sci.* 2020;21.

[50] Taylor RC, Cullen SP, Martin SJ. Apoptosis: controlled demolition at the cellular level *Nature Rev Mol Cell Biol.* 2008;9:231–241.

[51] McIlwain DR, Berger T, Mak TW. Caspase functions in cell death and disease *Cold Spring Harb Perspect Biol.* 2013;5:a008656.

[52] Singh R, Letai A, Sarosiek K. Regulation of apoptosis in health and disease: the balancing act of BCL-2 family proteins *Nature Rev Mol Cell Biol.* 2019;20:175–193.

[53] Youle RJ, Strasser A. The BCL-2 protein family: opposing activities that mediate cell death *Nature Rev Mol Cell Biol.* 2008;9:47–59.

[54] Hanahan D, Weinberg RA. The Hallmarks of Cancer *Cell.* 2000;100:57–70.

[55] Vogler M, Walter HS, Dyer MJS. Targeting anti-apoptotic BCL2 family proteins in haematological malignancies - from pathogenesis to treatment *Br J Haematol.* 2017;178:364–379.

[56] Khan N, Kahl B. Targeting BCL-2 in Hematologic Malignancies *Target Oncol.* 2018;13:257–267.

[57] Klanova M, Klener P. BCL-2 Proteins in Pathogenesis and Therapy of B-Cell Non-Hodgkin Lymphomas *Cancers (Basel).* 2020;12.

[58] Mihalyova J, Jelinek T, Growkova K, Hrdinka M, Simicek M, Hajek R. Venetoclax: A new wave in hematooncology *Exp Hematol.* 2018;61:10–25.

[59] Davids MS, Roberts AW, Seymour JF, et al. Phase I First-in-Human Study of Venetoclax in Patients With Relapsed or Refractory Non-Hodgkin Lymphoma *J Clin Oncol : official journal of the American Society of Clinical Oncology.* 2017;35:826–833.

[60] Bose P, Gandhi V, Konopleva M. Pathways and mechanisms of venetoclax resistance *Leuk Lymphoma.* 2017;58:1–17.

[61] Tam CS, Anderson MA, Pott C, et al. Ibrutinib plus Venetoclax for the Treatment of Mantle-Cell Lymphoma *N Engl J Med.* 2018;378:1211–1223.

[62] Jeon HJ, Kim CW, Yoshino T, Akagi T. Establishment and characterization of a mantle cell lymphoma cell line *Br J Haematol.* 1998;102:1323–1326.

[63] Zamò A, Ott G, Katzenberger T, et al. Establishment of the MAVER-1 cell line, a model for leukemic and aggressive mantle cell lymphoma *Haematologica.* 2006;91:40–47.

[64] Lai R, McDonnell TJ, O'Connor SL, et al. Establishment and characterization of a new mantle cell lymphoma cell line, Mino *Leuk Res.* 2002;26:849–855.

[65] Tohda S, Sato T, Kogoshi H, Fu L, Sakano S, Nara N. Establishment of a novel B-cell lymphoma cell line with suppressed growth by gamma-secretase inhibitors *Leuk Res.* 2006;30:1385–1390.

[66] Th'ng KH, Garewal G, Kearney L, et al. Establishment and characterization of three new malignant lymphoid cell lines *Int J Cancer.* 1987;39:89–93.

[67] Kluin-Nelemans HC, Limpens J, Meerabux J, et al. A new non-Hodgkin's B-cell line (DoHH2) with a chromosomal translocation t(14;18)(q32;q21) *Leukemia.* 1991;5:221–224.

[68] Hecht BK, Epstein AL, Berger CS, Kaplan HS, Hecht F. Histiocytic lymphoma cell lines: Immunologic and cytogenetic studies *Cancer Genet Cytogenet.* 1985;14:205–218.

[69] Al-Katib AM, Smith MR, Kamanda WS, et al. Bryostatin 1 down-regulates mdr1 and potentiates vincristine cytotoxicity in diffuse large cell lymphoma xenografts *Clin Cancer Res.* 1998;4:1305–1314.

[70] Uphoff CC, Drexler HG. Detection of Mycoplasma contamination in cell cultures *Curr Protoc Mol Biol.* 2014;106:28.4.1-14.

[71] Smith PK, Krohn RI, Hermanson GT, et al. Measurement of protein using bicinchoninic acid *Anal Biochem.* 1985;150:76–85.

[72] Ong SE, Blagoev B, Kratchmarova I, et al. Stable isotope labeling by amino acids in cell culture, SILAC, as a simple and accurate approach to expression proteomics *Molecular Cell Proteomics.* 2002;1:376–386.

[73] Chen X, Wei S, Ji Y, Guo X, Yang F. Quantitative proteomics using SILAC: Principles, applications, and developments *Proteomics.* 2015;15:3175–3192.

[74] Kim DI, Jensen SC, Noble KA, et al. An improved smaller biotin ligase for BioID proximity labeling *Mol Biol Cell.* 2016;27:1188–1196.

[75] Varnaitė R, MacNeill SA. Meet the neighbors: Mapping local protein interactomes by proximity-dependent labeling with BioID *Proteomics.* 2016;16:2503–2518.

[76] Holland PM, Abramson RD, Watson R, Gelfand DH. Detection of specific polymerase chain reaction product by utilizing the 5'—-3' exonuclease activity of Thermus aquaticus DNA polymerase *Proc Natl Acad Sci U S A.* 1991;88:7276–7280.

[77] Livak KJ, Schmittgen TD. Analysis of relative gene expression data using real-time quantitative PCR and the 2(-Delta Delta C(T)) Method *Methods.* 2001;25:402–408.

[78] Koopman G, Reutelingsperger CP, Kuijten GA, Keehnen RM, Pals ST, van Oers MH. Annexin V for flow cytometric detection of phosphatidylserine expression on B cells undergoing apoptosis *Blood.* 1994;84:1415–1420.

[79] Adli M. The CRISPR tool kit for genome editing and beyond *Nat Commun.* 2018;9:1911.

[80] Doench JG, Fusi N, Sullender M, et al. Optimized sgRNA design to maximize activity and minimize off-target effects of CRISPR-Cas9 *Nat Biotechnol.* 2016;34:184–191.

[81] Das AT, Tenenbaum L, Berkhout B. Tet-On Systems For Doxycycline-inducible Gene Expression *Curr Gene Ther.* 2016;16:156–167.

[82] Ryan J, Letai A. BH3 profiling in whole cells by fluorimeter or FACS *Methods.* 2013;61:156–164.

[83] Subramanian A, Tamayo P, Mootha VK, et al. Gene set enrichment analysis: a knowledge-based approach for interpreting genome-wide expression profiles *Proc Natl Acad Sci U S A.* 2005;102:15545–15550.

[84] Mootha VK, Lindgren CM, Eriksson KF, et al. PGC-1alpha-responsive genes involved in oxidative phosphorylation are coordinately downregulated in human diabetes *Nature genetics.* 2003;34:267–273.

[85] Albert MC, Brinkmann K, Pokrzywa W, et al. CHIP ubiquitylates NOXA and induces its lysosomal degradation in response to DNA damage *Cell Death Dis.* 2020;11:740.

[86] Zhong Q, Gao W, Du F, Wang X. Mule/ARF-BP1, a BH3-only E3 ubiquitin ligase, catalyzes the polyubiquitination of Mcl-1 and regulates apoptosis *Cell.* 2005;121:1085–1095.

[87] Oda E, Ohki R, Murasawa H, et al. Noxa, a BH3-only member of the Bcl-2 family and candidate mediator of p53-induced apoptosis *Science.* 2000;288:1053–1058.

[88] Yoshimura M, Ishizawa J, Ruvolo V, et al. Induction of p53-mediated transcription and apoptosis by exportin-1 (XPO1) inhibition in mantle cell lymphoma *Cancer Sci.* 2014;105:795–801.

[89] Autret A, Martin SJ. Emerging role for members of the Bcl-2 family in mitochondrial morphogenesis *Mol Cell.* 2009;36:355–363.

[90] Chong SJF, Marchi S, Petroni G, Kroemer G, Galluzzi L, Pervaiz S. Noncanonical Cell Fate Regulation by Bcl-2 Proteins *Trends Cell Biol.* 2020;30:537–555.

[91] Simoes ICM, Morciano G, Lebiedzinska-Arciszewska M, et al. The mystery of mitochondria-ER contact sites in physiology and pathology: A cancer perspective *Biochim Biophys Acta Mol Basis Dis.* 2020;1866:165834.

[92] Zinkel S, Gross A, Yang E. BCL2 family in DNA damage and cell cycle control *Cell Death Differ.* 2006;13:1351–1359.

[93] Jaufmann J, Franke FC, Sperlich A, et al. The emerging and diverse roles of the SLy/SASH1-protein family in health and disease-Overview of three multifunctional proteins *FASEB J.* 2021;35:e21470.

[94] Astoul E, Laurence AD, Totty N, Beer S, Alexander DR, Cantrell DA. Approaches to define antigen receptor-induced serine kinase signal transduction pathways *J Biol Chem.* 2003;278:9267–9275.